LATERAL FACIES VARIATION OF BASE SURGE DEPOSITS IN THE UBEHEBE HYDROVOLCANIC FIELD INVESTIGATED BY GROUND PENETRATING RADAR

by

BRUNO CAGNOLI

Laurea in Scienze Geologiche, Universita' di Bologna (Italia), 1993
M.Phil., Plymouth University (UK), 1997

A THESIS SUBMITTED IN PARTIAL FULFILMENT OF
THE REQUIREMENTS FOR THE DEGREE OF

DOCTOR OF PHILOSOPHY

in

THE FACULTY OF GRADUATE STUDIES

Department of Earth and Ocean Sciences

We accept this thesis as conforming
to the required standard

THE UNIVERSITY OF BRITISH COLUMBIA

September 2000

In presenting this thesis in partial fulfilment of the requirements for an advanced degree at the University of British Columbia, I agree that the Library shall make it freely available for reference and study. I further agree that permission for extensive copying of this thesis for scholarly purposes may be granted by the head of my department or by his or her representatives. It is understood that copying or publication of this thesis for financial gain shall not be allowed without my written permission.

Department of EARTH AND OCEAN SCIENCES

The University of British Columbia
Vancouver, Canada

Date Oct. 5, 2000

DE-6 (2/88)

ABSTRACT

Ground penetrating radar surveys were conducted in the Ubehebe hydrovolcanic field (Death Valley, California) in order to study the lateral facies variation of base surge deposits. Using low frequency antennae (50, 100 and 200 MHz), the lower stratigraphic boundary of the pyroclastic deposits was imaged, showing that their thickness can be estimated. Furthermore, different radar responses were obtained from base surge deposits and underlying sedimentary rocks, which enable their recognition when outcrops are unavailable. GPR data also confirmed the presence of small, eroded craters, which are partially filled by alluvium. In this case an unconformity between the overlying, horizontally bedded alluvium and the underlying bowl-shaped base surge deposits was recognized in the radar sections. GPR images collected with higher frequency antennae (900 MHz) show the presence of wavy reflections and that these reflections become increasingly less wavy and more plane-parallel away from the vent. These wavy reflections have been interpreted as GPR images of subsurface trains of climbing dune-forms, whose size decreases downflow. High-pass eigenimages of the 900 MHz profiles were computed in order to quantify the waviness of the reflections. The high-pass eigenimages act as a filter discarding the highly correlated parts of the traces and leaving the wavy reflections. For this reason, the energy of the eigenimages appears to be an index of the waviness of the reflections. The 900 MHz data showed also a downflow amplitude decrease of the reflections that can be used as a flow direction indicator when the vent position is unknown. This trend was displayed computing Fourier transforms and the average square of the sample points of the traces and probably reflects some aspects of the lateral facies variation of base surge deposits. This can be explained with a downflow increase of sorting and decrease of grain size and a consequent reduction of the differences between the beds, which, in turn, causes a reduction of the reflected energy. These results suggest that, although GPR profiles are traditionally used as 2-D images of the subsurface stratigraphy, they can be useful to obtain information about the heterogeneous distribution of subsurface physical properties.

TABLE OF CONTENTS

CHAPTER IV – Unshielded antennae and vertical resolution

CHAPTER V – Ground penetrating radar images of unexposed climbing dune-forms

CHAPTER VI – Downflow amplitude decrease of GPR reflections

CHAPTER VII – Quantification of the wavy reflections in GPR profiles using singular value decomposition

CHAPTER VIII – Cluster analysis of GPR profiles

CHAPTER IX – Summary

LIST OF TABLES

LIST OF FIGURES

ACKNOWLEDGMENTS

I am deeply indebted to Professor Tad Ulrych, whose intelligence and generosity made this thesis possible. Thank you Tad.

I am grateful to Professors Rosemary Knight and Michael Ort, who revised the first draft of this thesis.

Thanks a lot to Steve Cosway (Sensors and Software) for a generous discount, which enabled me the use of the PulseEKKO 1000.

Dr. Greg Valentine is gratefully acknowledged, as responsible editor, for reviewing Chapter 2, which has been published in the *Journal of Volcanology and Geothermal Research* (Cagnoli and Russell, 2000, *J.V.G.R.*, 96, 45-56). Francis Jones also provided a helpful discussion that improved both paper and Chapter 2.

I would like to thank Professor Lionel Wilson who revised Chapter 6, which is in press (Cagnoli and Ulrych, in press. Downflow amplitude decrease of ground penetrating radar reflections in base surge deposits. J.V.G.R).

Two other papers have been submitted: one to the *Journal of Volcanology and Geothermal Research* and one to the *Geophysical Journal International*.

I thank also the Rangers of the Death Valley Nation Park for the research permit.

The author of this thesis was awarded a *University Graduate Fellowship* (University of British Columbia) and a *NATO Fellowship*.

CHAPTER I

Introduction

1.1 Research purposes

Base surges are high velocity, turbulent flows produced by explosive magma-water interactions, which form tuff cones and tuff rings (Fisher and Schmincke, 1984; Cas and Wright, 1987). Field studies of base surge deposits have defined three facies: sandwave, planar and massive. However, there is disagreement in the literature about the inferred distribution of these facies with respect to the vent position. For example, the lateral facies variation model proposed by Wohletz and Sheridan (1979), which implies a downcurrent increase of grain concentration in the traveling flows, has been criticized and considered not acceptable from a sedimentological point of view. Sohn Y.K. and Chough S.K. (Sohn and Chough, 1989; Chough and Sohn, 1990; Sohn, 1996) distilled an alternative lateral facies sequence caused by a decelerating turbulent suspension with downcurrent flow dilution and increase of traction.

Because of the violent nature of the eruption and the high speed and temperature of the base surges it is impossible to study their transport and depositional processes directly. In order to understand their flow mechanisms and predict their behavior we must study the deposits they have left, but it is not always possible to find complete and satisfactory exposures. The purpose of this research is to study the lateral facies variation of base surge

deposits using ground penetrating radar (GPR) images. GPR enables continuous data collection from proximal to distal positions and can supply subsurface information between the few available outcrops. The Ubehebe hydrovolcanic field (Death Valley National Park, California) has been selected for such a study because it is composed of a continuous sheet of pyroclastic deposits, whose top is coincident with the ground surface (no soil is present). Furthermore, in Death Valley, the radar data collection is not disturbed by cultural electromagnetic noise (no town in the area).

I will try to answer two questions. 1) Is it possible to image and locate in the subsurface the three facies (massive, planar and sandwave) of the base surge deposits using ground penetrating radar? 2) Are there differences between the GPR data collected at different distances from the vent and, if so, why? In short, is it possible from the texture of GPR profiles (i.e. signal characteristics) to assess features such as grain size, degree of sorting etc. enabling a quantitative analysis of the facies? The final purpose of this study is to assess capabilities and limitations of GPR in studying the lateral facies variation of base surge deposits, where facies characteristics include: depositional structures, grain size, sorting, thickness of the deposits etc.

1.2 Ground Penetrating Radar

Ground penetrating radar (GPR) is a geophysical technique that uses the reflection of electromagnetic waves to image shallow subsurface geological structures (Ulriksen, 1982; Olhoeft, 1984; Davis and Annan, 1989; Mellett, 1990; Daniels, 1996; Reynolds, 1997). A high power pulse generator and transmitting antennae generate wide-band electromagnetic signals of known center frequencies that propagate through the subsurface and are reflected

(as well as refracted, diffracted, absorbed etc.) at interfaces characterized by changes in dielectric properties and electrical conductivity. Variations in these properties can be caused by several factors including changes in the water content, composition and texture of stratigraphic units. Reflected signals are then detected by receiving antennae and recorded with a conventional laptop computer.

In reflection profiling mode both transmitting and receiving antennae are moved along survey lines keeping their separation constant. At each antennae location, a single trace is collected, which comprises a series of amplitude values (sample points) equally spaced in time. These traces are then plotted sequentially, forming a GPR profile. GPR can sound down to as much as 20-40 m in low conductivity materials like dry sand, gravel and fresh water. On the other hand, in conductive materials such as clays, silts and soils with saline or contaminated pore water, the penetration is severely reduced (Davis and Annan, 1989). The attenuation is also frequency dependent: high frequencies are attenuated more than low frequencies (Cai and McMechan, 1995). This means that larger wavelengths have greater penetration (but less resolution) and smaller wavelengths have smaller penetration (but higher resolution).

The field experiments used to measure the subsurface velocity of the electromagnetic energy are called Common Mid Point (CMP) surveys (Annan et al., 1975; Fisher et al., 1992). In these experiments, the distance between receiving and transmitting antennae is increased after each measurement, while maintaining a fixed midpoint (Reynolds, 1997). In CMP profiles (which are graphs of travel time versus antennae separation), the air and ground waves plot as straight lines, whereas the reflected waves plot as hyperbolas. For the ground wave: $t = \frac{x}{v_g}$, where t is the travel time, v_g is the subsurface velocity of the

electromagnetic waves and x is the antennae separation (Annan et al., 1975). For the reflected waves: $t = \frac{1}{v_g}(x^2 + 4d^2)^{0.5}$, where d is the depth of the reflector (Annan et al., 1975). These hyperbolas enable an estimate of the subsurface velocity of the reflected waves. The air wave travels through the air at approximately 0.3 m/ns.

GPR has wide use in geology, glaciology, engineering, archeology, forensic and environmental sciences (Daniels, 1996; Reynolds, 1997). Examples of GPR studies of sedimentary rocks are Jol and Smith (1991), Gawthorpe et al. (1993), Smith and Jol (1992), Smith and Jol (1995), Beres et al. (1995), Bristow et al. (1996), Smith and Jol (1997) and McMechan et al. (1997). This technique promises to be useful with pyroclastic rocks as well, although GPR investigations of pyroclastic deposits are still in their infancy. Attempts to study pyroclastic deposits with GPR made the work of Russell and Stasiuk (1997 and *in press*) who ran GPR surveys over recent volcanic deposits in western Canada and over the Late Bronze Age deposits in Santorini (Greece) respectively. McCoy et al. (1992) is another example of GPR application to pyroclastic deposits in Santorini, while Pilon et al. (1991) investigated the underground stratigraphy of the Meteor Crater in Arizona.

1.3 Base surges

Base surges are due to explosive interactions between magma and water (phreatomagmatic eruptions). They are highly expanded, low particle concentration, turbulent flows capable of moving in all directions radial to the vent (Fisher and Schmincke, 1984; Cas and Wright, 1988). They can contain three phases: solid fragments, volcanic gases and water (steam). Water vapor moves along with the pyroclasts and may segregate, rising

above the surge and leaving dry deposits, but can also condense during transport resulting in wet deposits (Wohletz, 1986). Large-scale vaporization of sea or ground water is widely recognized to be very important in explosive volcanism although volcanologists are aware of the complexity of the physical and chemical phenomena involved (Wohletz, 1986). These turbulent flows are initiated by an explosive thrust, but, because their density is higher than that of the atmosphere, they are gravity controlled. This means that they tend to follow topographic lows, but can also climb obstacles because of their energy and turbulent nature. According to Sohn Y.K. and Chough S.K. (Sohn and Chough, 1989; Chough and Sohn, 1990; Sohn, 1996) during flowage the grain transport mechanism changes from suspension to surface traction, but a rapid deposition from high concentration suspension without tractional transport is expected near the vent.

Phreatomagmatic juvenile clasts are characteristically fine grained because of the high degree of fragmentation caused by the magma-water interaction (when efficient fuel/coolant interactions occurs). The fragments are glassy, poorly vesicular and nearly equant and blocky in shape (Fisher and Schmincke, 1984; Heiken and Wohletz, 1992). The phreatomagmatic explosions form maars, tuff rings and tuff cones that are common volcanic landforms. Their deposits are thick around the vent, thinning away from it and are composed of a lot of thin beds and laminae ranging in thickness from few millimeters to several tens of centimeters, but most are less than 10 cm thick (Fisher and Schmincke, 1984). They are composed of many thin beds because, typically, the eruptions comprise a large number of short eruptive pulses (surges). Usually the base surge deposits do not reach distances more than 10 km from the vent location.

1.4 Ubehebe hydrovolcanic field

The Ubehebe hydrovolcanic field is located in the northern part of the Death Valley National Park (California), on the slope of the Tin Mountains at about 800 m above sea level (Crowe and Fisher, 1973). The volcanic field probably formed during Holocene time (Crowe, 1990) and includes at least 12 craters within an area of 3 km^2; the associated deposits cover an area no less than 15 km^2 (Crowe and Fisher, 1973). These pyroclastic deposits are alkali basalt in composition (Crowe and Fisher, 1973) and were emplaced by base surges. The two main craters appear to be situated on a north-trending fault line (Von Engeln, 1932; Roddy, 1968; Crowe, 1990). The pyroclastic deposits rest upon a thick (~ 500 m) sequence of sandstones and conglomerates (Crowe and Fisher, 1973). This sequence, fractured and faulted, crops out also within the Ubehebe crater.

The craters are divided into four areas including: a western and southern group of craters, Ubehebe crater and Little Hebe Crater (Crowe and Fisher, 1973). The western crater cluster includes seven craters, whereas four craters make up the southern crater cluster. They are tuff rings with small rims that are built mainly of base surge beds (with subordinate amounts of fall deposits). Generally, in tuff rings, the beds dip inward and outward with respect to the crater depression (Cas and Wright, 1987). The Ubehebe crater is a maar (700-800 m in diameter and 235 m deep), cut below the general ground level and surrounded by a tuff ring with maximum thickness of 50 m at the crater rim, decreasing downflow with a dip of 10°-15°. The Ubehebe crater was formed by the last and largest eruptive episode of this volcanic field. The surges flowed undisturbed from its vent, but some moved uphill within the gullies sloping down from the Tin Mountains (Crowe and Fisher, 1973). Little Hebe

Crater is a small cone comprising agglutinated spatter overlain by base surge beds derived from Ubehebe Crater. It has a diameter of 100 m and a depth of 20 m.

1.5 Lateral facies sequences in base surge deposits

Introduction

Base surge beds display three facies, called respectively sandwave, planar and massive. The term sandwave is applied to beds with climbing dune-forms, undulating surfaces and internal cross lamination. The planar facies consists of plane-parallel beds and laminae with upper and lower contacts generally planar and parallel to one another. Massive beds are without internal organization of the fragments and are thicker than the beds showing the other two facies.

There are different opinions in the literature about the lateral facies variations in base surge deposits. Sigurdsson et al. (1987) describe surge deposits that are dune bedded throughout most of their extent. Fisher and Waters (1970) and Waters and Fisher (1971) suggest that the lateral facies variation in base surge deposits can change from one volcano to another. Surges are also thought to change downcurrent into a bipartite flow comprising a high-concentration, laminar lower part and a dilute, turbulent upper part (Fisher, 1983). Unfortunately the lack of exhaustive measurements and widely applied rigorous facies analysis prevents a real comprehensive model for base surges (Sohn and Chough, 1989). Scientists agree that more work needs to be done to study the facies of base surge deposits. Where there seems to be general agreement is that the supporting mechanism of the fragments in base surges is mainly the turbulence because of the presence of tractional

sedimentary structures such as cross-stratification and horizontal lamination. These structures result from grain-by-grain tractional transport implying low grain concentration. Nevertheless, it is important to bear in mind that, usually in a single flow, different mechanisms of grain support are dominant at different stages of its life (Blatt et al., 1980). Base surges like turbidity currents are density currents, but this does not help to delineate a fluid dynamic model. These flows could be described as non-uniform, unsteady, non-linear, free-boundary flows (Allen, 1985) causing the despair of fluid dynamicists!

The lateral facies sequences

Wohletz and Sheridan (1979) suggested a downflow facies variation for dry base surge deposits from sandwave near the vent, to massive in intermediate positions and planar in the most distal sections (Fig. 1.1), whereas Sohn and Chough (1989), Chough and Sohn (1990) and Sohn (1996) distilled the following lateral facies sequence from dry Korean base surge deposits: 1) proximal massive deposits, 2) intermediate plane-parallel and dune bedded deposits and 3) distal plane-parallel laminated deposits (Fig. 1.1). The Korean model is interpreted in terms of a turbulent suspension that decelerates with distance from the vent and whose grain concentration decreases and degree of traction increases downflow. On the contrary, the model by Wohletz and Sheridan (1979) assumes a deflation of the flow resulting in an increase of the grain concentration downcurrent when massive beds are deposited (this deposition decreases again the concentration of the flow so that plane-parallel laminae are produced in more distal positions). In the model by Wohletz and Sheridan

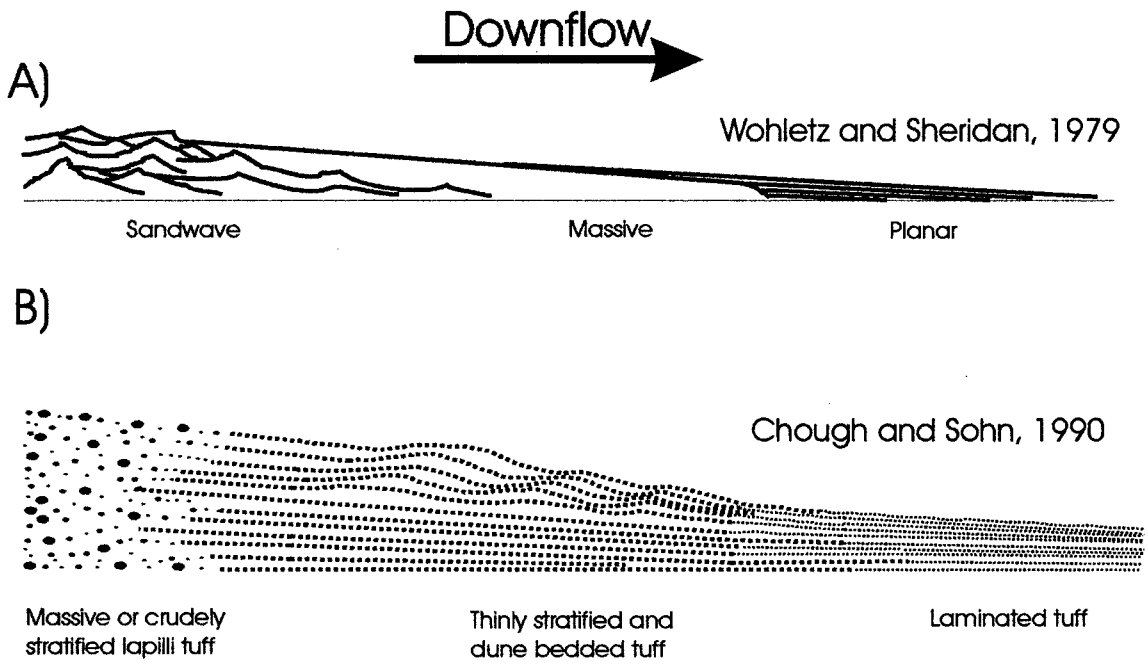

Fig. 1.1. In the model suggested by Wohletz and Sheridan (1979) a proximal cross-bedded facies passes downflow within 500 m to a massive and reversely graded bed facies that is replaced further away by a planar facies in the most distal positions. These authors have studied base surge deposits up to 1 km from the crater rim. Bed thickness decreases very rapidly in the direction of transport in the cross bedded facies, but not in the massive facies where the variation is not systematic. In the studied deposits, the parameter phi (sorting) ranges from 1.6 to 1.88 and the grain size from 0.177 mm to 30 mm. In the model suggested by Chough and Sohn (1990), the general thickness of the deposit as well as the individual bed thickness and grain size decrease in the direction of transport for almost 3 km. The thickness of the beds varies from about 1m near the crater to < 10 cm in the distal part. This lateral facies variation model begins with disorganized lapilli tuff and passes downcurrent into stratified lapilli tuff. The latter is succeeded most commonly by undulatory waveforms, less commonly by climbing dunes and stratified tuff. These bedforms decrease in wavelength and amplitude downcurrent and transform into either planar-bedded or mantle bedded tuff.

(1979) the flow is highly turbulent in proximal positions so that traction structures (such as sandwaves) are formed before the deposition of massive beds. Lajoie and Stix (1992) prefer the lateral facies variation model proposed for the Korean base surge deposits, because of its similarity to turbidity current deposits.

In the wet-surge deposits of Linosa island (Italy), Lajoie et al. (1992) described a proximal section showing that more than 80 % of the beds are massive, a medial section where more than 50 % of the beds are parallel-laminated and a more distal section where most deposits have dune-type cross bedding. The Korean lateral facies sequence and that described by Lajoie et al. (1992) are pretty similar if we consider that the most distal portion of the sequence in Linosa may have been lost because deposited on sea water, i.e. wet or dry surges can have similar lateral facies sequence (Lajoie et al. 1992). Lajoie and Stix (1992) say that the lateral facies variation model for the Korean and Italian surge deposits is new and insufficiently tested, but they consider it an excellent working hypothesis.

In particular, Sohn and Chough (1989) found six lateral facies sequences (LFS), representing downcurrent transformations of various base surges with different physical properties. Four LFS begin with poorly sorted and massive lapilli tuff and transform down-current into thinly stratified units that are either planar-bedded, undulatory bedded or climbing dune-bedded. In these LFS, the near-vent deposits are generally unstratified because of the rapid deposition from highly concentrated suspension without tractional transport. Whereas the down-current transformation of massive lapilli tuff into stratified units is indicative of an increasing degree of traction and sorting due to flow dilution. Further increase in the tractional phase results in the development of undulatory waveforms. A fifth LFS begins with unstratified lapilli tuff and is crudely stratified downcurrent. This is thought

to be the deposit of wet surge lacking hydraulic sorting because of the cohesion of damp ash (the ash in a steam-rich flow becomes wet and sticky affecting the facies of the deposits). The last LFS comprises well-sorted lapilli tuff near the vent and thin-bedded tuff in distal areas. It seems to have been deposited by combined falls and surges.

Fisher and Schmincke (1984) think that the facies model proposed by Wohletz and Sheridan (1979) can provide statistical summations of many flows through time in a particular place, but cannot be applied to processes, which occur laterally within a single flow. The model suggested by Wohletz and Sheridan (1979) has been obtained using a Markov analysis to characterize sections and analyze vertical bed-forms distributions as a function of distance from the vent in 12 locations. The problem is that each section records the deposition of several different surges with different size and energy. This means that in the same location there can be proximal and distal deposits left by different surges. For this reason, there is a distinct possibility that Wohletz and Sheridan (1979) did not obtain information about the lateral facies variation in these deposits. Rather, they evaluated the most likely occurrence of the different facies in each single location (Fisher and Schmincke, 1984). The differences between the lateral facies sequence by Wohletz and Sheridan (1979) and by Sohn (1996) are also due to different definitions of the different facies. For example, Wohletz and Sheridan (1979) define the "sandwave facies" as a combination of sandwave and massive beds, whereas the "massive facies" is a combination of massive, sandwave and planar beds.

Base surges and turbidity currents

Lajoie and Stix (1992) suggest similarities between flow and depositional processes of sedimentary and pyroclastic deposits. On the other hand, Cas and Wright (1987) think that

there is no hydrodynamic equivalence between turbidity currents and surges and, although both are gravity controlled, they produce different facies. Gravity controlled means that they are both density currents that travel due to density differences between the flow and the atmosphere because of the presence of dispersed particles (Allen, 1985). Cas and Wright (1987) even suggest that it is probably premature to propose simple facies variations model for base surge deposits (i.e. something similar to the Bouma sequence) because of their complexities. Base surges can be dry, hot, wet, cold and have different degree of condensation, intensity of fragmentation and explosive thrust. These authors think that even if the turbidity currents can be considered the closest sedimentary analogue to base surges (because they are both turbulent) the similarity cannot be extended any further because the base surges are complex three phases mixtures while the turbidity currents are not (Cas and Wright, 1987). Cas and Wright (1987) also criticize the use of terms like "dune" or "antidune" to describe the cross lamination in base surge deposits. I personally agree and prefer to call the structures responsible for the sandwave facies "climbing dune-forms" as in Cas and Wright (1987) even if in this thesis sometimes they are called sandwaves for short. Also Allen (1982) criticized the hydrodynamic interpretation of the sandwave bed forms as antidunes. Similarly, Boudon and Lajoie (1989) observed that the subaqueous and pyroclastic dunes have several differences. Floodplain and subacqueous information is not applicable to base surge deposits.

1.6 Preliminary geologic survey (summer 1998)

I carried out a preliminary geological survey of the Ubehebe hydrovolcanic field during the summer 1998 to design the location of the GPR traverses and examine the characteristics of the base surge deposits in this area.

The main field observations were:

1) The lateral facies variation model by Wohletz and Sheridan (1979) does not take into account the presence of massive beds and beds showing coarse tail reverse grading which crop out along the rim of the Ubehebe Crater.
2) The facies map by Wohletz and Sheridan (1979) does not take into consideration the entire area covered by the base surge deposits, but includes only 1 km around the Ubehebe Crater. There are base surge deposits up to 4 km north of Ubehebe Crater (Troxel and Strand, 1964; Strand, 1967).
3) North of Ubehebe Crater there are insufficient outcrops, but the presence of the base surge deposits is certain (Strand, 1967), because the top of the deposits is coincident with the ground surface (no soil is present). The northern sector promised to be the area where it should be possible to find a complete lateral facies sequence (because the base surge deposits reach the largest distance from the vent and they are not covered by alluvial fans) and where GPR should be able to fill the gap of information between the few available exposures.
4) In the gullies south and west of the Ubehebe crater there are no outcrops entirely composed of climbing dune-forms (i.e. there are no vertical successions of climbing dune-forms). I found only horizontal successions of sandwaves (in places more than ten

dune-forms in successions). This is how I expect to see them in the GPR profiles collected in the area north of Ubehebe Crater.

1.7 Discussion

I believe that the discrepancies between field evidences and the lateral facies variation model suggested by Wohletz and Sheridan (1979) as well as the intriguing, more recent lateral facies sequences distilled by Y.K Sohn and S.K. Chough (Sohn and Chough, 1989; Chough and Sohn, 1990; Sohn, 1996) show that the lateral facies sequence in base surge deposits is still an open problem in volcanology. Is the model suggested by Wohletz and Sheridan (1979) correct? Is the lateral facies sequence distilled by Y.K Sohn and S.K. Chough valid in the Ubehebe Crater area as well? The area north of the Ubehebe Crater seems a perfect place to answer those questions because it is where the base surge deposits reach the largest distance from the Ubehebe Crater and, for this reason, where their lateral facies sequence has more chances to be complete (in the northern area the deposits are not disturbed by the presence of the other small craters and they are not covered by alluvial fans). Because of lack of outcrops in the northern sector, we need an instrument, like GPR, capable of imaging the subsurface. Base surge deposits have characteristics suitable for study by GPR, because they are fine-grained, which should reduce the extent of the electromagnetic scattering and even more importantly, the beds in these deposits are typically thin, which means that when the depth of penetration of the electromagnetic waves is limited, the GPR profiles are still representative.

A 3-D study of the geometry of sandwaves should also be very interesting. Cross bedding is a very important structure able to indicate depositional environments, palaeoflow

velocities and palaeo-current directions (Rubin, 1987). This study can be attempted using high-resolution antennae and running a closely spaced grid of GPR profiles over a sandwave. I am also particularly interested in the extraction from GPR data of information concerning the subsurface that would be otherwise impossible to obtain in areas without exposures. For example, it should be interesting to numerically characterize the texture of GPR profiles and compare proximal and distal traces. Some differences are expected because there is a downflow decrease of grain size and thickness of the beds and increase of sorting in these deposits. I believe that the most ambitious target is the use of GPR data without outcrop calibration (i.e. comparison) to extract "real" geological information. The design of parameters to characterize the textures of the GPR sections and the use of appropriate signal processing techniques is necessary to pursue this target.

The study of the deposits left by base surges is necessary because the violent nature of their eruptions and the high speed and temperature of the flows prevent a direct study of their transport and depositional processes. Base surges are not rare and strange natural phenomena. On the contrary, they have left their deposits in densely populated areas like Honolulu, Mexico City, Campi Flegrei (Napoli), Auckland and Manila and they can strike again anywhere and anytime a magmatic intrusion moves upward and meets a body of water (sea, lake or just ground water).

CHAPTER II

GPR survey of the Ubehebe hydrovolcanic field using 50, 100 and 200 MHz antennae

2.1. Introduction

This chapter presents preliminary ground penetrating radar (GPR) data obtained from surveys conducted with 50, 100 and 200 MHz antennae in the Ubehebe hydrovolcanic field. The purpose of these surveys is to assess capabilities and limitations of GPR in imaging the subsurface features of basaltic base surge deposits. It is important to test the resolution of the different antennae (comparing GPR profiles and outcrops) and measure the velocity of propagation of the electromagnetic waves. An important question is: can we obtain GPR images of climbing dune-forms? It is also interesting to evaluate the possibility to recognize the presence in the subsurface of different, unexposed lithologies. The GPR images of pyroclastic rocks presented in this chapter constitute a database that is useful to suggest appropriate antenna frequencies to study the lateral facies variation of base surge deposits (do we need frequencies higher than 200 MHz?). GPR data can be collected relatively easily and quickly, but the application of this technique to the study of pyroclastic rocks is only in its infancy.

Furthermore, in the Ubehebe hydrovolcanic field, there are 12 craters of different sizes. The larger craters can be easily identified in the field. The smaller cannot, because they are

partially eroded and filled by alluvium. For this reason, profiles have been run to confirm the presence of the smaller craters. Fig. 2.1 shows a map of the Ubehebe hydrovolcanic field, where the locations of the crater rims (Fig. 2.2) are based on field and air photo mapping. The bottom of some craters has been sedimented by alluvial material deriving from reworked base surge deposits or by thin veneers of clay resulting from ephemeral lakes (Crowe and Fisher, 1973). Clay represents a problem for radar surveys because it causes strong attenuation of electromagnetic waves due to its electrical conductivity (Reynolds, 1997).

In order to understand what the GPR profiles would have imaged, samples were collected and thin sections cut to investigate the nature of the fragments constituting the pyroclastic deposits. The thin sections show that these deposits contain not only juvenile volcanic fragments (glass for example), but also fragments of quartz and other rock material derived from the underlying sedimentary rocks, which are exposed also within the Ubehebe Crater.

2.2 Data collection and data presentation

All radar data were collected using a commercial PulseEKKO 100 instrument, manufactured by Sensors and Software Inc., with a 1000 V transmitter. The GPR was controlled by a Husky FC-486 laptop computer. Topographic profiles were measured by a Nikon D-50 total station and used to move the first datum of each trace into the correct vertical position. The GPR surveys were carried out using 50, 100 and 200 MHz antennae. The 50 MHz antennae permitted imaging of deeper structures at lower resolutions, whereas the 200 MHz antennae experiments provided higher resolution images of the shallow portion of the deposits. The 100 MHz antennae have intermediate resolution and depth of

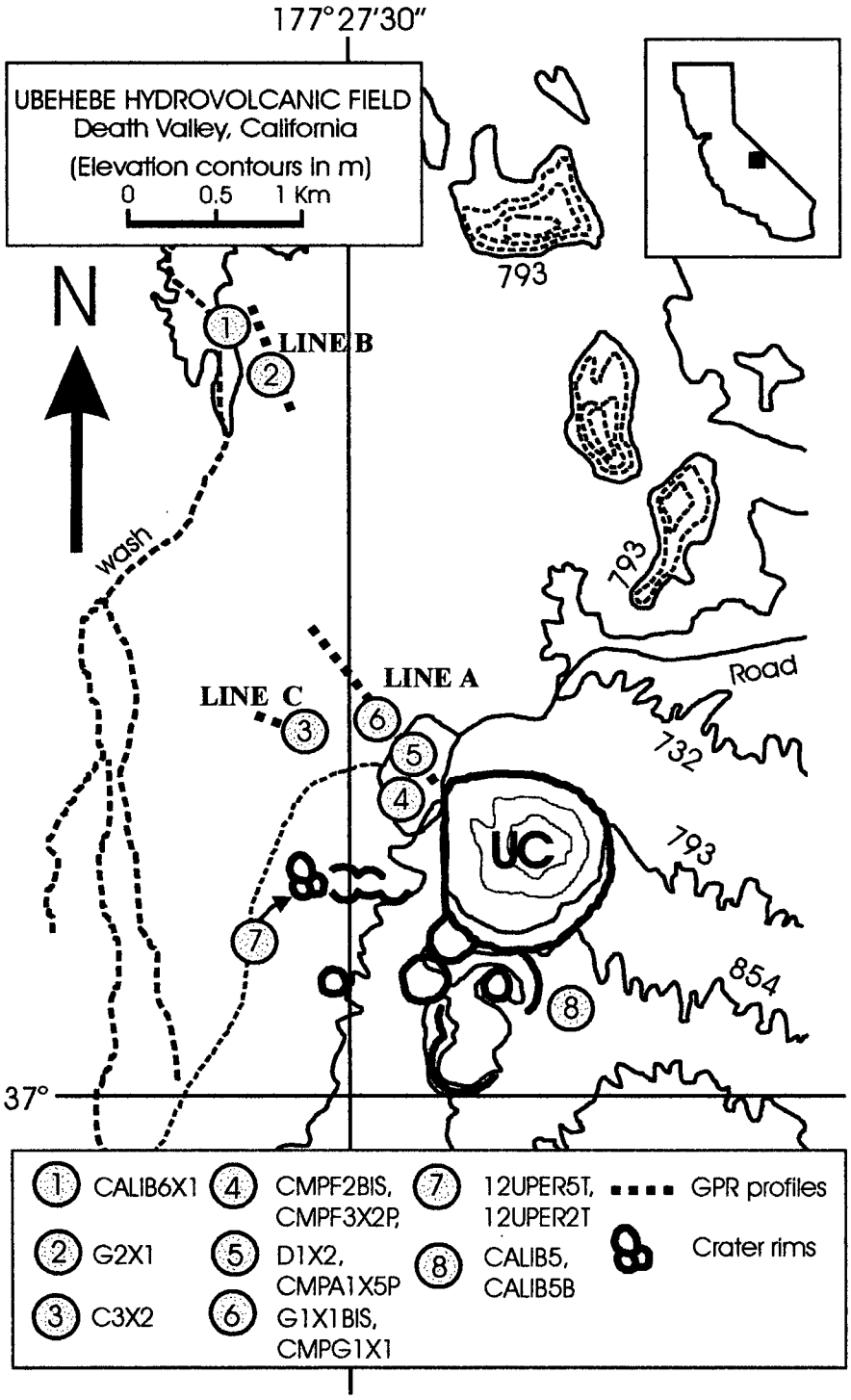

Fig. 2.1. Map of the Ubehebe hydrovolcanic field with locations of the GPR lines A, B and C. UC stands for Ubehebe crater, the largest one. The numbers show the locations of the GPR profiles described in Chapter 2. The inset to the upper right shows map location within California.

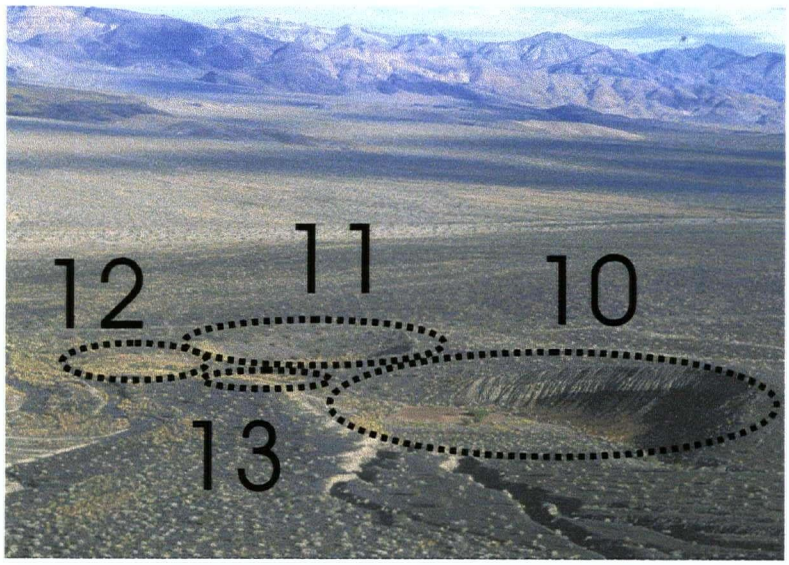

Fig. 2.2. Field photograph showing a portion of the western crater cluster of the Ubehebe hydrovolcanic field, with location of the smaller craters number 12 and number 13.

penetration. Table 2.1 summarizes the parameters used in each GPR survey. Radar profiles are displayed after applying a signal saturation correction filter (dewow) and an automatic gain control (AGC). Data were processed using the software PulseEKKO© (Sensors and Software Inc.). In all radar profiles the position of the antennae is represented along the horizontal axis and the two-way signal travel time is along the vertical axis. All profiles have no vertical exaggeration. The locations of the data described in the text are shown in Fig. 2.1.

2.3 GPR profiles: methods and results

Common Mid Point (CMP) surveys

Common Mid Point (CMP) surveys were run to compute the average velocity of the electromagnetic waves in the subsurface and provide a basis for converting two-way travel times to depths. The results of fifteen CMP profiles, run with the three antennae frequencies (Fig. 2.3), suggest that the velocity of the reflected electromagnetic waves in the upper part of the base surge deposits are between 0.095 – 0.1 m/ns. These velocities were computed using the software Gradix© (Interpex Ltd.).

Calibrations

Several comparisons (calibrations) between outcrops and GPR profiles were carried out to assess the resolution of the antennae and evaluate the characteristic radar response of the different lithologies. For example, Fig. 2.4 presents two profiles (CALIB5B and CALIB5) run with 200 MHz antennae, which are parallel to an outcrop showing horizontal, parallel laminae and beds with a maximum thickness of 10 cm. Two small climbing dune-forms are

Table 2.1. GPR data collection and presentation parameters.

Profile Name	Frequency (MHz)	Antennae separation (m)	Step size (m)	Stacks No. [b]	AGC type [c]
CMPF2BIS	200	[a]	0.2	128	0.25 [d]
CMPF3X2P	200	[a]	0.2	128	0.25 [d]
CMPG1X1	100	[a]	0.5	128	0.25 [d]
CMPA1X5P	50	[a]	1	64	0.25 [d]
CALIB5B	200	0.5	0.1	128	0.5 [d]
CALIB5	200	0.5	0.1	128	0.5 [d]
CALIB6X1	100	1	0.25	128	0.5 [d]
D1X2	200	0.5	0.1	128	0.5 [d]
C3X2	200	0.5	0.1	64	200 [e]
G1X1BIS	100	1	0.25	128	0.5 [d]
G2X1	100	1	0.25	128	0.5 [d]
12UPER5T	50	2	0.5	64	0.1 [d]
12UPER2T	200	0.5	0.1	64	1 [d]

A signal saturation correction filter (dewow) was applied to all profiles.

[a] In CMP surveys the antennae separation increases after each measurement.

[b] Stacks No. is the number of traces collected at each survey position that was averaged to increase the signal to noise ratio.

[c] AGC = automatic gain control.

[d] Dynamic gain limiting scheme; [e] manual gain limiting scheme (PulseEKKO© software).

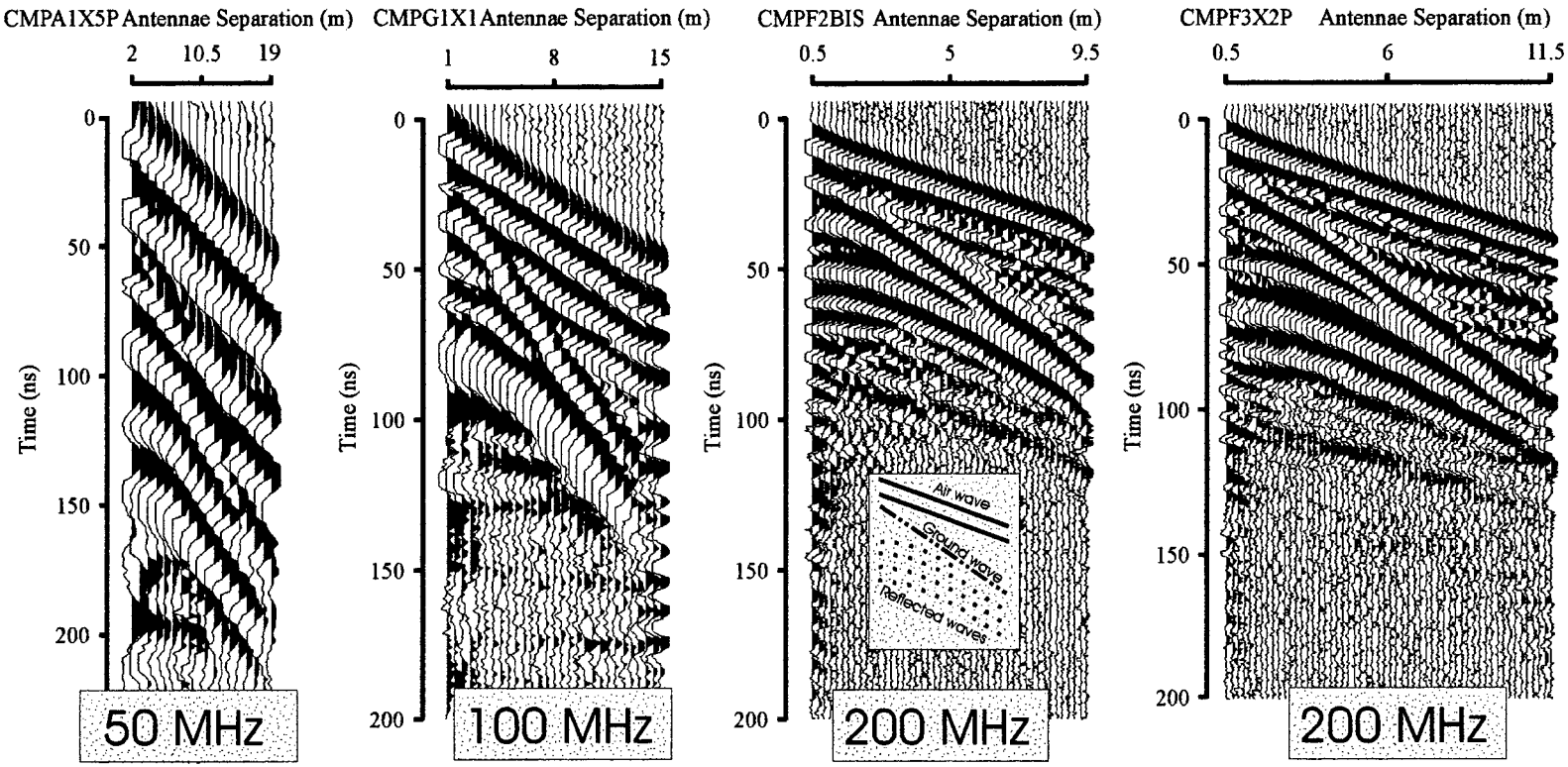

Fig. 2.3. Examples of Common Mid Point (CMP) profiles obtained using different frequencies. The reflected waves suggest velocities of the electromagnetic waves in the upper part of the base surge deposits between 0.095 and 0.1 m/ns.

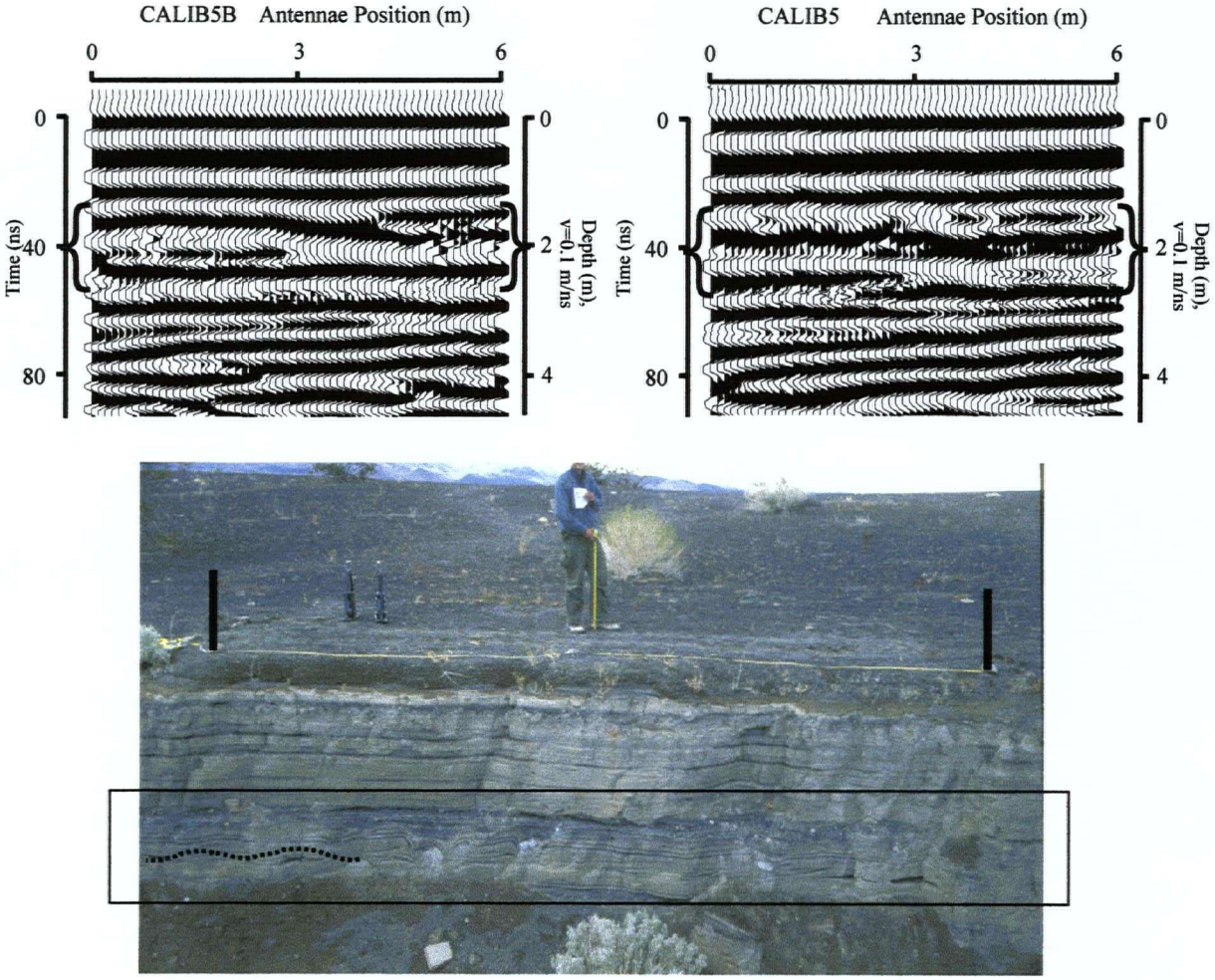

Fig. 2.4. Comparison between outcrop and GPR profiles run with 200 MHz antennae between the two black bars in the photograph. CALIB5 and CALIB5B are located respectively 1.5 and 0.5 m from the edge of the gully. The tape held by the field assistant is 1 m long. The dotted line in the photograph shows the position of two climbing dune-forms. Parenthesis (in the profiles) and rectangle (in the photo) show the area that is not affected by air and ground waves. When evaluating thickness, note that the surfaces of the outcrop and photograph are not parallel.

present in the lower, left corner. The two profiles CALIB5B and CALIB5 are located 50 cm and 1.5 m respectively, from the edge of the gully. Two important observations can be made, 1) both profiles show parallel reflections, but are not identical and 2) the climbing dune-forms are not clearly identifiable.

Calibration profile CALIB6X1 (Fig. 2.5) was run with 100 MHz antennae. The aim of this calibration is to identify the buried sedimentary rocks that underlie the base surge deposits (Crowe and Fisher, 1973), where no exposures are available. This profile is parallel to an outcrop (located along the wash, north of the Ubehebe crater, Fig. 2.1) showing an inclined stratigraphic contact between pyroclastic deposits and sandstones. The surface of the outcrop and the profile are a few meters apart. In Fig. 2.5, the deeper reflections are labeled A and an inclined reflection is labeled CO.

GPR profiles of the base surge deposits

GPR profiles were collected along three lines (A, B and C) north of the Ubehebe Crater (Fig. 2.1), using 200 and 100 MHz antennae. Line A is proximal and 900 meters long, line B is distal and 600 meters long, and line C is 180 meters long. The GPR profiles of lines A and B are located downhill from, and along directions radial to, Ubehebe Crater. They are situated in the central part of the northern valley, where the deposits are probably thicker and less disturbed by an irregular paleotopography. They are also positioned to avoid small hillocks that probably correspond to paleotopographic highs. These highs could have disturbed the regular flow of the turbulent base surges affecting the characteristics of the deposits. Line C is located above a small hill not far from the Ubehebe crater. All surveys

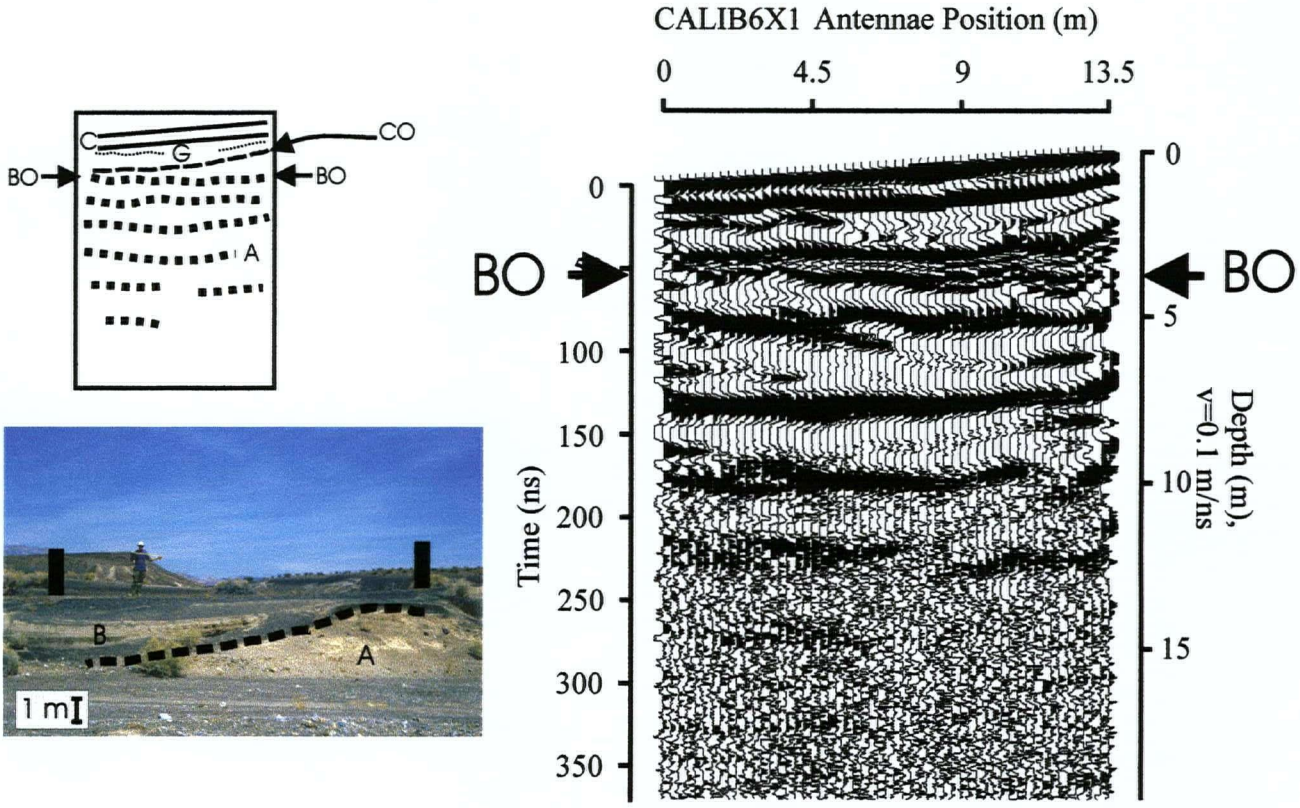

Fig. 2.5. Comparison between outcrop and GPR profile CALIB6X1 run with 100 MHz antennae. The profile is located between the two black bars in the photograph. Topographic correction has been applied. A stands for sedimentary rocks (sandstones), B for base surges, CO for the contact between base surges and underlying sedimentary rocks. BO is the base of the outcrop positioned taking into account its height; C is the air wave and G may be the ground wave or a reflection from the base surge deposits. To evaluate thickness, note that the surfaces of the outcrop and the photograph are not parallel.

have been carried out directly above the top of the base surge deposits (Strand, 1967) because there is no soil in the area.

Profile D1X2 (Fig. 2.6) is a portion of a 200 MHz survey, which is representative of those collected along lines A and B. This profile shows monotonous, parallel reflections that are locally wavy and discontinuous. It was collected relatively close to the Ubehebe Crater rim, where the base surge deposits are 50 m thick. Profile C3X2 (Fig. 2.7), which presents more complex reflections, was run with 200 MHz antennae along line C on the slope of a little hill facing Ubehebe Crater. Two main features can be observed: 1) angular unconformities (onlaps) between reflections H and K, and 2) the wavy reflections K.

Profiles G1X1BIS and G2X1 (Fig. 2.8) were carried out with 100 MHz antennae in the northern valley between the Ubehebe Crater and the wash (Fig. 2.1), where no outcrops are available. These experiments were run to estimate the thickness of the base surge deposits. G1X1BIS is located in proximal position relatively close to the Ubehebe Crater, whereas G2X1 is distal. In both profiles, two sets of reflections (A and B) with different wavelength along the traces can be observed. These reflections have been compared to those of CALIB6X1 for interpretation.

GPR profiles of the craters

GPR profiles were also collected along lines running through the centers of the craters, but no exposures are available for calibration. Unfortunately, surveys run in the larger craters returned no useful information probably because of a thin surface layer of clay that severely reduced the penetration depth of the radar signal. An example of a profile run within one of the smaller craters (e.g. No. 12, Fig. 2.2) is shown in Fig. 2.9. The center of the crater and the

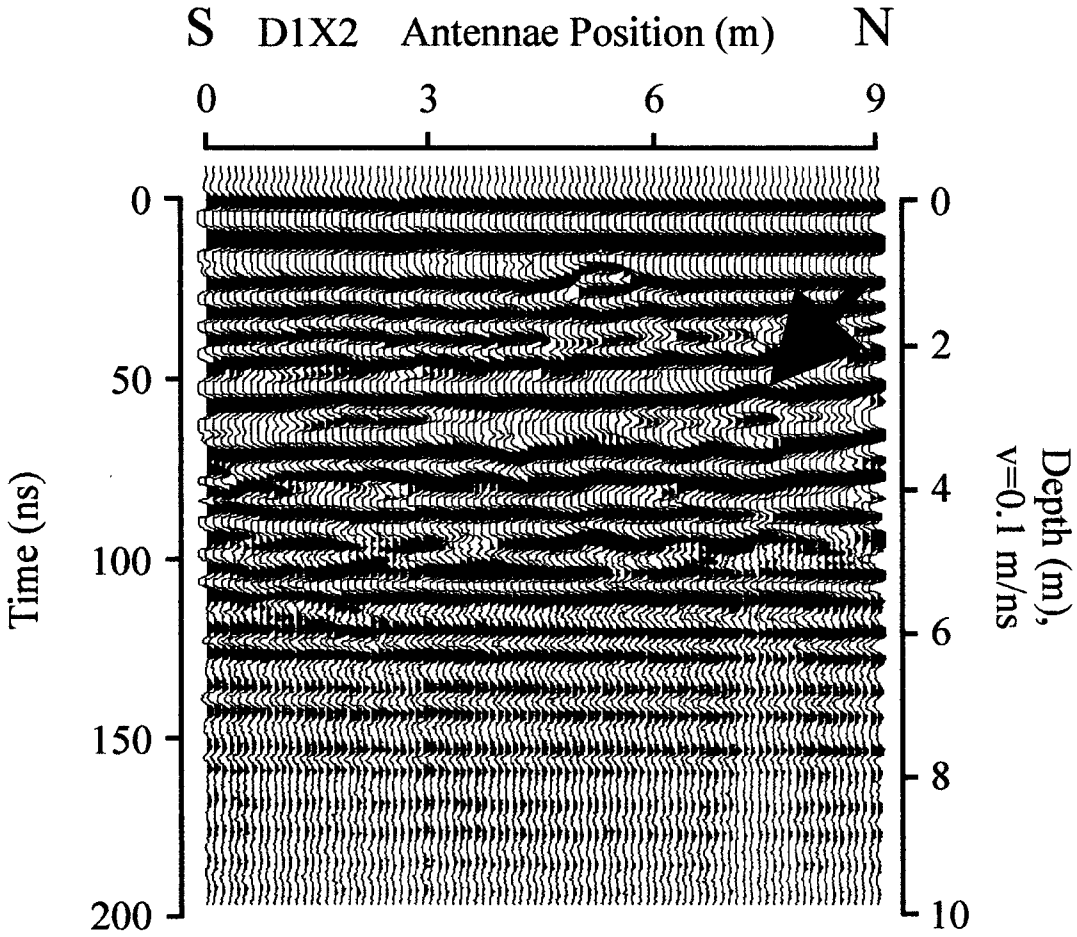

Fig. 2.6. Portion of a GPR profile collected along line A using 200 MHz antennae. The reflections are parallel and sometimes discontinuous or wavy (arrow).

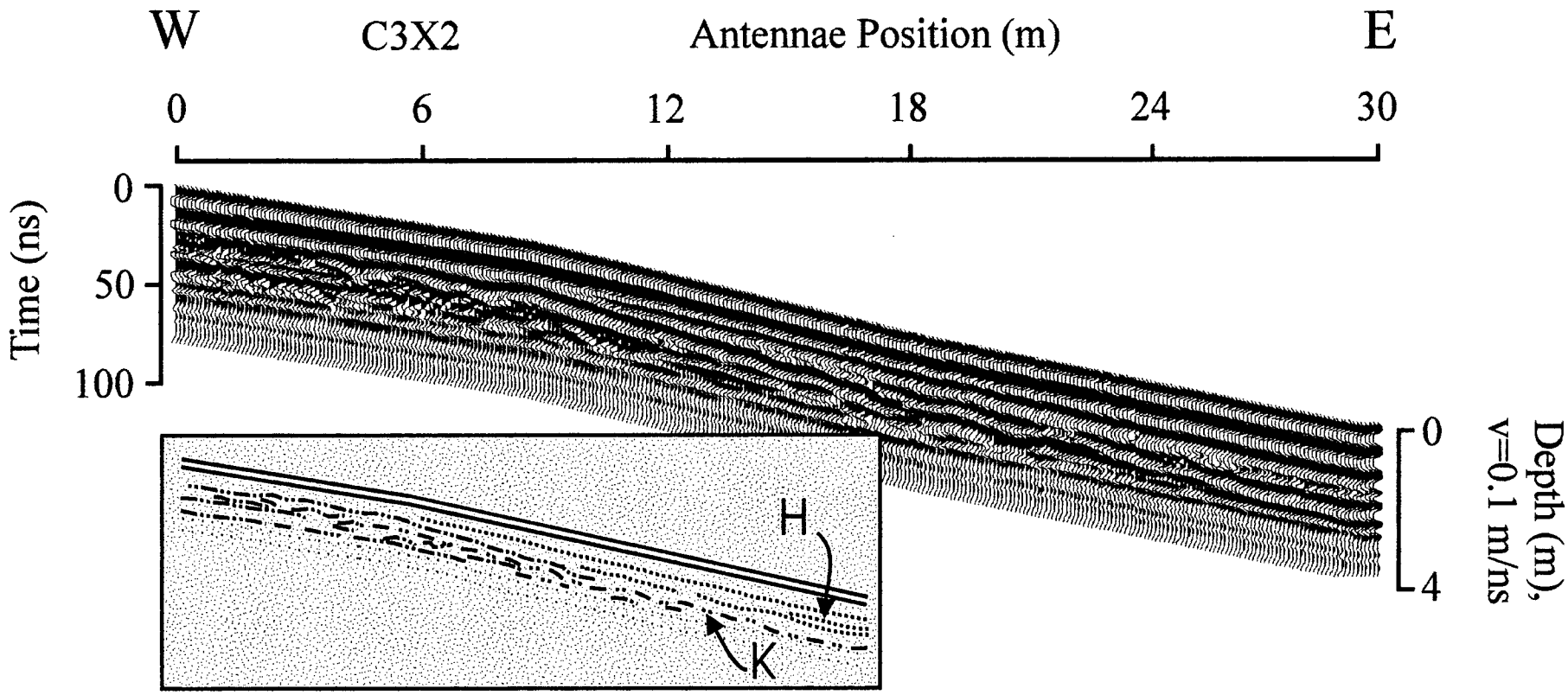

Fig. 2.7. GPR profile collected along line C with 200 MHz antennae. The slope faces Ubehebe Crater. Reflections H and the underlying, wavy reflections K form angular unconformities.

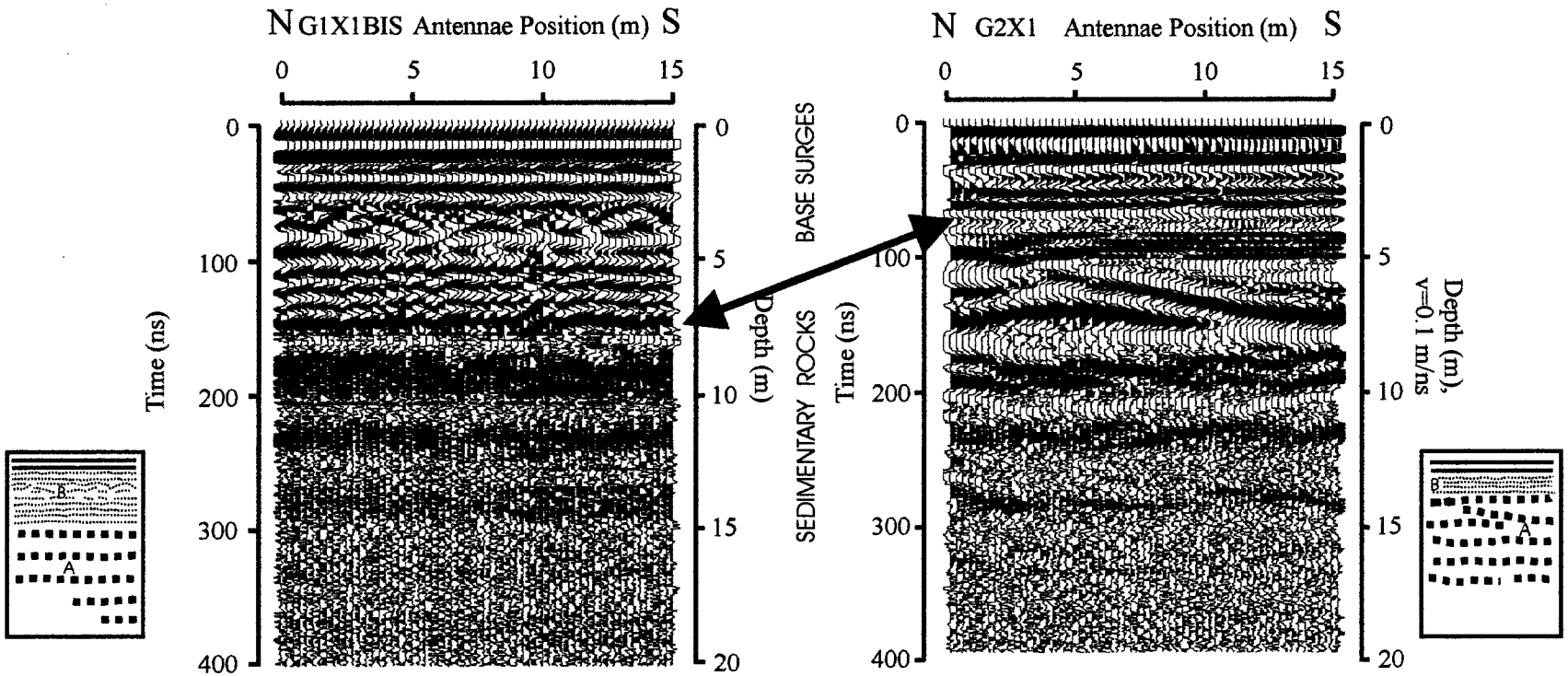

Fig. 2.8. Profiles G1X1BIS (proximal) and G2X1 (distal) were run with 100 MHz antennae. They show the base of the base surge deposits (arrows). The insets present the interpretation of the profile, where A stands for sedimentary rocks and B for base surges.

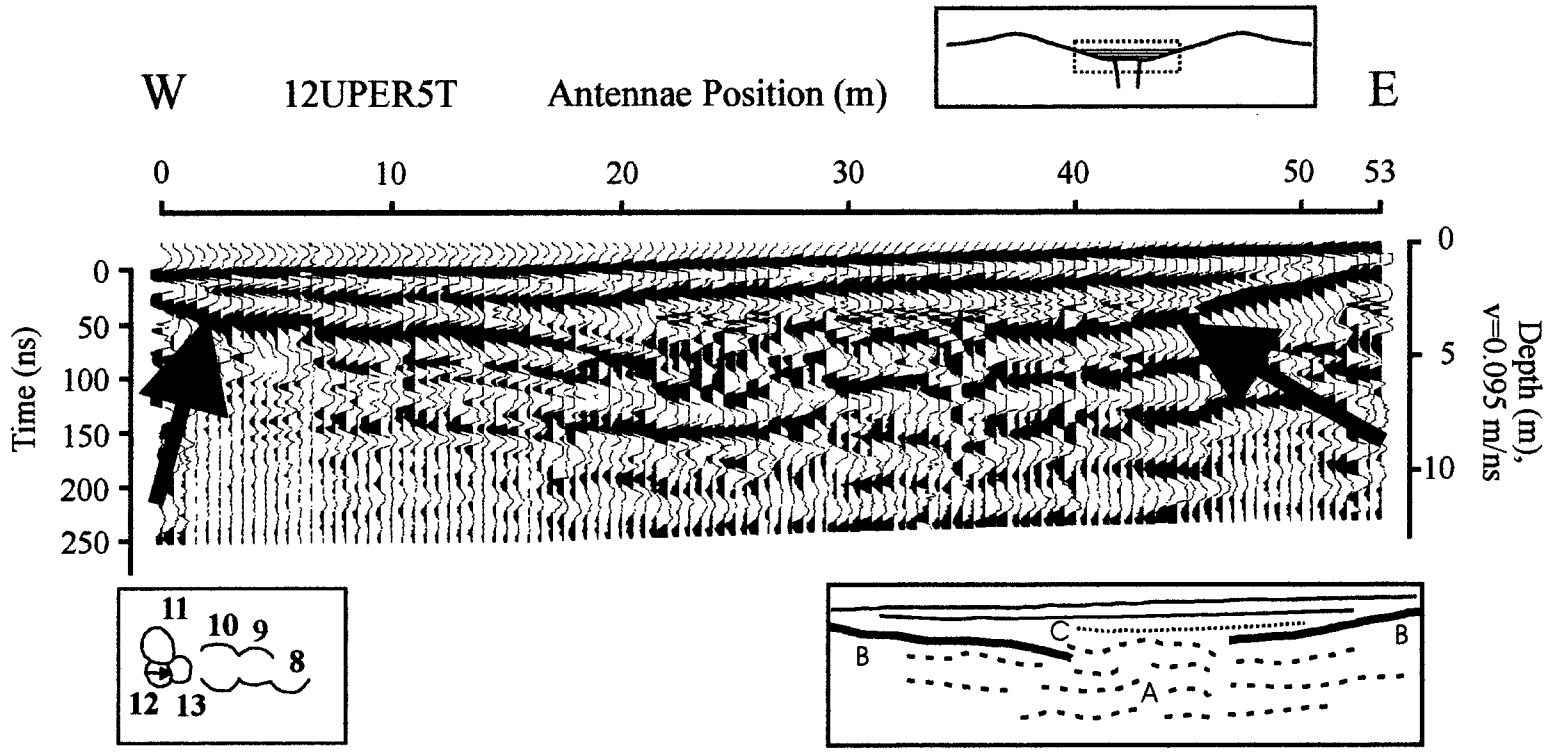

Fig. 2.9. GPR profile for Crater No. 12 obtained with 50 MHz antennae. Insets show field location of survey in the western crater cluster (lower left) and position of profile relative to cross-section through idealized crater (upper right). Lower right inset represents line diagram interpretation of the profile, which shows bowl shaped reflections B (arrows) and an angular unconformity between reflections B and C.

center of the profile are coincident and the orientation of the survey is shown in the figure. This profile was done with 50 MHz antennae and presents bowl-shaped reflections (B), which are disrupted in the center (discontinuous reflections A). An angular unconformity (onlap) between reflections B and C is also visible. Fig. 2.10 presents the radar profile run with higher frequency antennae (200 MHz) over the eastern margin of the same crater showing the unconformity between the reflections B and C with higher resolution.

2.4 Discussion

Common Mid Point (CMP) surveys

The Common Mid Point profiles, run with 50, 100 and 200 MHz antennae and shown in Fig. 2.3, present reflected waves, i.e. hyperbolas, which are well visible. The velocities suggested by the shallow reflections (0.095 – 0.1 m/ns) have been used to draw the vertical depth scale in the GPR profiles. The direct ground waves have not been used to evaluate the subsurface velocities, because they probably do not represent good average values for the bulk deposits.

Calibrations

Regarding the profiles CALIB5B and CALIB5, note that signals between 0 – 25 ns are caused by a combination of direct air and ground waves and that the GPR signals have penetrated deeper than the height of the outcrop. For this reason, only the central portion of the profile can be directly compared to the lower part of the exposure (Fig. 2.4). In spite of that, useful observations can be made. For example, a comparison between the GPR profiles

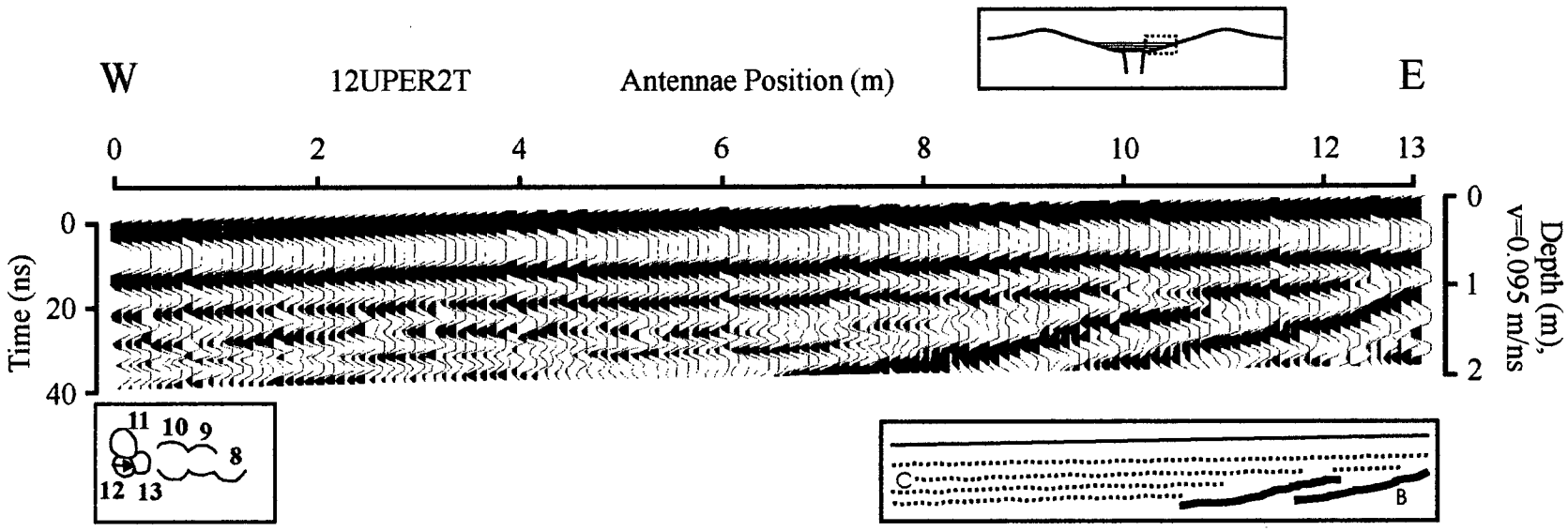

Fig. 2.10. GPR profile for Crater No. 12 with 200 MHz antennae. Insets show field location of survey in the western crater cluster (lower left) and position of profile relative to cross-section through idealized crater (upper right). This profile derives from the eastern edge of the crater. The lower right inset shows the angular unconformities between two sets of reflections labeled B and C.

and the correspondent outcrop (Fig. 2.4) shows that there are more discontinuities, beds and laminae, in the deposits than reflections in GPR profiles. This confirms that, even with the highest frequency antennae of our radar system (i.e. 200 MHz), the resolution is low and it is not possible to recognize the climbing dune-forms located in the lower left corner of the exposure. In the Ubehebe Craters area the climbing dune-forms have a maximum wave height of only 24 cm (Crowe and Fisher, 1973). It is also interesting that the two profiles CALIB5B and CALIB5, although only 1 m apart, are different, probably because of the relatively high lateral variability of these deposits.

The comparison between outcrop and profile CALIB6X1 (Fig. 2.5) suggests that features labeled A are reflections from the sandstones, which stratigraphically underlie the pyroclastic deposits. These reflections are deeper than the height of the outcrops, but the interpretation is consistent with Crowe and Fisher (1973), who suggest that sedimentary rocks are several hundred meters thick. The inclined reflection CO can be interpreted as the contact between the two lithologies. Its shape differs from that of the contact in the photograph, probably because of the typical lateral variability of these deposits (the surface of the outcrop and the profile are parallel but a few meters apart). The event G, with shorter wavelength, could be a reflection; however, it also may be the ground wave travelling through the top of the base surge deposits. Unfortunately, in this profile, most reflections from the base surge deposits (between 0 and 20-25 ns) are masked by air and ground waves, which probably affect also the reflection from the contact between sandstones and base surges. Furthermore, reflections from the contact between the surface of the outcrop and a small pile of rock debris (talus) in front of it may have disturbed the other events above the

base of the outcrop BO (Fig. 2.5). For this reason, the reflections A below the outcrop are probably the most reliable for calibration purposes of the sedimentary rocks.

GPR profiles of base surge deposits

Calibrations CALIB5B and CALIB5 also suggest that profile D1X2 (Fig. 2.6), located where no outcrops are available, presents reflections that are less numerous than the discontinuities in the deposit (horizontal laminae and beds). These discontinuities have an attitude that changes locally, forming wavy reflections, but the low resolution does not enable the recognition of the details. Here, probably only structures within the base surge deposits have been imaged, because they are almost 50 meters thick around the crater rim (Crowe and Fisher, 1973). Profile C3X2 (Fig. 2.7) presents angular unconformities between reflections H and the wavy reflections K. In this case, the unconformities can be explained by the fact that these kinds of deposits are thinner over palaeo-topographic highs and thicker over palaeo-topographic lows (Cas and Wright, 1987). At the top of the hill, the beds are thinner and the reflections disappear because of the low resolution, resulting in unconformities. The interpretation of the wavy reflectors K is more difficult. They may be due to beds deformed plastically under the influence of gravity on the slope of the hill (a typical feature of wet base surge deposits). Unfortunately the resolution is too low to be able to interpret these features reliably.

The results of calibration CALIB6X1 give insight for interpreting the GPR profiles in Fig. 2.8, located where no outcrops are available. In this case the reflections A have larger wavelength similar to those of profile CALIB6X1 and are probably due to the sedimentary rocks, whereas the upper reflections B have smaller wavelength and are probably caused by

the base surges. The presence of the base surge deposits is certain because their top constitutes the ground surface. In reality, the signal wavelengths of the events A in G1X1B are not exactly like those in G2X1, probably because of a different content of moisture or other variables (which are not always possible to identify clearly) in the rocks as well as along their stratigraphic contact. But these profiles certainly show a downward change in character, suggesting changes in the subsurface conditions (Reynolds, 1997). It is also true that, G1X1BIS is noisier (and maybe with multiples) than G2X1 and that this noise (boosted by the automatic gain control) affects the reflections A in G1X1BIS more than in G2X1. The two sets of reflections A and B form radar sequences which are the fundamental stratigraphic units identifiable in GPR profiles and define two genetically different packages of strata (Gawthorpe et al., 1993). Similar concepts apply to stratigraphic analysis of seismic data (Mitchum et al., 1977). The two different lithologies produce different radar response in the GPR profiles because they have two different compositions, textures and probably moisture content. The profiles in Fig. 2.8 also enable an assessment of the thickness of the base surge deposits: probably no more than 7 m in G1X1BIS (relatively proximal position) and 3-4 m in G2X1 (more distal).

GPR profiles of the craters

Fig. 2.9 shows an example of a profile run within one of the smaller and less recognizable crater. Here, the section of the bowl-shaped crater depression (reflections B) filled by alluvial material is well visible. In this case, the crater beds (reflections B) and the overlying horizontal alluvial deposits (reflections C) form an angular unconformity (onlap). The presence of the alluvium was verified by field inspection of the ground surface (there is

no soil in the area) and its maximum thickness can be estimated in the profile: probably no more than 4-5 meters. This estimate is limited by the fact that individual reflections in GPR profiles are not single spikes but wavelets comprising more than one peak (Robinson and Treitel, 1980; Daniels, 1996). The vent may be located where the underlying reflections A are disrupted in the center, although the vertical discontinuity between conduit and country rocks is not identifiable.

Profile 12UPER2T, run with 200 MHz antennae (Fig. 2.10), shows the onlap within the same crater, with more details and higher resolution. According to Gawthorpe et al. (1993) reflection terminations, where two reflectors converge to produce triple junctions (toplap, onlap or downlap) can indicate non-depositional hiatuses. These terminations identify radar sequence boundaries. In this case the two radar sequences are: 1) a lower one composed of the surge deposits and 2) an upper one composed of the alluvium.

2.5 Conclusions

Our results prove that in areas with simple stratigraphy, ground penetrating radar is useful in imaging shallow structures. In particular, ground penetrating radar permits evaluation of thickness of base surge deposits and alluvial material, although it can be difficult to identify precisely the position of the reflectors in the underground, because each reflection comprises more than one peak. Stratigraphic unconformities can also be imaged in the near subsurface. Furthermore, the location of small, eroded craters (which are filled by alluvium and difficult to recognize in the field) can be confirmed when bowl-shaped reflections are imaged, but the presence of conductive material, like clay, can strongly reduce the depth of penetration of the electromagnetic waves. Our data shows also that it is possible

to distinguish base surge deposits and the underlying sandstones, because they have different radar responses. It is important to bear in mind that ground penetrating radar antennae also receive signals reflected from features, which are not directly below them and for this reason a GPR profile cannot be considered a true geologic cross section. Regarding the study of the lateral facies variation, it is clear that the 200 MHz antennae have too little resolution to locate unexposed sandwaves in the subsurface and that higher frequency antennae are necessary.

CHAPTER III

GEOSTATISTICAL ANALYSIS OF GPR PROFILES

3.1 Introduction

Rea and Knight (1998) made geostatistical analysis of GPR profiles in order to characterize and quantify heterogeneities in the subsurface. The purpose of their analysis was to look for a characteristic GPR signature associated with specific depositional environments (Tercier et al., submitted). For example, they used the *range* of a semivariogram to quantify the continuity (and dip direction) of the reflections in GPR sections and consequently of the reflectors in the deposits (Knight et al., 1997). In this chapter, semivariograms of GPR profiles collected in the Ubehebe area have been computed and described to test this technique and characterize quantitatively the GPR images in order to study the lateral facies variation of the base surge deposits. The GPR data were collected using a PulseEKKO 100 instrument with 200 MHz antennae.

3.2 Geostatistics

Geostatistics deals with regionalized variables, that (unlike random variables) have continuity from point to points, but the changes are so complex that cannot be described by

any tractable deterministic function (Davis, 1986; Armstrong, 1998). In order to express the rate of change of a regionalized variable along a specific direction, a parameter called semivariance is estimated for distances that are multiples of the spacing Δ between samples. The semivariance is the sum of the squared differences between pairs of points separated by the distance Δh, i.e.

$$\gamma_h = \sum_i^{n-h} (X_i - X_{i+h})^2 / (n-h),$$

where X_i is a measurement of a regionalized variable taken at location i and X_{i+h} is another measurement taken h intervals away (Davis, 1986; Armstrong, 1998). The number of points is n and the number of comparisons between pairs of points is n-h.

The plot of the semivariances versus the different values of h is called semivariogram. When Δh is a small distance, the semivariance is a small value because the points we are comparing are very similar. When the distance Δh is increased, the points being compared are less and less closely related to each other and their differences become larger, resulting in larger values of the semivariance. At some distance the points being compared are so far apart that they are not related to each other. In this case, their squared differences become equal in magnitude to the variance around the average value. The *range* of the regionalized variable is the distance at which the semivariance approaches the variance. In this case the semivariance no longer increases and the semivariogram develops a flat region called *sill*.

Usually the discrete, experimental semivariograms are modeled by a continuous function evaluated at any distance (Clark, 1979). For example, the exponential model is:

$$\gamma(h) = c\left[1 - \exp\left(-\frac{3h}{a}\right)\right],$$

where c is the sill and a is the range. Furthermore, a semivariogram is said to present a *hole effect* whenever its growth is not monotonic but presents peaks and valley, i.e. holes (Journel and Froidevaux, 1982). The *hole effect* suggests that data separated by larger distances are actually more similar than closer ones (Isaaks and Srivastava, 1989). The *hole effect* is modeled by:

$$\lambda(h) = c\left\{1 - \left[\left(\exp - \frac{h}{\delta}\right)\cos\frac{2\pi h}{\lambda}\right]\right\},$$

where δ is a factor to model the damping of the *hole effect* amplitude with increasing lag and λ is the *hole effect* wavelength (Journel and Froidevaux, 1982). Finally, when a semivariogram is said to show a *nugget effect*, it means that does not go through the origin but assume some nonzero value for h equals to zero (Journel and Froidevaux, 1982). Any linear combination of models (called nested models) is permitted.

3.3 Geostatistical analysis: method and results

Semivariograms of GPR profiles collected in the Ubehebe area with 200 MHz antennae have been computed using the software package GSWIN (developed by Scullard, Knight and co-workers at UBC). This software enables the selection of a window within a GPR profile, where the semivariogram is computed using the amplitude values of the radar traces. An automatic gain control (AGC) was first applied to the data to correct for the violation of stationarity due to the decay of amplitude down the trace (Rea and Knight, 1998).

Fig. 3.1 presents three semivariograms of GPR profiles collected with 200 MHz antennae along line A (profiles A1X2 and A6X2) and line B (profile B1X2). The map in Fig. 2.1 shows the location of these lines in the Ubehebe hydrovolcanic field. The windows

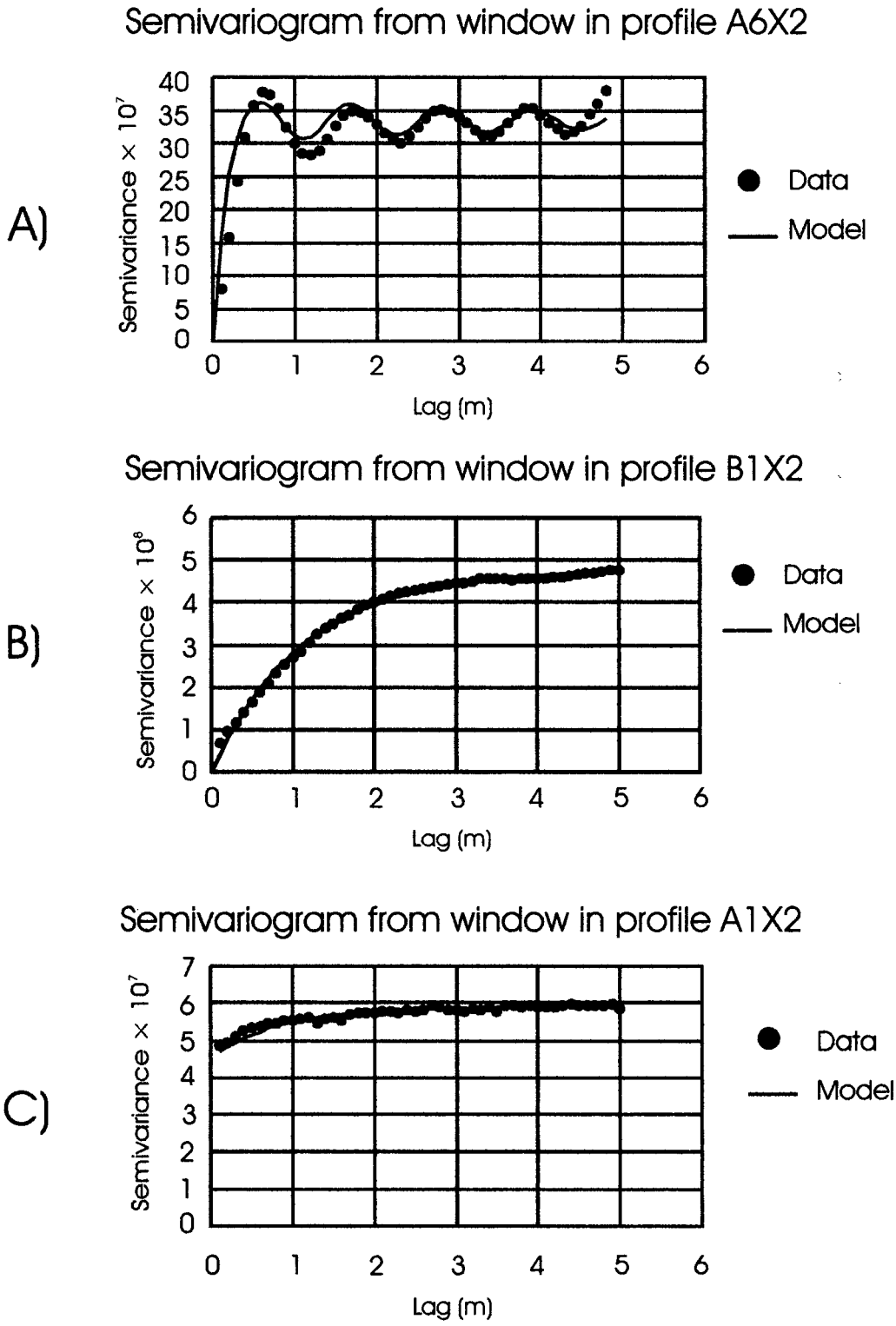

Fig. 3.1. Semivariograms from profiles A6X2, B1X2, A1X2 (computed along the horizontal direction). In plot A, an exponential model plus an hole effect fit the experimental semivariogram, in plot B the model is an exponential one, in plot C an exponential model plus a nugget effect fit the experimental semivariogram.

selected for the calculations are shown in Fig. 3.2, 3.3 and 3.4. These windows are narrow along the time axis in order to select only a specific radar texture. The semivariograms have been computed along the horizontal direction, because the deposits are composed of sub-horizontal beds and laminae. Finally, a model equation has been fitted to the experimental semivariogram.

The semivariogram in Fig. 3.1a has been computed selecting a window in the central part of profile A6X2 (Fig. 3.2). This semivariogram shows a combination of a *hole effect* (with a wavelength equals to 1.12 m) and an exponential model (with range equals to 0.4 m). The semivariogram in Fig 3.1b has been computed selecting a window in the central part of profile B1X2 (Fig. 3.3). This experimental semivariogram is well fitted by an exponential model with range equal to 3.38 m. The semivariogram in Fig 3.1c has been computed selecting events in the lower part of profile A1X2 (Fig. 3.4). In this case, an exponential model plus a *nugget effect* fit well the experimental semivariogram.

3.4 Discussion

The semivariogram in Fig. 3.1a presents a well visible *hole effect* and shows the capability of geostatistical analysis to highlight the presence of periodicity in the data set. The wavelength of the oscillation of the *hole effect* can be considered approximately equal to the wavelength of the cycles in the data (Rea and Knight, 1998). In Fig. 3.1a the wavelength of the *hole effect* is 1.12 m. This value is close to the wavelength of the sandwaves in the Ubehebe area (Crowe and Fisher, 1973) and the wavy reflections in the GPR profile could be images of climbing dune-forms, although the low resolution of the 200 MHz antennae does not enable a reliable interpretation.

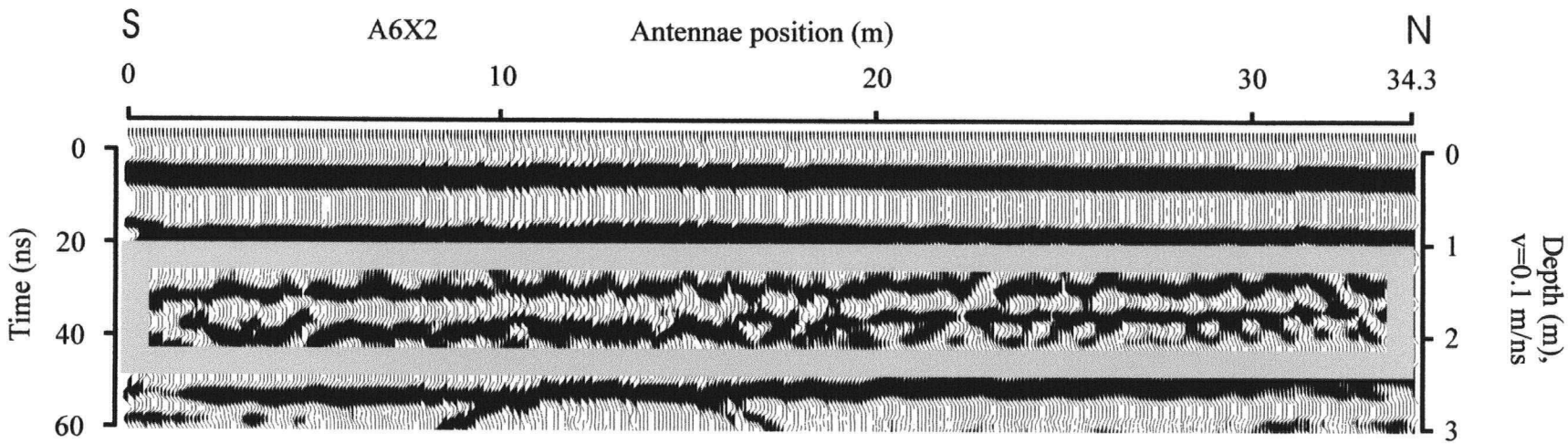

Fig. 3.2. Profile A6X2. The rectangle shows the portion of the data, which has been used to compute the semivariogram.

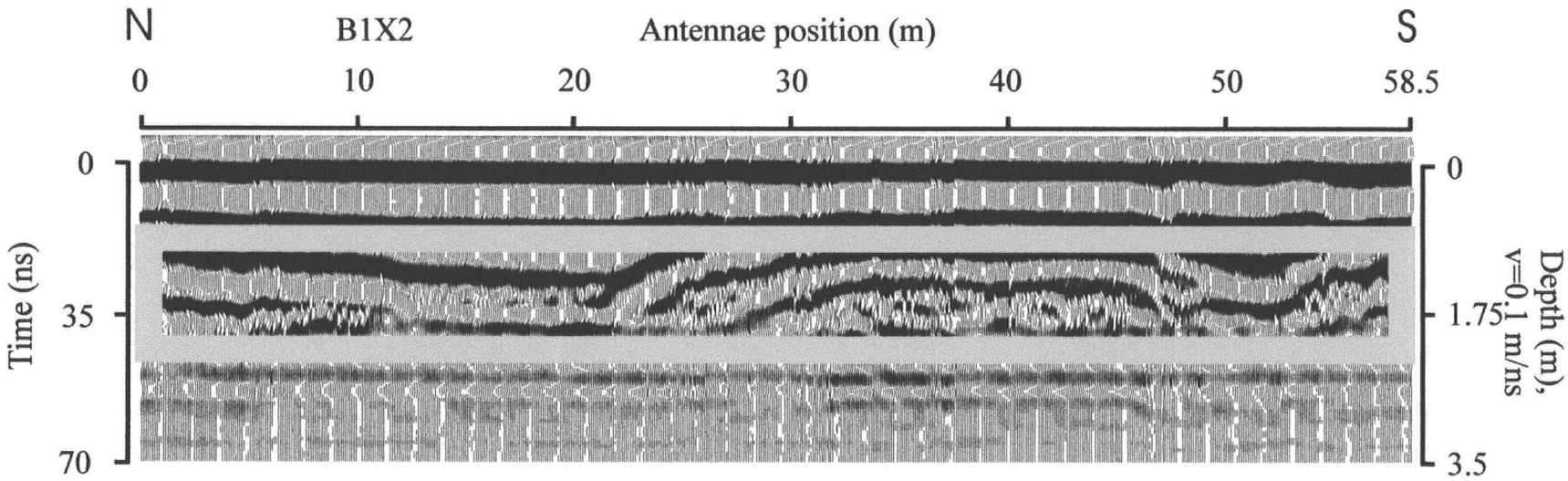

Fig. 3.3. Profile B1X2. The rectangle shows the portion of the data, that has been used to compute the semivariogram.

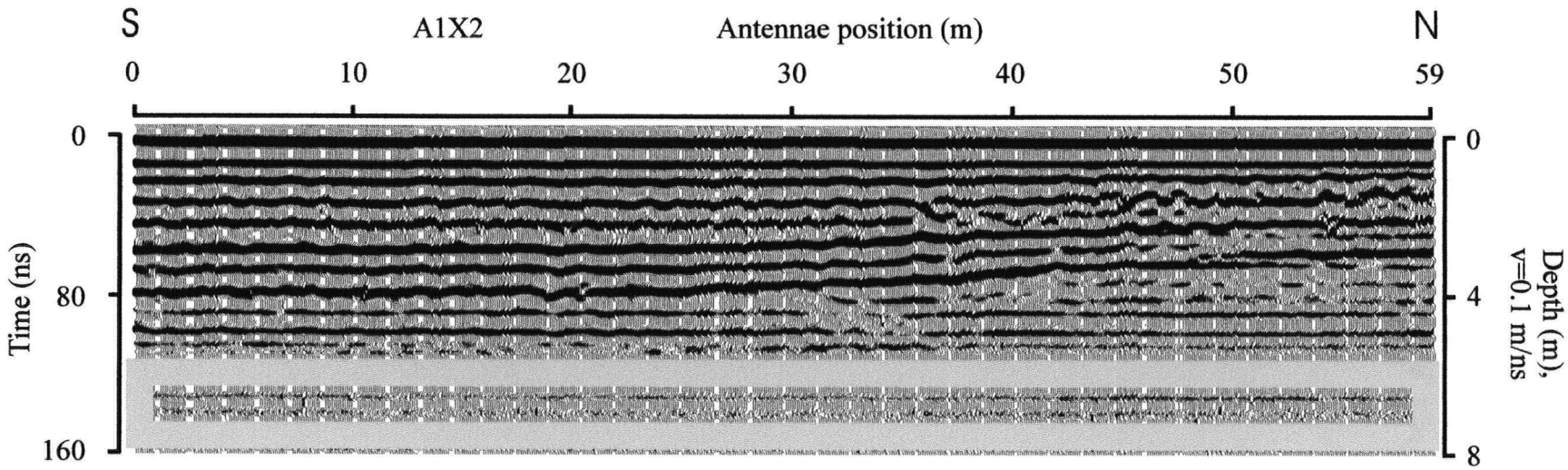

Fig. 3.4. Profile A1X2. The rectangle shows the portion of the data, that has been used to compute the semivariogram.

The semivariogram in Fig. 1b does not present the *hole effect*, suggesting a lack of periodicity in the data set (i.e. no climbing dune-forms in the deposits). This agrees with the fact that profile B1X2 is located in distal position where only plane parallel laminated beds are visible in the nearby outcrops along the wash. On the other hand, the *nugget effect* shown in Fig. 1c is due to nearby values, which are erratic (Davis, 1986; Isaaks and Srivastava, 1989). Finally, I have not used the *range* of the semivariograms to quantify the linear continuity of the reflections (as in Rea and Knight, 1998), because, in these profiles, most of the reflections are continuous and sub-horizontal along their entire length.

CHAPTER IV

Unshielded antennae and vertical resolution

4.1 Introduction

The purpose of this chapter is to describe a simple field experiment to assess the presence of artifacts related to console and computer position in GPR profiles collected with unshielded antennae. These artifacts can be underestimated in radar profiles, but can potentially affect the results of data processing such as a numerical comparison of the traces. An evaluation of the theoretical vertical resolution of different antennae frequencies is also shown. These considerations are necessary to select an appropriate radar system to study the lateral facies variation of base surge deposits in the Ubehebe hydrovolcanic field.

4.2 Experiment to evaluate artifacts related to console-computer position

This experiment has been carried out using a PulseEKKO 100 system with 200 MHz antennae (which are unshielded) and consists in keeping the antennae always in the same position, while console and computer have been moved back and forward, but gradually away from the antennae (the distance ranges from 5 to 10 m). At each console position, ten traces were collected. Fig. 4.1 shows the generated GPR profile.

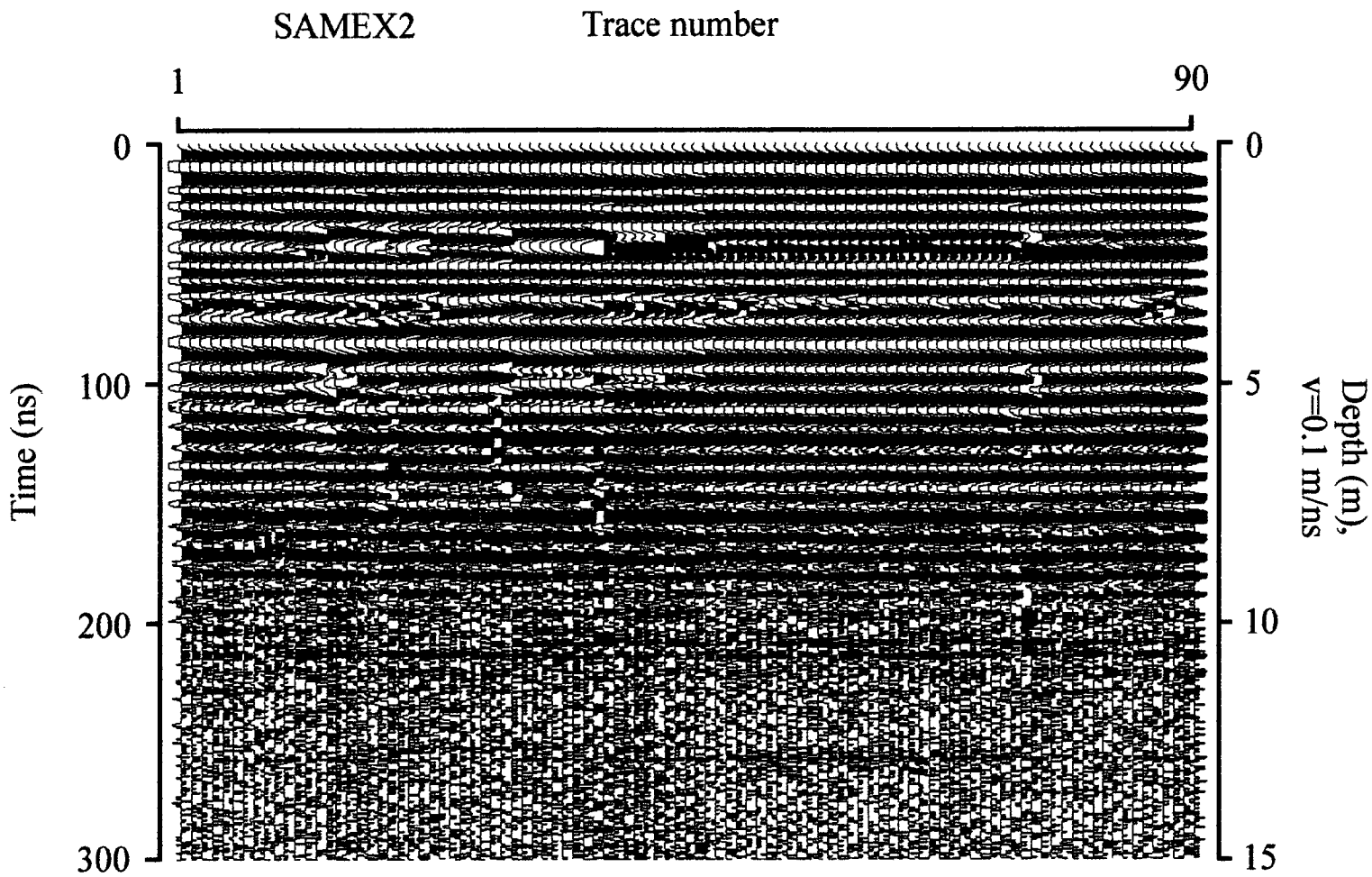

Fig.4.1. Profile SameX2 obtained with 200 MHz antennae, which have been kept in the same position while console and computer have been moved to different locations.

In order to compare the traces of this GPR profile, their average square of the sample points (x) has been computed, i.e.

$$\frac{1}{N}\sum_{1}^{N} x_k^2 ,$$

where 1<k<N and N is the number of sample points. The upper part of each trace has been clipped to eliminate ground and air waves and only the time window between 30 and 100 ns has been used. These calculations were performed using MATLAB® routines. A signal saturation filter (dewow) was applied to the profiles, but no automatic gain control (AGC) to avoid possible data distortion. This parameter is plotted in Fig. 4.2 and the overlapping traces of the GPR profiles are shown in Fig. 4.3.

4.3 Vertical resolution

Table 4.1 shows the theoretical vertical resolution of different antenna frequencies computed following Reynolds (1997). The theoretical vertical resolution is considered to be equal to one-quarter of the wavelength (Reynolds, 1997), and, for example, in a medium where the velocity v of the electromagnetic waves is equal to 0.1 m/ns, the wavelengths λ of 200, 100 and 50 MHz signals are 0.5, 1 and 2 m respectively. The wavelengths have been computed from $v = \lambda f$, where f is the frequency.

4.4 Discussion

Only small differences between the traces are discernible in profile SAMEX2 (Fig. 4.1), but these differences become more visible in the plot of the average square of the sample points (Fig. 4.2). These differences cannot be due to the subsurface geology, because the

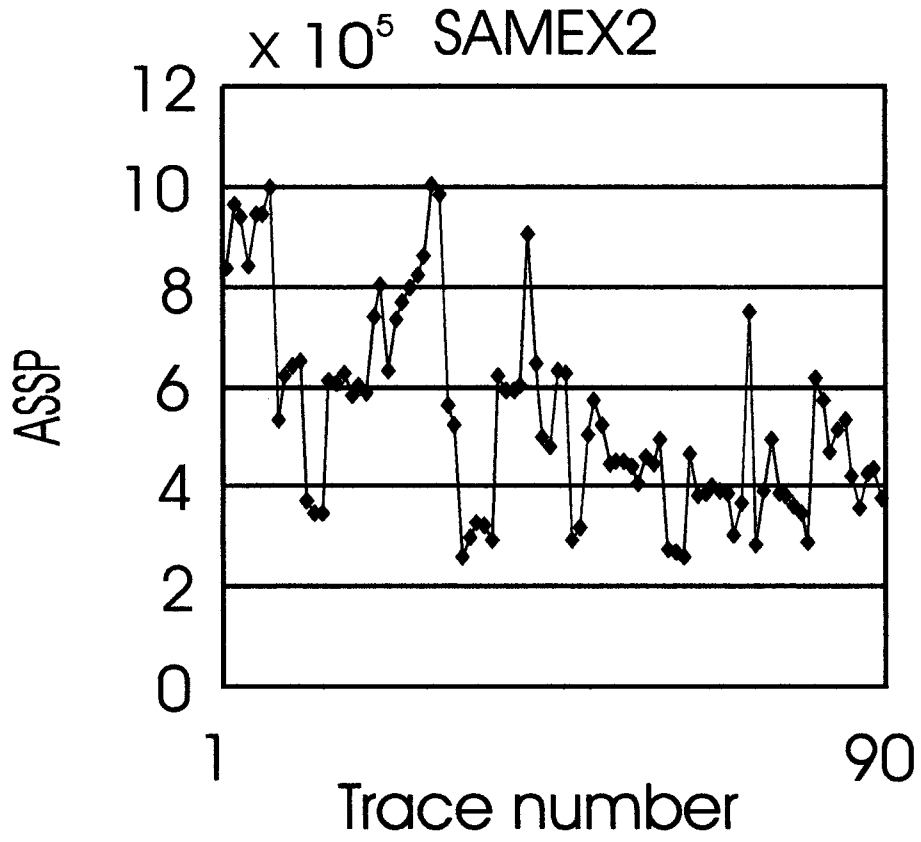

Fig. 4.2. Average square of the sample points (ASSP) of the traces in profile SameX2.

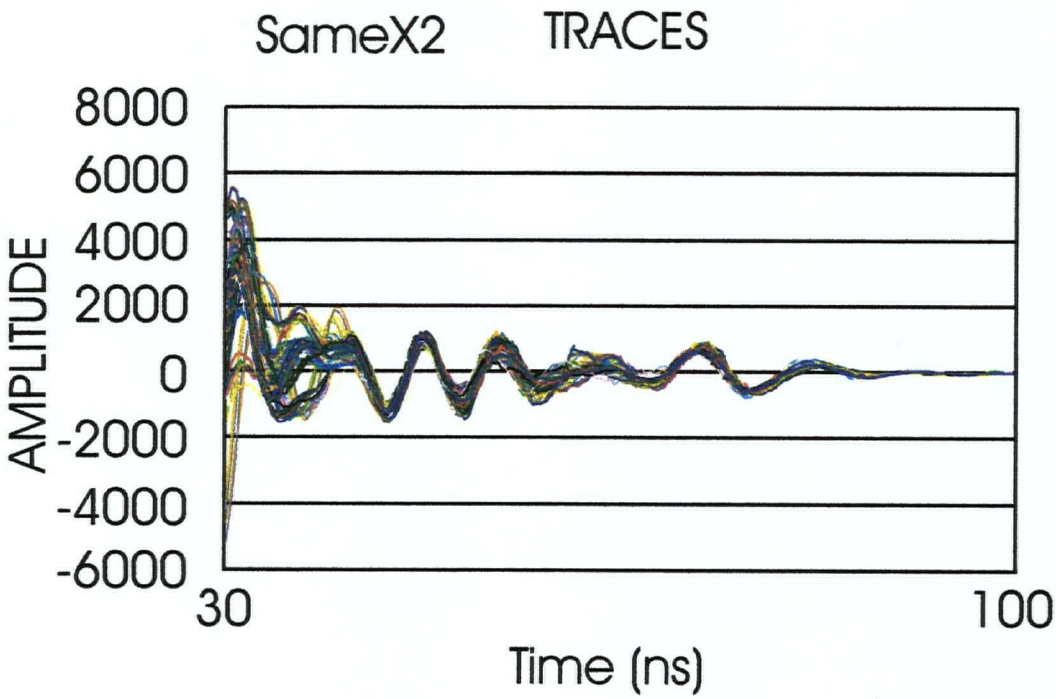

Fig. 4.3. Overlapping traces of profile SAMEX2.

antennae have been kept always in the same position. The decrease of the average square of the sample points (when the distance between antennae and console increases) suggest that the artifacts are probably due to the computer and the cable connecting computer and console, which are strong sources of radio frequency noise (Sensors and Software, 1996). This decrease does not appear regular, because, console and computer have been moved back and forward although gradually away from the antennae. It is important to stress that these artifacts can be easily ignored in a GPR profile and for this reason similar experiments should always be carried out to establish the presence and magnitude of undesired components in the data.

Is it really possible to image climbing dune-forms using ground penetrating radar? Their average height in the Ubehebe area is about 12 cm, ranging from 24 to about 3 cm (Crowe and Fisher, 1973). The 200 MHz antennae have a resolution that is quite close to this wave height (Table 4.1), but the true resolution can be much smaller than the theoretical one. It is important to remember that field evidence suggests that it is unlikely to find vertical sequences of climbing dune-forms (Chapter 1, paragraph 6). If we want to locate them we need antennae with frequency higher than 200 MHz.

4.5 Conclusion

As stated in Chapter 1, the purpose of my research projects is the study of the lateral facies variation of base surge deposits using ground penetrating radar. This encompasses, for example, the location of the climbing dune-forms in the subsurface and a numerical comparison of the traces collected at different distances from the vent. In order to pursue this project, I believe that it is not appropriate to use unshielded antennae, because of the possible

Table 4.1. Theoretical vertical resolution[a] of different antennae frequencies.

Frequency MHz	Wavelength m	Resolution m
10	10	2.5
12.5	8	2
25	4	1
50	2	0.5
100	1	0.25
110	0.91	0.23
200	0.50	0.13
225	0.44	0.11
400	0.25	0.06
450	0.22	0.06
500	0.20	0.05
900	0.11	0.03
1000	0.10	0.03
1200	0.08	0.02

[a] The theoretical vertical resolution is equal to ¼ of the wavelength (Reynolds, 1997). The wavelength λ has been computed from $v = \lambda f$, where v is the electromagnetic wave velocity equal to 0.1 m/ns and f is the frequency.

presence of artifacts related to the console and computer position (or even reflections from object situated above the ground surface, see Appendix II). Furthermore, the location of sandwaves, which are relatively small in the Ubehebe area, requires frequencies higher than 200 MHz. Unfortunately, the PulseEKKO 100 instrument can only make use of unshielded antennae with frequency smaller or equal to 200 MHz. The GPR profiles collected with this instrument show efficiently the major subsurface discontinuities (Chapter 2), but they are not suitable to highlight small differences between the traces. An instrument with shielded and higher frequency antennae must be used (for example the PulseEKKO 1000).

CHAPTER V

Ground penetrating radar images of unexposed climbing dune-forms

5.1 Introduction

The purpose of the research presented in this chapter is to locate unexposed climbing dune-forms in the base surge deposits of the Ubehebe hydrovolcanic field using high frequency ground penetrating radar surveys. Base surge beds display three facies, called respectively sandwave, planar and massive (Fisher and Schmincke, 1984; Cas and Wright, 1988). The term sandwave is applied to beds with climbing dune-forms, undulating surfaces and internal cross lamination. The planar facies consist of plane-parallel beds and laminae with upper and lower contacts generally planar and parallel to one another. Massive beds are without internal organization of the fragments and are thicker than the beds of the other two facies. In this thesis the terms "sandwaves" and "climbing dune-forms" are used interchangeably. The localization of the climbing dune-forms with respect to the vent position is important to formulate lateral facies variation models of these deposits. These models are necessary to understand the transport and emplacement mechanisms of base surges.

I want to stress here that because of the violent nature of their eruptions and the high speed and temperature of the flows it is impossible to study base surge transport and

depositional processes directly. To understand their flow mechanism and predict their behavior we must study their deposits. Unfortunately, such a study is usually restricted to just the few outcrops available in the field, but a continuous outcrop from the most proximal to the most distal locations is not available in the northern sector of the Ubehebe area. This is the sector where the deposits reach the largest distance from the crater and where there are more chances to find a complete lateral facies sequence, because the deposits are not covered by alluvial fans. The lack of outcrops makes the study of the lateral facies variation more difficult, but GPR can provide valuable, additional information supplementing traditional geologic surveys. Unfortunately the use of relatively low frequency antennae (50, 100 and 200 MHz) prevented the identification of the climbing dune-forms in Chapter 2.

5.2 Field observations

The vertical exposures of the base surge deposits have been carefully examined to place the radar profiles in a known geologic context. These outcrops are concentrated in the gullies nearby the Ubehebe Crater (mostly east, south and only a few of them west of the crater). North of the Ubehebe Crater, there are virtually no outcrops with the exception of the few exposures along the wash and some along the paved road (Fig. 5.1). A couple of field observations are particularly useful to complete the GPR survey. First, there are beds showing massive facies or coarse tail reverse grading (with grain size ranging from ash to blocks up to 15 cm in diameter) along the southwest rim of the Ubehebe Crater (Fig. 5.2). Proximal massive deposits indicate a quick emplacement by high concentration flow, whereas inverse grading suggests shear stresses and dispersive pressure

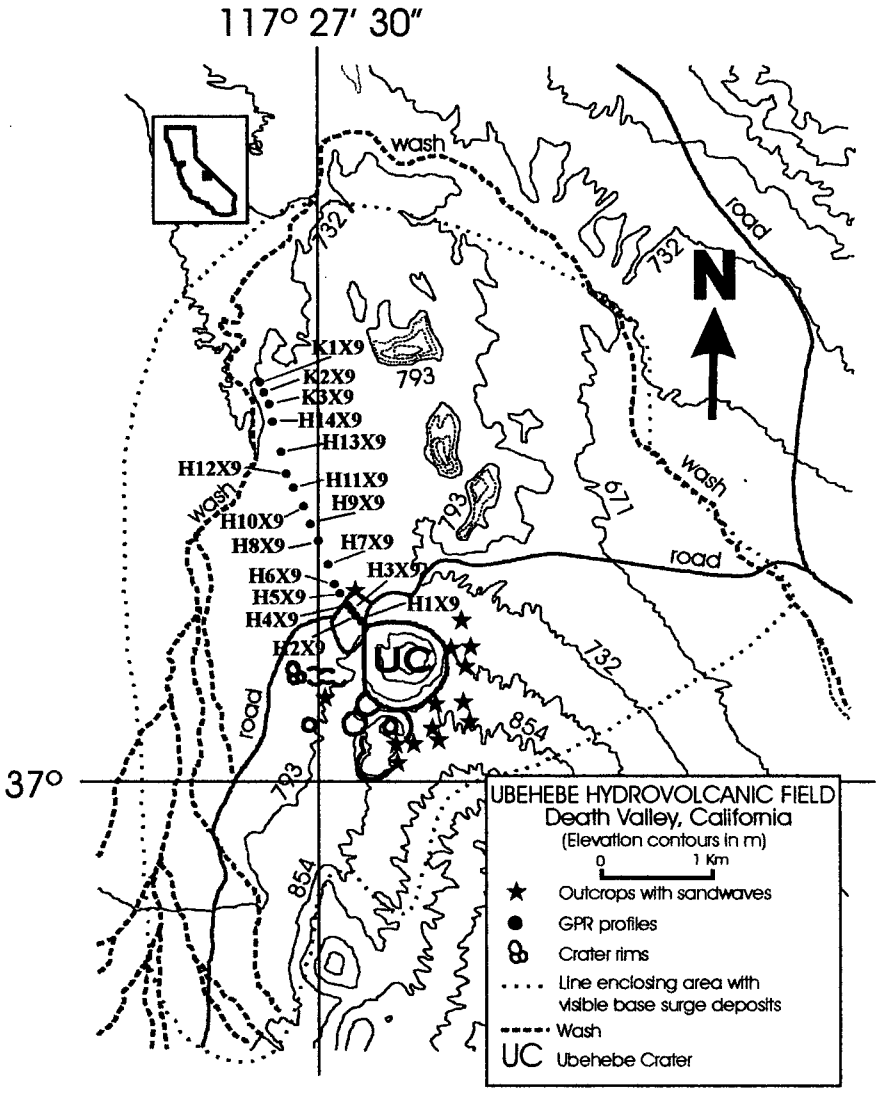

Fig. 5.1. Map of the Ubehebe hydrovolcanic field with positions of the GPR profiles. UC stands for Ubehebe Crater, the largest one. The inset to the upper left shows map location within California.

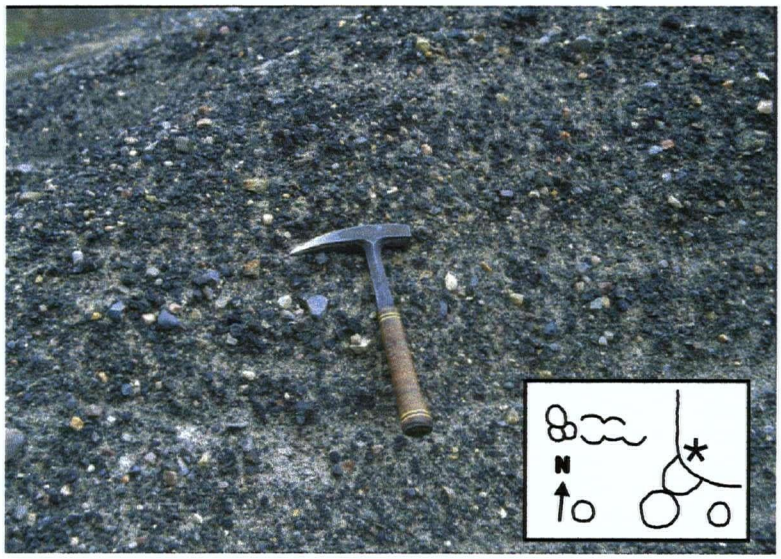

Fig. 5.2. Field photograph of deposits from outcrop on rim of Ubehebe Crater. The inset shows the position of the exposure (asterisk) in the crater cluster. The deposit comprises juvenile and accessory fragments and is massive. The grain size ranges from ash to lapilli.

in high concentration flow (Chough and Sohn, 1990). Second, I have recorded with a GPS unit the positions of the climbing dune-forms visible in the outcrops (stars in Fig. 5.1).

5.3 Data collection and data presentation

All radar data have been collected using the ground penetrating radar PulseEKKO 1000 (manufactured by Sensors and Software Inc.) that makes use of a 200 V transmitter. A field computer Husky FC-486 has been used to control the radar system. All GPR surveys have been carried out using 900 MHz antennae with a step size equal to 2 cm, antennae separation equal to 17 cm and 32 stacks. The number of stacks is the number of traces collected at each survey position that has been averaged to increase the signal to noise ratio. Radar profiles are displayed after applying a signal saturation correction filter (dewow) and an automatic gain control (AGC). Data were processed using the PulseEKKO© software (Sensors and Software Inc.). In all radar profiles the position of the antennae is represented along the horizontal axis and the two-way signal travel time is along the vertical axis. All profiles have no vertical exaggeration. The locations of the data described in the text are shown in Fig. 5.1.

5.4 GPR profiles: method and results

Common Mid-Point (CMP) surveys

Several CMP experiments have been carried out using 900 MHz antennae. Fig. 5.3 shows an example collected in the same location of profile H1X9. The hyperbolas suggest a subsurface velocity of the reflected electromagnetic waves equal to 0.12 m/ns. This value has

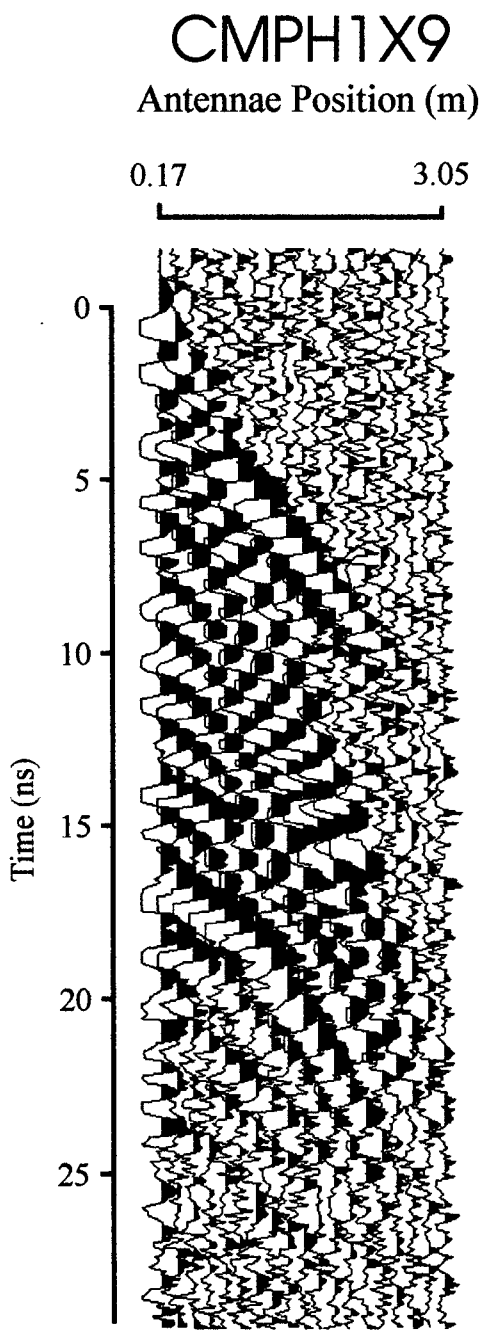

Fig. 5.3. Common Mid Point (CMP) profile collected with 900 MHz antennae in the same location of H1X9. The hyperbolas suggest a subsurface velocity of the reflected electromagnetic waves equal to 0.12 m/ns.

been computed using the software Gradix© (Interpex) and used to draw the vertical depth scale in GPR profiles.

GPR Profiles

The GPR profiles have been collected in the northern part of the hydrovolcanic field downhill from, and along a direction radial to, Ubehebe Crater (Fig. 5.1). These profiles are situated in the central part of the northern valley, where the base surge deposits are probably thicker and less disturbed by an irregular paleotopography. They are also positioned to avoid small hillocks that probably correspond to paleotopographic highs. These highs could have disturbed the regular flow of the turbulent base surges affecting the characteristics of the deposits (Valentine, 1987).

During the surveys, the antennae have always been in contact with the top of the base surge deposits (Strand, 1967), because there is no soil in the area and the top of the deposits forms the ground surface. Furthermore, the data have been collected at the end of the hot season (summer) and there was no evidence of moisture (i.e. the imaged deposits were dry). The presence of water would have affected the radar data. The salient features of the GPR profiles are highlighted below (a side view of the figures is recommended to better recognize the geometry of the reflections).

(a) Profile H1X9 (Fig. 5.4) shows two sets of horizontal, wavy reflections labeled A and B, which are characterized by the presence of shorter reflections below the crests. The lower set has particularly well visible crests. The reflections in this profile are subhorizontal and subparallel. This profile is the most proximal and is located approximately 550 m from the

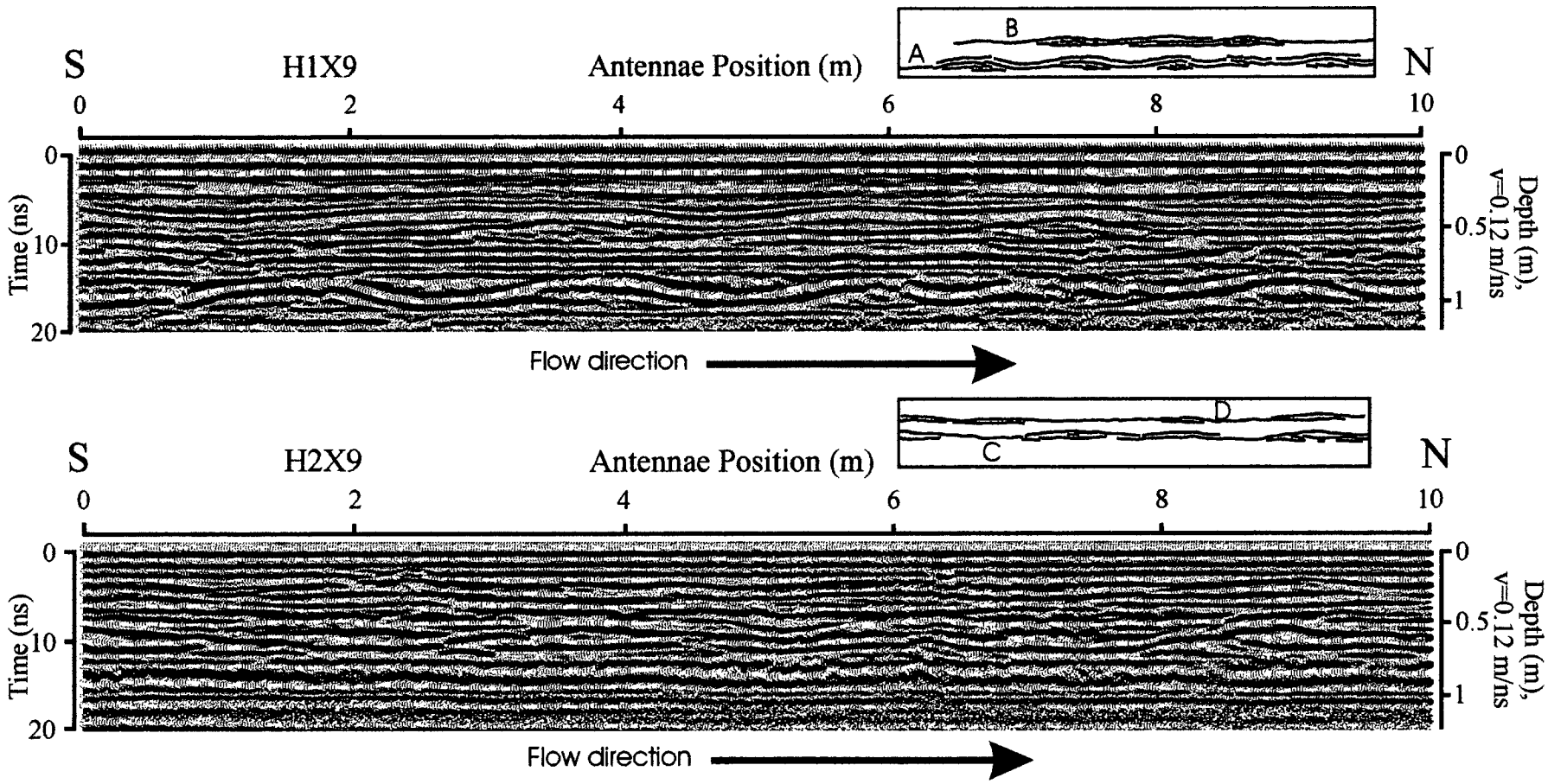

Fig. 5.4. GPR profiles H1X9 and H2X9 collected with 900 MHz antennae. The insets show the position of the sets of wavy reflections. Note the short reflections below the crests.

center of the Ubehebe Crater (Fig. 5.1). The GPR profile in Fig. 5.5 is a close-up of the leftmost crest of the lower set of wavy reflections.

(b) Profile H2X9 (Fig. 5.4) shows a set of horizontal, wavy reflections (labeled C) with shorter reflections below the crests. A second set (D) of wavy reflections may be located in the upper part of the profile. The reflections in this profile are subhorizontal and subparallel.

(c) Profile H3X9 (Fig. 5.6) shows two sets of horizontal, wavy reflections (E and F) with shorter reflections below the crests. The reflections in this profile are subhorizontal, and subparallel.

(d) Profile H4X9 (Fig. 5.6) shows two sets (G and H) of horizontal, wavy reflections with shorter reflections below the crests. The reflections in this profile are subhorizontal and subparallel.

(e) Profile H5X9 (Fig. 5.7) shows two sets (I and J) of horizontal, wavy reflections with other reflections immediately below the crests. The wave heights are smaller than those in the more proximal profiles. The reflections in this profile are subhorizontal and subparallel.

(f) Profile H6X9 (Fig. 5.7) has two sets of horizontal, wavy reflections (K and L) with reflections below the crests. The wave heights are smaller than those in the more proximal profiles. The reflections in H6X9 are subhorizontal and subparallel. This profile is located about 900 m from the center of Ubehebe Crater (Fig. 5.1).

(g) Profile H7X9 (Fig. 5.8) shows one set (M) of horizontal and slightly wavy reflections with shorter reflections below the crests, but their identification is uncertain because the wave heights are small. Other wavy reflections are located in the lower portion of the profile. The reflections in this profile are subhorizontal and subparallel.

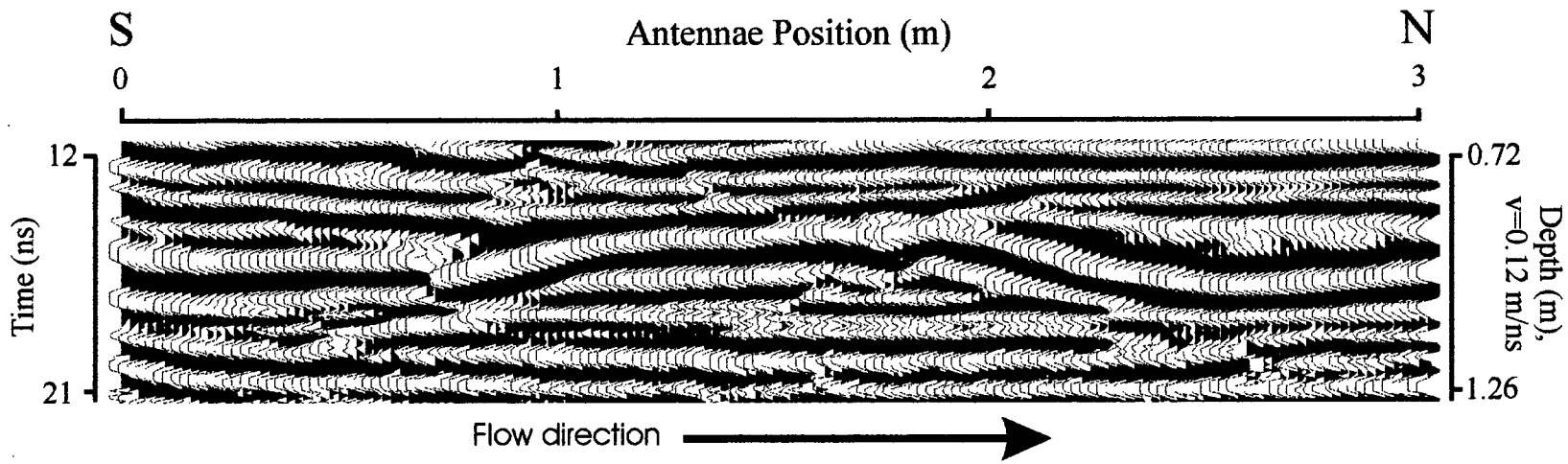

Fig. 5.5. Close-up of the leftmost crest of the set A of wavy reflections in profile H1X9.

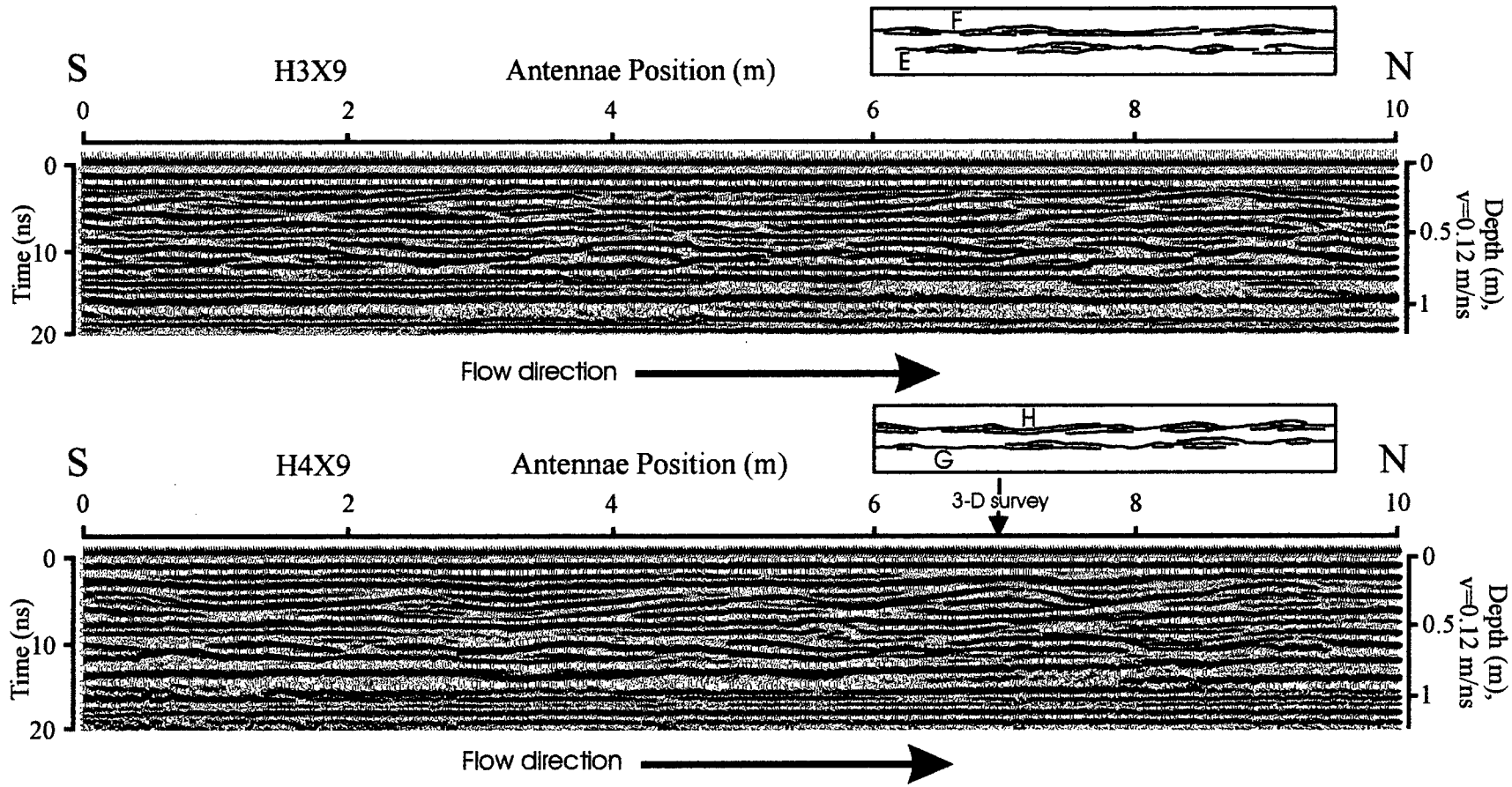

Fig. 5.6. GPR profiles H3X9 and H4X9 collected with 900 MHz antennae. The insets show the position of the sets of wavy reflections. The vertical arrow in H4X9 indicates the location of the 3-D survey.

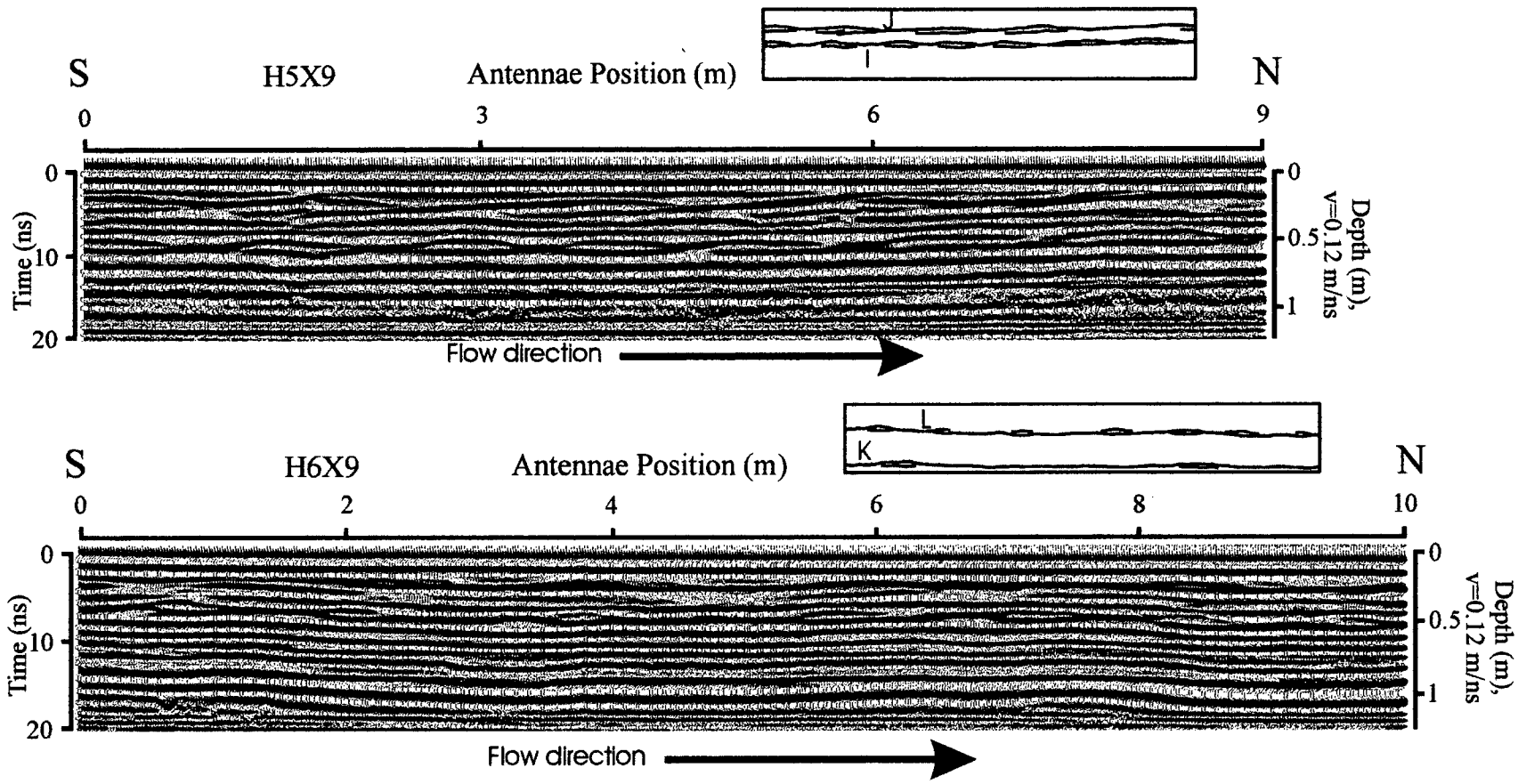

Fig. 5.7. GPR profiles H5X9 and H6X9 obtained with 900 MHz antennae. The insets show the position of the sets of wavy reflections.

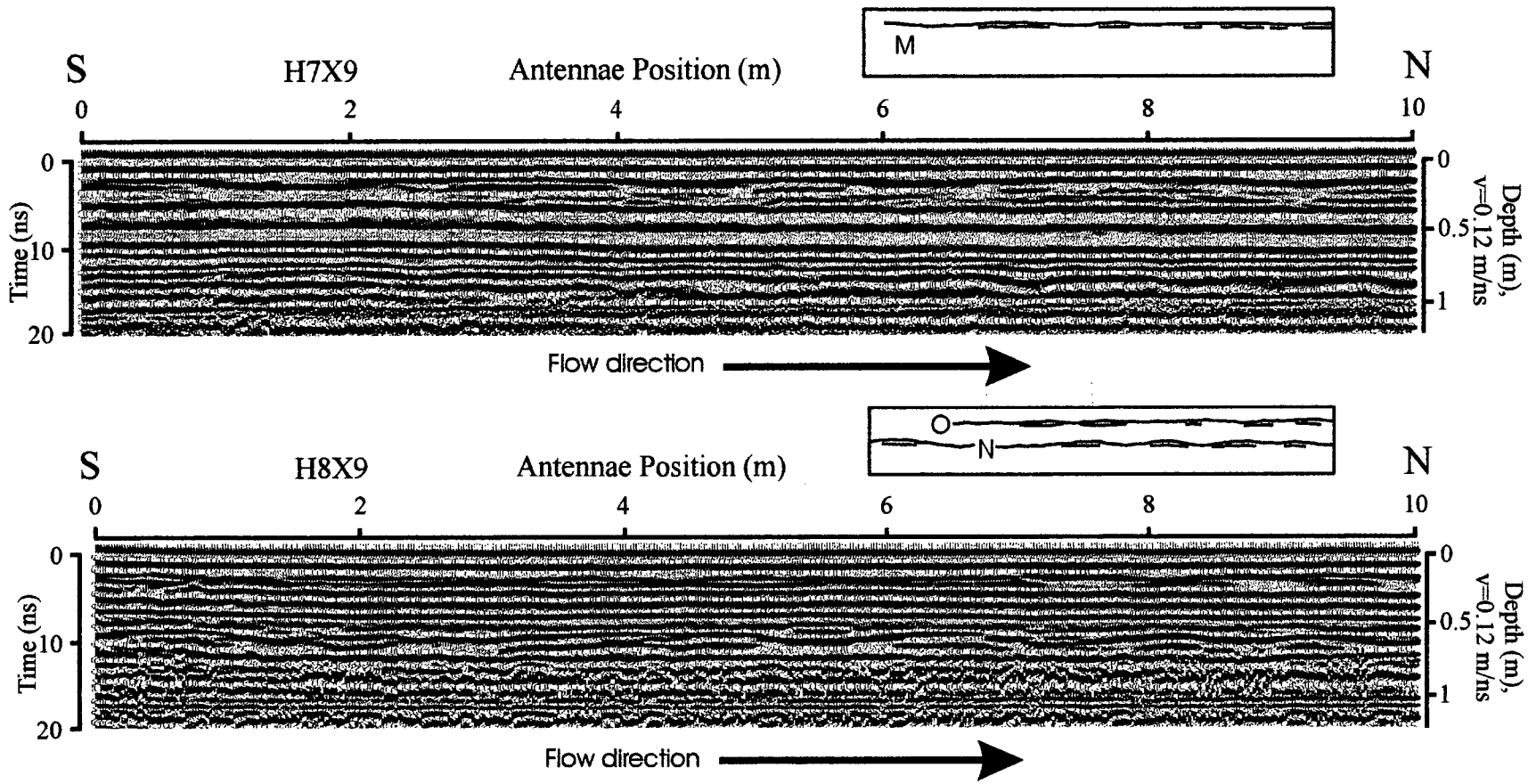

Fig. 5.8. GPR profiles H7X9 and H8X9 collected with 900 MHz antennae. The insets show the position of the sets of wavy reflections.

(h) Profile H8X9 (Fig. 5.8) shows a set (N) of horizontal, wavy reflections with shorter reflections below the crests. An upper set O has smaller wave heights and it is not easily visible. The reflections in this profile are subhorizontal and subparallel. In the lower portion of the profile the reflections are slightly disrupted.

(i) Profile H9X9 (Fig. 5.9) shows one set (P) of horizontal, wavy reflections with shorter reflections below the crests. The reflections in this profile are subhorizontal and subparallel and in the lower portion are slightly disrupted. This profile is located 1500 m from the center of the Ubehebe Crater. A trench was dug in correspondence to one of the crests to study the geometry of the laminations in the subsurface. Fig. 5.10 shows a climbing dune-form exposed within the trench.

(j) Profile H10X9 (Fig. 5.9) shows one set (Q) of horizontal, wavy reflections with shorter reflections below the crests. The reflections in this radargram are subhorizontal, and subparallel and become slightly disrupted in the lower part.

(k) Profile H11X9 (Fig. 5.11) shows one set (R) of horizontal, wavy reflections with shorter reflections below the crests. The reflections in this profile are subhorizontal and subparallel and slightly disrupted in the lower portion.

(l) In profile H12X9 (Fig. 5.11), the reflections are subhorizontal and subparallel. Slightly wavy reflections are labeled S. Others disrupted and slightly wavy reflections are visible in the lower part of the profile.

(m) In profile H13X9 (Fig. 5.12) the reflections are subhorizontal and subparallel. Some reflections are discontinuous or slightly wavy (for example those shown by the arrows in Fig. 5.12).

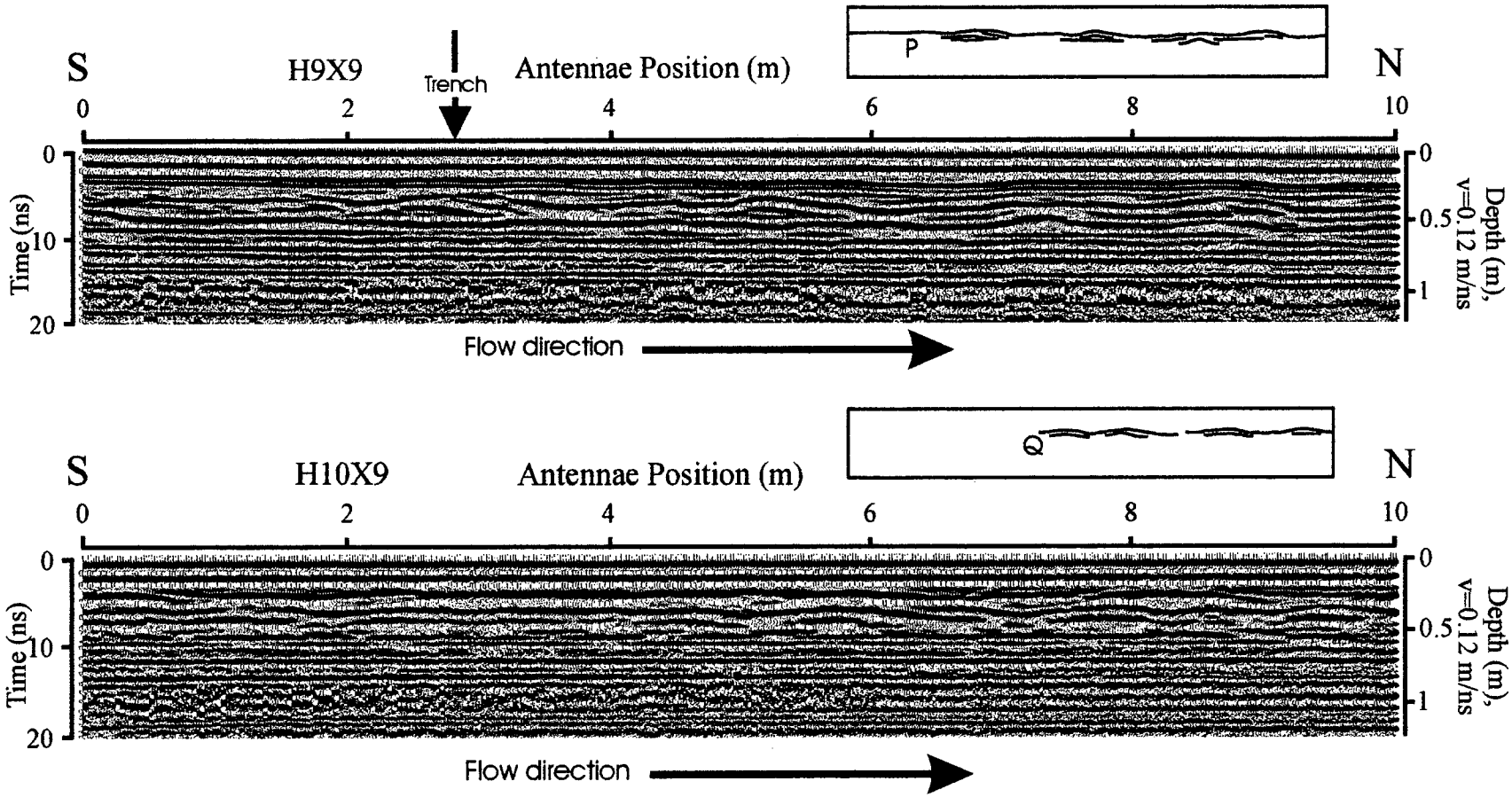

Fig. 5.9. GPR profiles H9X9 and H10X9 collected with 900 MHz antennae. The insets show the position of the sets of wavy reflections. The arrow indicates the location of the trench of Fig. 5.10.

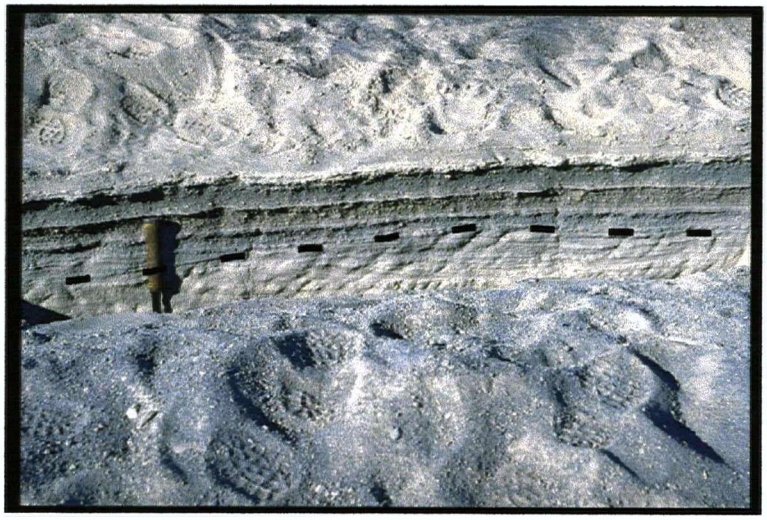

Fig. 5.10. Trench dug parallel to profile H9X9, where one of the crests of the wavy reflections is located (see arrow in Fig. 5.9). The exposure shows the presence in the subsurface of a climbing dune-form (dashed line).

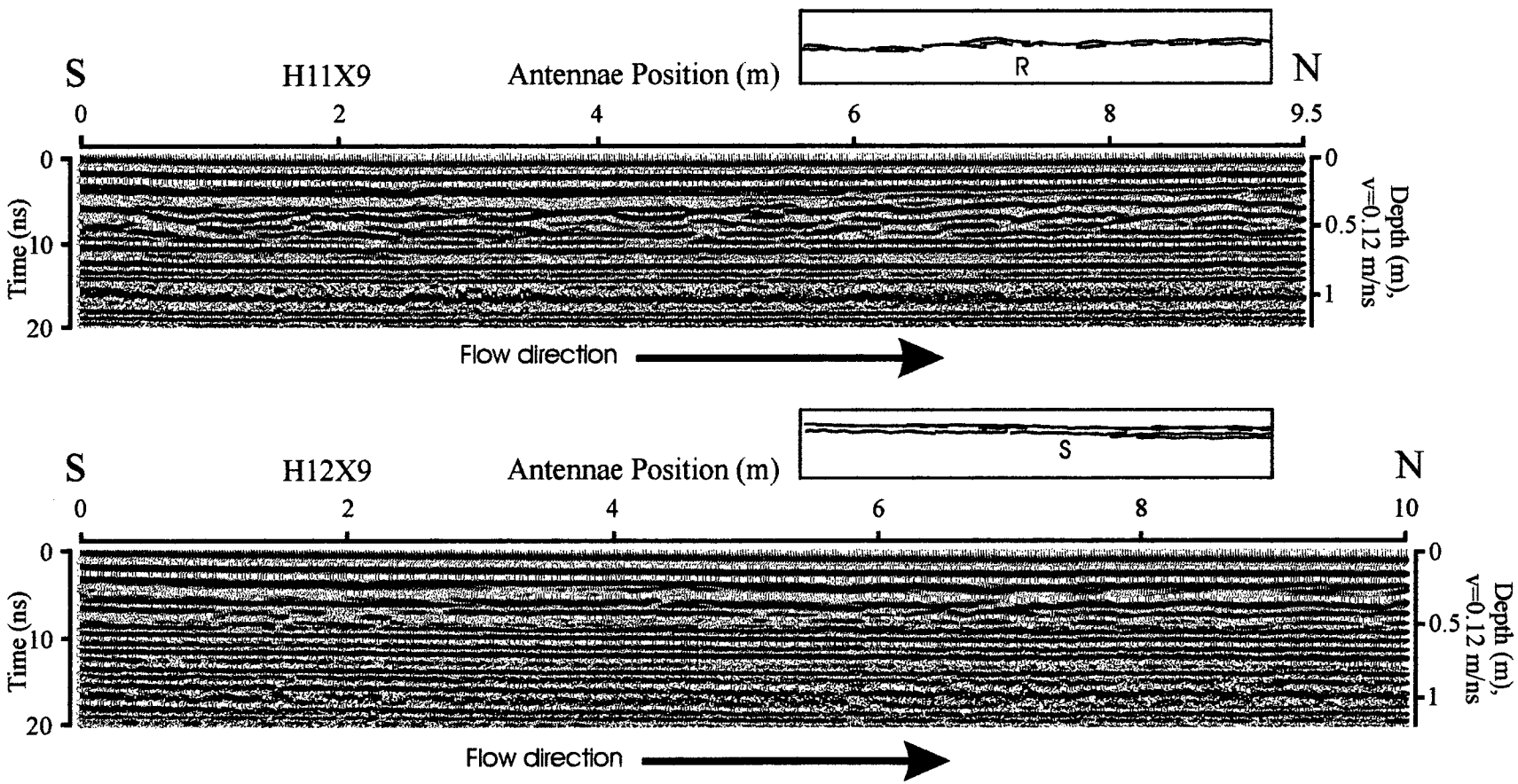

Fig. 5.11. GPR profiles H11X9 and H12X9 collected using 900 MHz antennae. The insets show the position of wavy reflections.

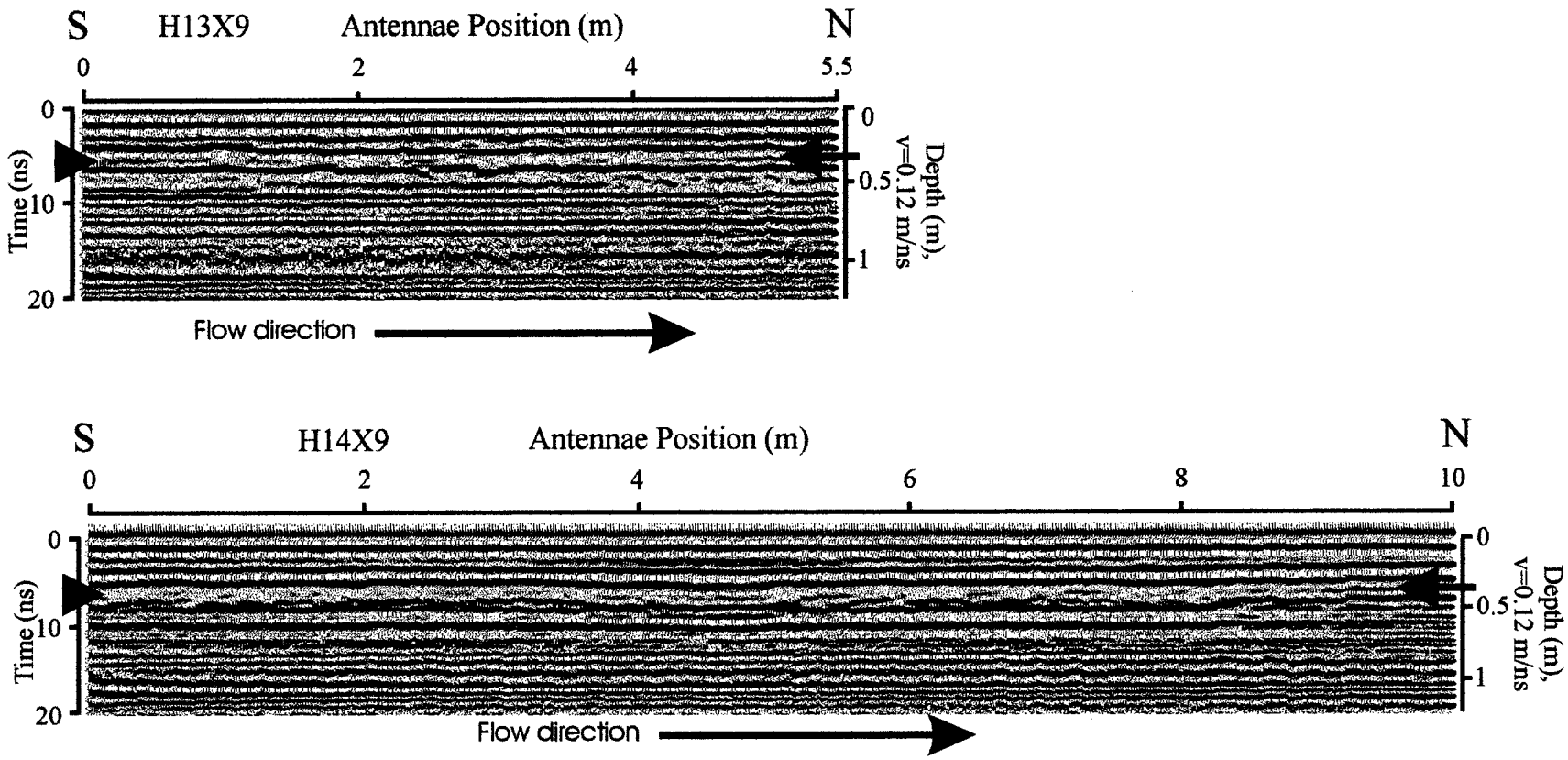

Fig. 5.12. GPR profiles H13X9 and H14X9 collected with 900 MHz antennae. The reflections are sub-horizontal and sub-parallel. Some are discontinuous or slightly wavy (arrows).

(n) In profile H14X9 (Fig. 5.12), the reflections are subhorizontal and subparallel. There are also discontinuous or slightly wavy reflections (for example those shown by the arrows in Fig. 5.12).

(o) In profile K3X9 (Fig. 5.13), the reflections are subhorizontal and subparallel (some are discontinuous). In the right part of the profile (within the ellipse) the reflections become slightly wavy.

(p) Profile K2X9 (Fig. 5.13) shows subhorizontal and subparallel reflections (some are discontinuous). Reflections intersecting at small angles are visible in the right half of the profile (inside the ellipse).

(q) Profile K1X9 (Fig. 5.14) shows subhorizontal and subparallel reflections (some are discontinuous and/or slightly wavy). This profile is located about 2800 m from the center of the Ubehebe Crater, where distal base surge deposits occur (Strand, 1967).

5.5 Three dimensional survey

A 3-D survey comprising nine parallel GPR profiles has been carried out 7 meters from the starting point of H4X9 (Fig. 5.6) in correspondence to a crest of wavy reflections. The purpose of these measurements is a three dimensional image of this subsurface structure. The parallel profiles are 2.5 m long and 25 cm apart. Profile AGRPA4 (Fig. 5.15A) is one of these profiles, located in the middle of the 3-D survey area (Fig. 5.16A) and showing the crest of the wavy reflections. The set of parallel profiles has been transformed into a data cube (Fig. 5.16A) and processed using the software EKKO-3D© (Sensors and Software) and T3D© (Fortner Research LLC). Fig. 5.16B shows a vertical slice of the data cube (positioned close to profile AGRPA4) and two time slices, i.e. horizontal sections of the deposit.

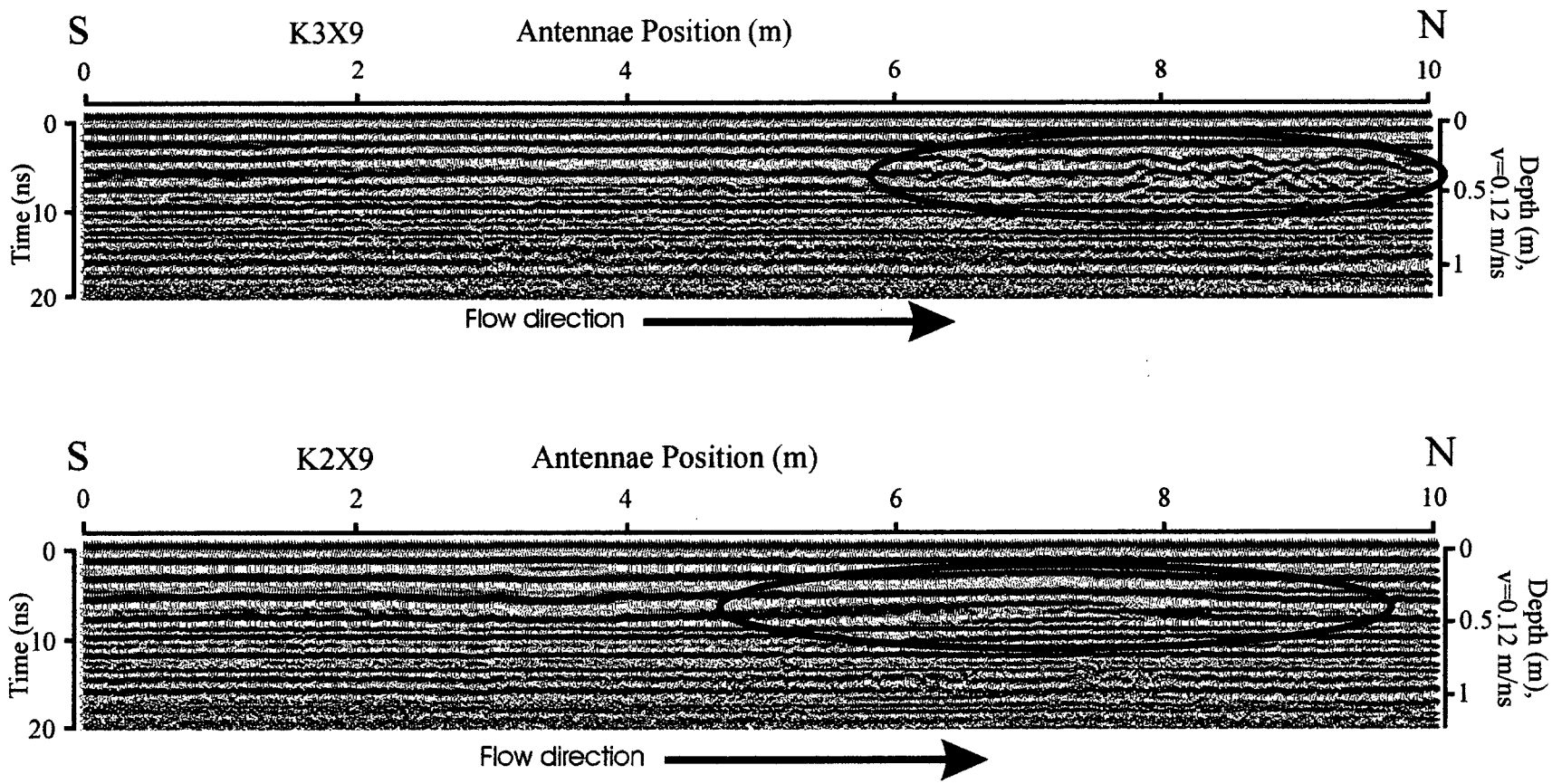

Fig. 5.13. GPR profiles K3X9 and K2X9 collected with 900 MHz antennae (K3X9 is more proximal than K2X9). The ellipses show the position of wavy reflections in K3X9 and reflections intersecting at small angle in K2X9.

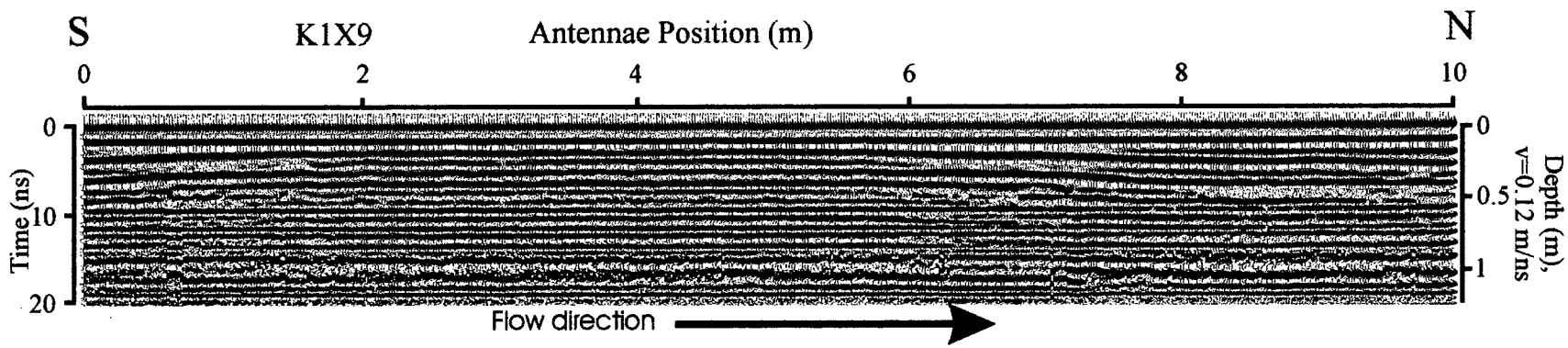

Fig. 5.14. GPR profile K1X9 collected with 900 MHz antennae. This profile is the most distal and shows sub-horizontal and sub-parallel reflections.

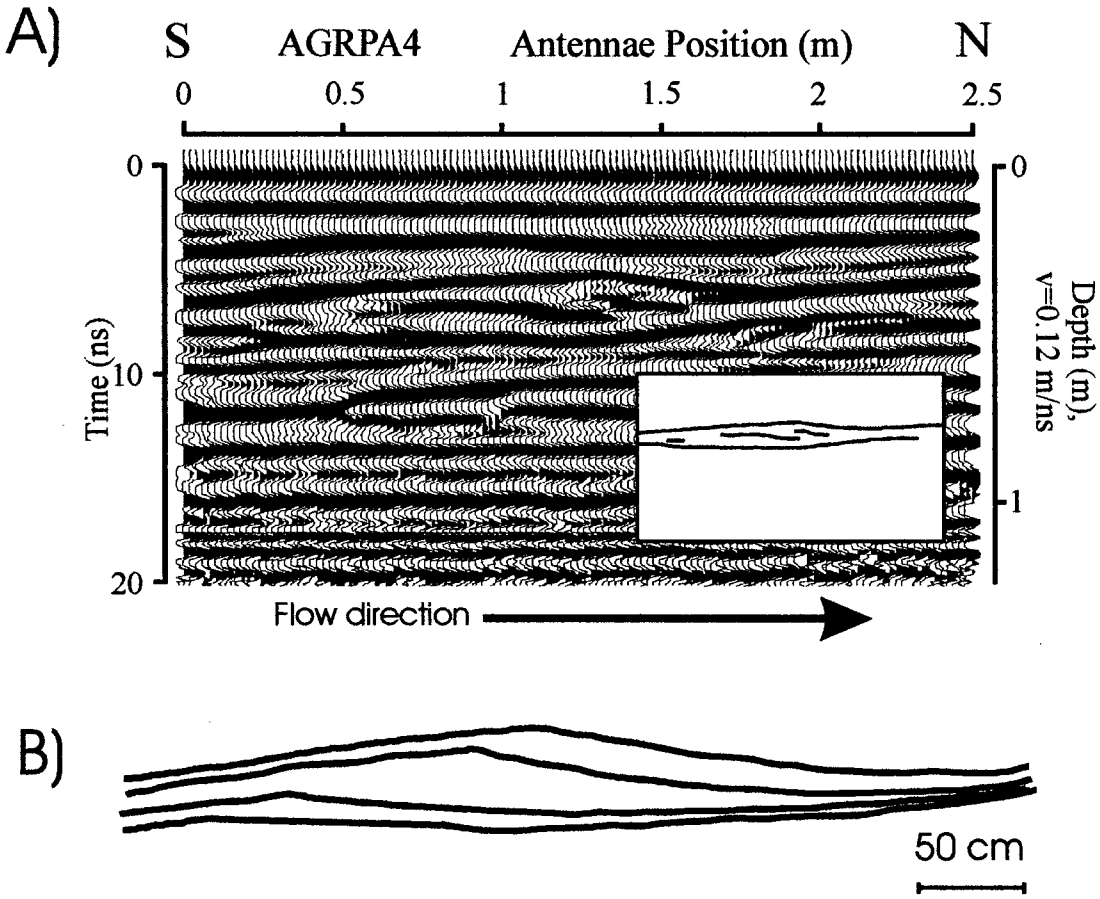

Fig. 5.15. A) GPR profile AGRPA4 obtained with 900 MHz antennae. This is one of the nine parallel profiles of the 3-D survey. The center of the 3-D survey area is located 7 meters from the starting point of H4X9. The inset shows the position of a crest of wavy reflections. B) Sketch of a climbing dune-form from a photo of a base surge deposit in Cas and Wright (1987), page 122.

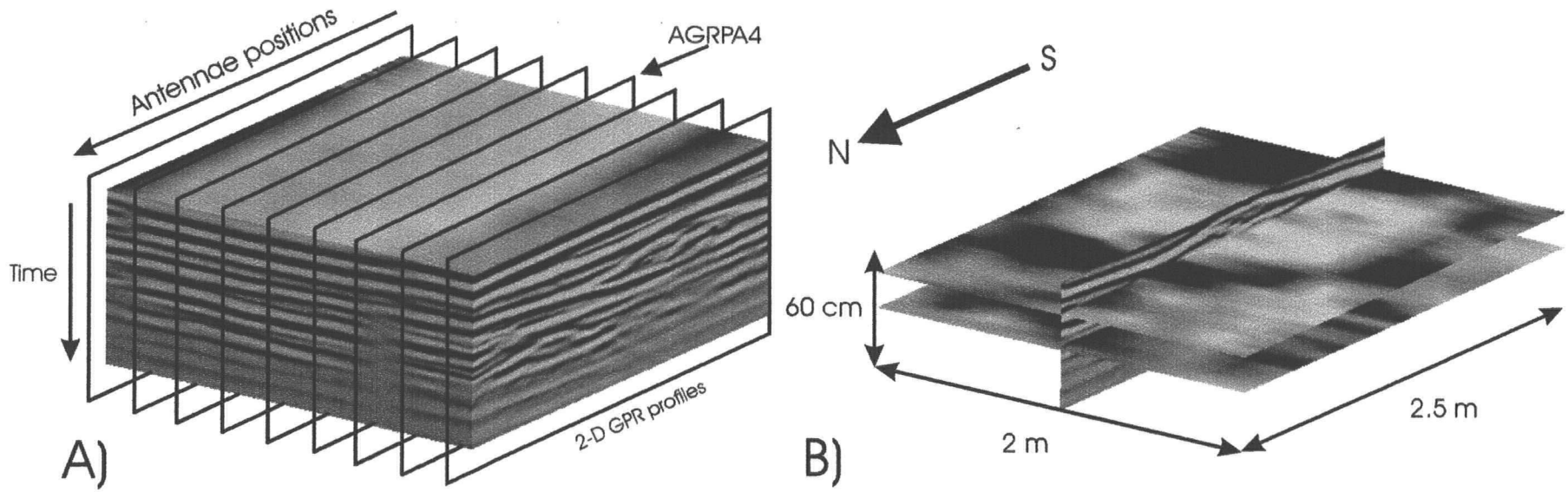

Fig. 5.16. A) Data cube obtained from nine, equally spaced GPR profiles, shown as rectangles in the figure. The position of profile AGRPA4 is also indicated. The center of the 3-D survey area is located 7 meters from the starting point of H4X9. B) One vertical and two horizontal slices of the data cube showing respectively vertical and horizontal sections of a climbing dune-form. The flow direction is from South to North.

5.6. Discussion

The relatively small depth of penetration (1.2 m) of the 900 MHz waves does not limit the representativeness of the GPR profiles because most of the beds in base surge deposits are relatively thin (Fisher and Schmincke, 1984). The limited depth of penetration is well compensated by the high resolution, that is visible comparing the data described here and those collected in the same area with 200 MHz antennae (Chapter 2). Furthermore, the reflections from beds and laminae are not disturbed by diffraction hyperbolas (Reynolds, 1997), which are not present in the profiles. The lack of diffraction hyperbolas suggests that large ballistic blocks are not an important component in the deposits where we ran our surveys. On the other hand, the presence of disrupted reflections in the lower parts of some profiles (for example H8X9, H9X9, H10X9, H11X9, H12X9) is probably due to noise magnified by the automatic gain control.

The sets of wavy reflections in profiles H1X9, H2X9, H3X9 and H4X9 are almost certainly caused by the presence in the subsurface of trains of climbing dune-forms. Fig. 5.5 is a close-up of the leftmost crest of the lower set of wavy reflections in H1X9. One of these crests can be easily recognized also in profile AGRPA4 (Fig.5.15A). A comparison between the shape of the crests and a sketch of a climbing dune-form (Fig. 5.15B) from a photo in Cas and Wright (1988), page 122, shows that they are quite similar. It is interesting to note that the lee side of the crests is concave-upward in Fig. 5.5, 5.15A and 5.15B as well as in other figures. In any case, the interpretation of the wavy reflections as climbing dune-forms is confirmed by the sandwave exposed in the trench (Fig. 5.10). This trench was excavated in correspondence to one of the crests in profile H9X9 (Fig. 5.9). This relatively small

subsurface structure is particularly useful to demonstrate the capability of the 900 MHz antennae to locate sandwaves. Furthermore, the images of sandwaves in the proximal radar profiles agree with the presence of sandwaves in the outcrops nearby the Ubehebe Crater (stars in Fig. 5.1). Among the proximal profiles, the individuation and interpretation of the upper set (D) of wavy reflections in H2X9 is probably the most uncertain.

The wavy reflections in profiles H5X9, H6X9, H8X9, H10X9 and H11X9 can be due to the presence of sandwaves in the subsurface. In these cases, the wave heights are smaller than in the four most proximal profiles, but the presence of sandwaves as far as H9X9 is demonstrated by the trench. The origin of the slightly wavy reflections in profiles H7X9, H12X9, H13X9, H14X9 and K3X9 is more uncertain. They may be due to the presence in the subsurface of small sandwaves or just undulatory laminations and beds. On the other hand, profile K2X9 shows essentially plane parallel reflections, but those intersecting at small angles are difficult to interpret reliably because of lack of detail. The downflow decrease of grainsize and bed thickness in base surge deposits probably requires, in the more distal positions, higher frequency antennae to better resolve the smaller features. Finally, the survey K1X9 shows only plane-parallel laminated reflections and not climbing dune-forms. K1X9 is the most distal profile. It is interesting to compare profile H1X9 (collected with 900 MHz antennae, Fig. 5.4) and profile A1X2 (Fig. 3.4, Chapter 3), collected with 200 MHz antennae. They were collected exactly in the same place, but the 200 MHz profile has not enough resolution and does not show the real structure of the subsurface. This demonstrates that the theoretical resolution of the different antennae frequency anticipated in Chapter 4 is probably different from the real one.

In GPR profiles, there is no evidence (such as diffraction hyperbolas due to larger fragments or a peculiar, different radargram texture) of the presence of massive beds. The field observation of massive deposits (Fig. 5.2) along the southwest rim of the Ubehebe crater suggests that this facies can be proximal. This observation agrees with the lateral facies variation models distilled by Chough and Sohn (1990), where massive deposits are the most proximal. It is possible that, in the sector where we ran our survey, the proximal, massive deposits collapsed inside the crater during the explosive widening of the Ubehebe Crater. Syn- and\or post-eruption partial slumpings are still visible along the rim of this large maar (Crowe and Fisher, 1973). It is also well known from the study of turbidity current deposits that not necessarily all facies of a lateral sequence are always present and, also in base surge deposits, incomplete sequences are more common than complete ones (Chough and Sohn, 1990). It is also true that the limited depth of penetration of the 900 MHz signals prevented the study of deeper beds. In any case, it is important to take into consideration that the interpretation of radar data is affected by the limited resolution inherent in GPR profiles.

The downflow, lateral facies sequence described in Sohn (1996) comprises: 1) proximal massive deposits, 2) intermediate plane-parallel stratified and dune-bedded deposits, and 3) distal plane-parallel laminated deposits. The GPR profiles collected in the Ubehebe hydrovolcanic field can be interpreted as images of the intermediate to distal portion of the lateral facies sequence by Chough and Sohn (1990), because the most proximal and intermediate radargrams show wavy reflections (i.e. sandwaves) together with plane-parallel reflections (i.e. plane-parallel beds), whereas the distal profiles present increasingly more plane-parallel reflections (Fig. 5.18). But, the relative low resolution of the radar data does not allow a reliable interpretation of the plane-parallel reflections. They could be due for

example to plane-parallel laminated beds, fall deposits or thin massive beds. It is interesting to note that the GPR profiles confirm a decrease away from the vent of the size (i.e. wavelength and wave height, which are proportional) of the sandwaves as reported in the literature (Fisher and Schmincke, 1984; Cas and Wright, 1988; Chough and Sohn, 1990). This feature could be used to assess flow directions from GPR data when the position of the vent is unknown, but the decrease downflow of the size of the sandwaves is not regular. For example in profile H9X9, the sandwaves are larger than in some of the previous, more proximal profiles.

Using a Markov analysis of vertical bed form transitions, Wohletz and Sheridan (1979) suggested a lateral facies variation model where the "sandwave" facies is proximal, the "massive" one is intermediate and the "planar" facies is distal. The difference between the models distilled by Wohletz and Sheridan (1979) and those distilled by Sohn and Chough (1989) and Chough and Sohn (1990) are probably in part due to differences in the definition of the facies (Valentine and Fisher, 2000). For example, Wohletz and Sheridan (1979) define the "sandwave facies" as a combination of sandwave and massive beds, whereas the "massive facies" is a combination of massive, sandwave and planar beds. It is also probably true that a Markov analysis of vertical bed form transition produces a statistical summation of many flows through time in a specific location and may not be indicative of lateral variations within a single flow (Fisher and Schmincke, 1984). Unfortunately, GPR data alone cannot demonstrate the presence of one lateral facies sequence or the other, because the resolution is not high enough to locate thin, fine-grained massive beds, which could be present for example in medial positions such as in the model suggested by Wohletz and Sheridan (1979).

In short the interpretation of the GPR profiles is not unique because of the relative low resolution of the data.

A 3-D data volume is particularly useful to study underground structures, because subsurface geological features are three dimensional in nature. The 3-D data can then be explored using 3-D image processing software, enabling view of subsurface structures that would be impossible in the field. For example, a data cube can be cut and a section obtained in any direction. In particular, time slices (i.e. horizontal sections) are useful to generate contour maps of underground surfaces. Fig. 5.16A shows a data cube positioned in correspondence to a crest of wavy reflection (a sandwave) along profile H4X9. The vertical slice in Fig. 5.16B shows the crest. The upper horizontal section, on the other hand, shows an approximately circular black ring that is probably where the reflection of the top of the sandwave intersects that horizontal plane.

5.7 Conclusion

In conclusion, I believe that GPR data can provide useful subsurface information and can integrate traditional geologic surveys especially where there are only few exposures. For example, the GPR surveys conducted north of the Ubehebe Crater allowed images of base surge deposits that would be otherwise impossible to study because of lack of outcrops in this sector. Here, GPR profiles located trains of climbing dune-forms, whose size decreases downflow. GPR allows also a three-dimensional study of subsurface structures that would be impossible in the field.

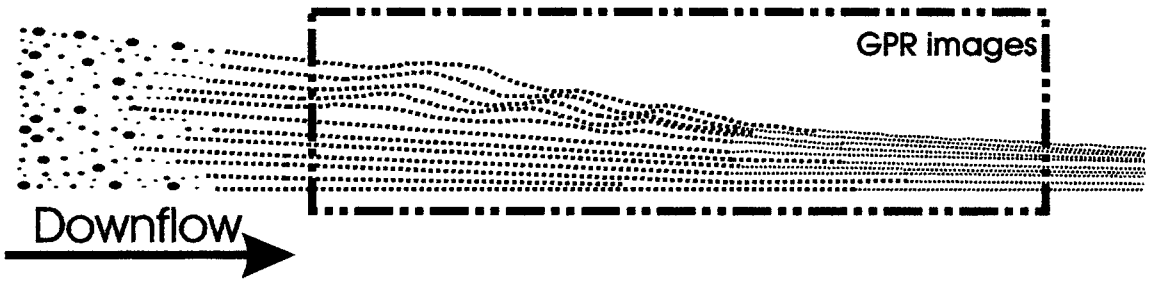

Fig. 5.17. Lateral facies sequence in base surge deposits by Chough and Sohn (1990). The rectangle shows one possible interpretation of the geometry of the reflections in the radar profiles.

CHAPTER VI

Downflow amplitude decrease of GPR reflections

6.1 Introduction

A topic of ongoing research in rock physics is the attempt to evaluate properties of unexposed rocks (such as their textural features, composition or water content) directly from ground penetrating radar data (Rea and Knight, 1998). This should be possible because reflections in GPR profiles are caused by subsurface dielectric discontinuities, which can be, for example, due to differences in texture, chemical composition or water content of the litostratigraphic units. Although GPR profiles are traditionally used as 2-D images of the subsurface stratigraphy, they probably contain more information, but the extraction of this information is not straightforward and constitutes virtually a new research field. The purpose of this chapter is to show that GPR data can record subsurface heterogeneities related to the lateral facies variation, which, even if not obvious in GPR profiles, can be discerned comparing numerically the individual radar traces. I assume that quantitative differences in the traces relate to changes in the physical properties of the pyroclastic deposits.

6.2 Data collection

Some of the GPR profiles analyzed in this chapter have been described in Chapter 5. The data collection characteristics are summarized here again, because they directly affect the interpretations of the results. Data were collected using the ground penetrating radar PulseEKKO 1000 (manufactured by Sensors and Software) that makes use of a 200 V transmitter. A field computer Husky FC-486 controlled the radar system. All data presented here were collected with 900 MHz antennae (which are shielded) to obtain high-resolution images of the shallow subsurface. The maximum depth of penetration is about 1.2 m, for this reason only base surge deposits have been imaged, because in this area, they are thicker than 1.2 m (Chapter 2). Throughout the GPR survey, the collection parameters were kept constant to enable comparisons between the traces. Survey parameters include: antennae separation equal to 17 cm, step size equal to 2 cm and 32 stacks. The number of stacks is the number of traces collected at each antennae position, which are averaged to increase the signal to noise ratio. In order to minimize the presence and magnitude of artifact related to the console position (Chapter 4), antennae and console were kept at a constant distance of no less than 20-25 m during the entire data collection. The magnitude of these artifacts in this data set has been evaluated in a field experiment described in a later paragraph.

GPR profiles have been collected along a flow direction north of the Ubehebe Crater (Fig. 6.1). The first letter of their names is H or K (Fig. 6.1). These profiles are 10 meters long and present subparallel, subhorizontal and sometimes wavy reflections (Chapter 5). A portion of one of them is shown in Fig. 6.2. All surveys have been carried out directly in contact with the top of the base surge deposits (Strand, 1967) because there is no soil in the area. These profiles are situated in the central part of the northern valley, where the deposits

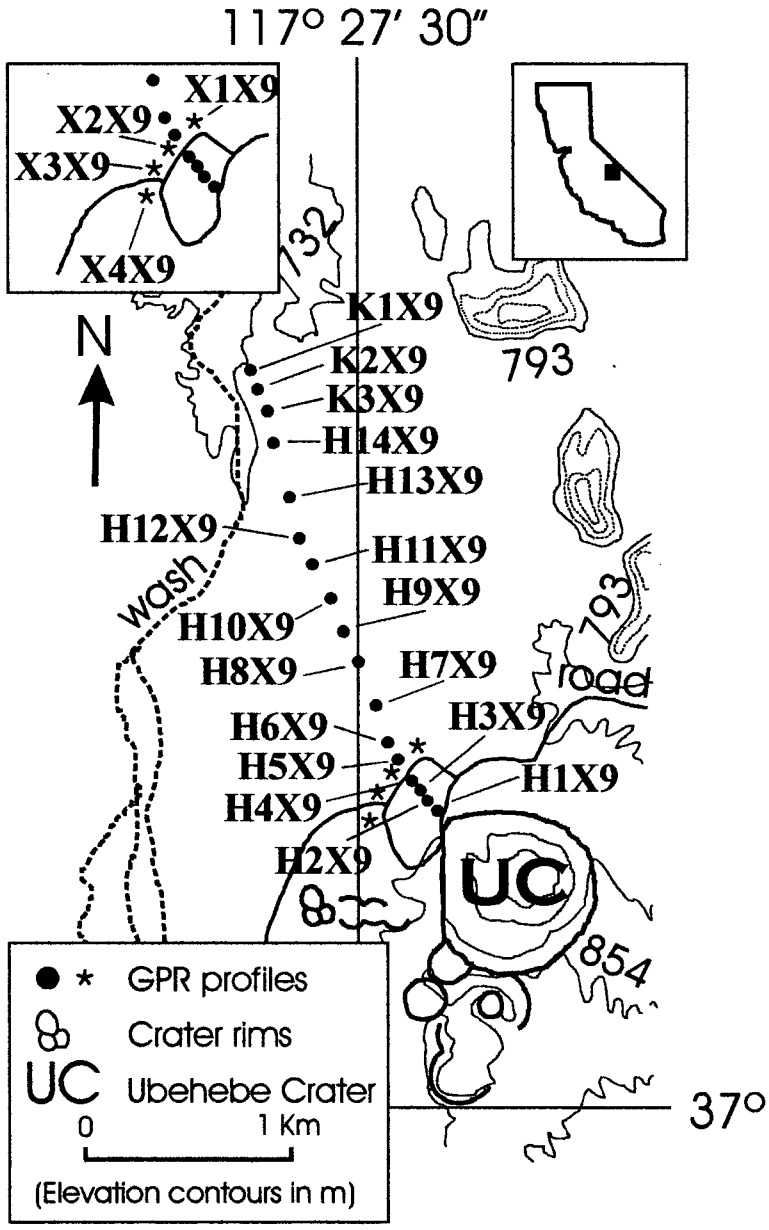

Fig. 6.1. Map showing the locations of the GPR profiles collected with 900 MHz antennae along the flow direction radial to the Ubehebe Crater.

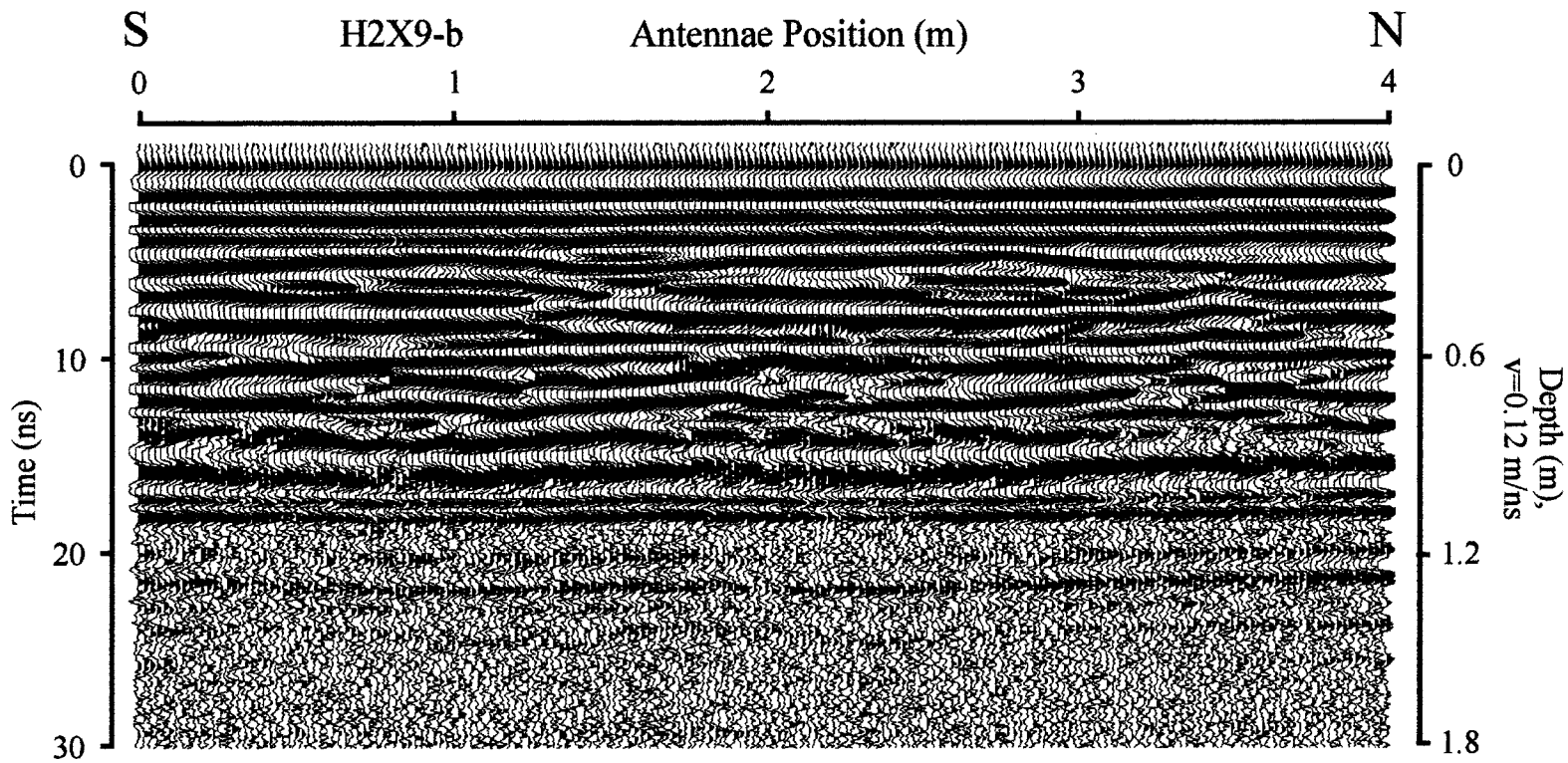

Fig. 6.2. Portion of GPR profile H2X9-b collected using 900 MHz antennae. An automatic gain control (AGC) has been applied for display purposes only in order to boost the weaker signals at later time, because the signal strength decreases with increasing time.

are probably thicker and less disturbed by an irregular paleotopography. They are positioned to avoid small hillocks that probably correspond to paleotopographic highs. These highs could have disturbed the regular flow of the turbulent base surges affecting the lateral facies variation of their deposits. Furthermore, in the entire data set, there is no evidence of large ballistic blocks that would have caused diffraction hyperbolas (Reynolds, 1997). The deposits were also dry, because the data were collected at the end of the summer. Reflections from large ballistic blocks and/or water could have masked the change in radar response due to the lateral facies variations in the base surge deposits.

One Common Mid Point (CMP) profile (Annan et al., 1975; Reynolds, 1997) has been collected in the same location of each GPR profile to evaluate the subsurface velocity of the electromagnetic waves. Fig 6.3 presents one of the most proximal CMP (CMPH2X9 coincident with H2X9) and the most distal (CMPK1X9 coincident with K1X9). It is important to note that well discernible hyperbolas due to reflections from subsurface beds can be identified only in proximal CMP profiles and not in the distal ones (Fig. 6.3). In any case, the visible hyperbolas suggest an electromagnetic wave velocity equal to 0.12 m/ns. Finally, four GPR profiles were collected along a flow perpendicular direction (Fig 6.1). The first letter of their names is X (Fig. 6.1). Only four flow perpendicular profiles were collected, because profiles distributed along a larger distance would have probed deposits from other flows, which traveled along the other directions radial to Ubehebe Crater.

6.3 Data analysis: methods and results

Traces from the different flow parallel profiles have been plotted separately and compared visually and numerically after application of a signal saturation correction filter

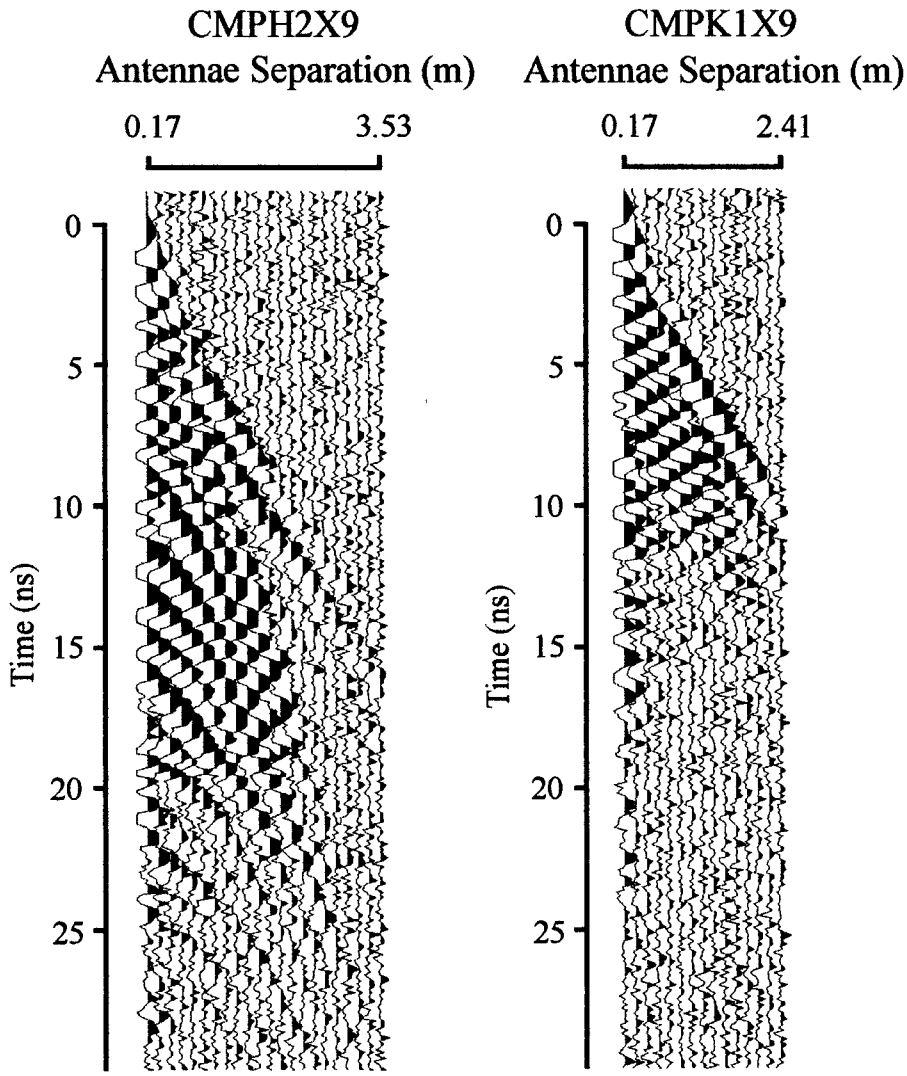

Fig. 6.3. Proximal (CMPH2X9) and distal (CMPK1X9) Common Mid Point profiles collected using 900 MHz antennae. The hyperbolas in CMPH2X9 suggest a subsurface velocity of the electromagnetic waves equal to 0.12 m/ns. The distal profile CMPK1X9 does not present visible hyperbolas.

(dewow). The first 8 ns of each trace were clipped to eliminate ground and air waves. These earlier events have much higher amplitudes than the deeper reflections and would have strongly biased the results of any numerical comparison of the traces. For this reason, always the same time window between 8 and 23 ns has been used. No gain functions have been applied to avoid possible distortion of the data. All calculations were made using MATLAB® routines.

Fig. 6.4 presents one of these comparisons involving one trace from each profile, whereas Fig. 6.5 shows the amplitude spectra of the Fourier transform. The average square of the sample points (ASSP) constituting the traces has also been computed (i.e. $\frac{1}{N}\sum_{1}^{N} x_k x_k$, where 1<k<N and N is the number of sample points x). This parameter is equivalent to the zero lag autocorrelation (Stearns and David, 1996) and has been plotted versus the distance of the mid position of each profile from the center of the Ubehebe Crater. Fig. 6.6 shows the ASSP of the traces in Fig. 6.4, whereas Fig. 6.7 presents the ASSP of nine other sets of traces, again one from each flow parallel profiles. The different traces from the same profile are equally spaced along its length for representativeness reasons. Fig. 6.8, 6.9 and 6.10 show respectively traces, amplitude spectra and ASSP values of the traces from the flow perpendicular profiles (those labeled X in Fig. 6.1).

Fig. 6.4 and Fig. 6.5 show that the amplitudes of the reflections of the traces and of the main peaks of the amplitude spectra decrease downflow. Also the ASSP of the traces (Fig. 6.6) forms a unidirectional data set as suggested by its decrease in the same direction. A similar trend is visible in the plots of the ASSP of the other traces from the same flow parallel profiles (Fig. 6.7). These trends are irregular, but it is clear that the most proximal values are larger then the most distal ones. Furthermore, the traces from the flow

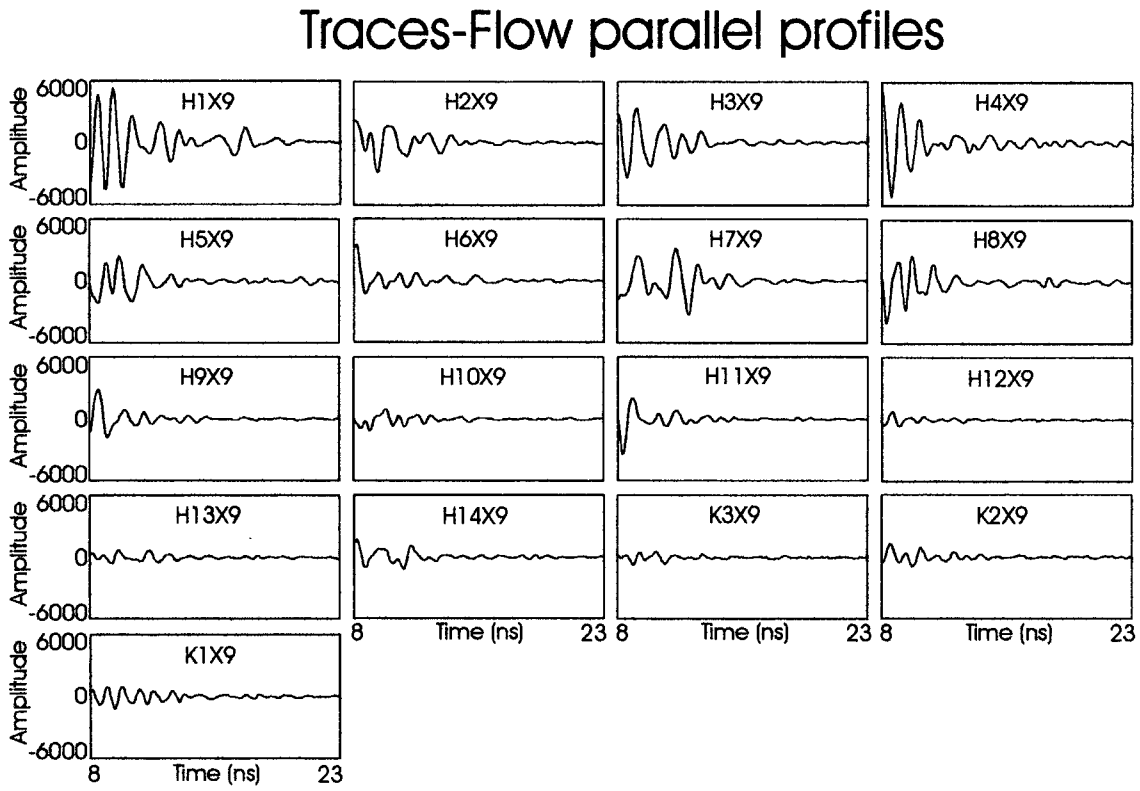

Fig. 6.4. Comparison of one trace from each flow parallel profile. The names of the profiles are indicated in the plots. The amplitudes are in microvolts.

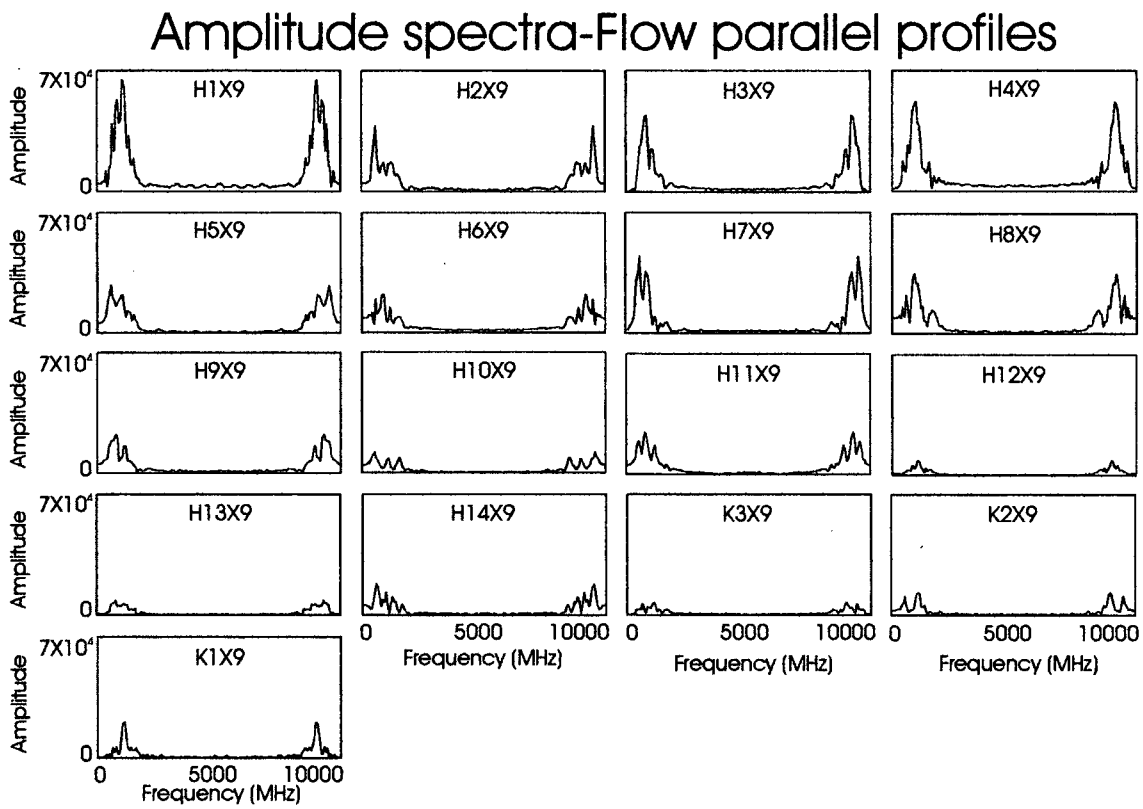

Fig. 6.5. Comparison of amplitude spectra of the traces in Fig. 6.4. The name of the profiles are indicated in the plots. The Nyquist frequency is 5000 MHz.

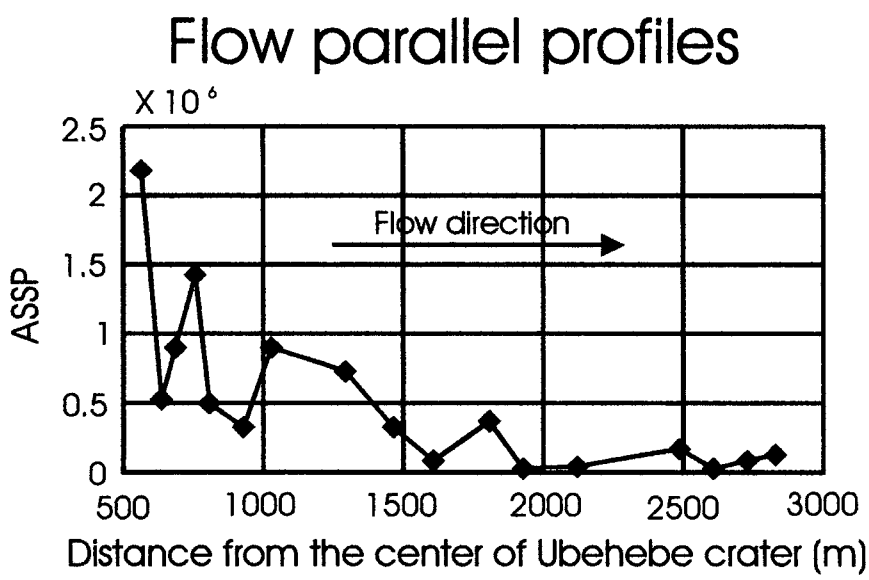

Fig. 6.6. Average square of sample points (ASSP) of the traces in Fig. 6.4 plotted versus the distance from the center of the Ubehebe Crater.

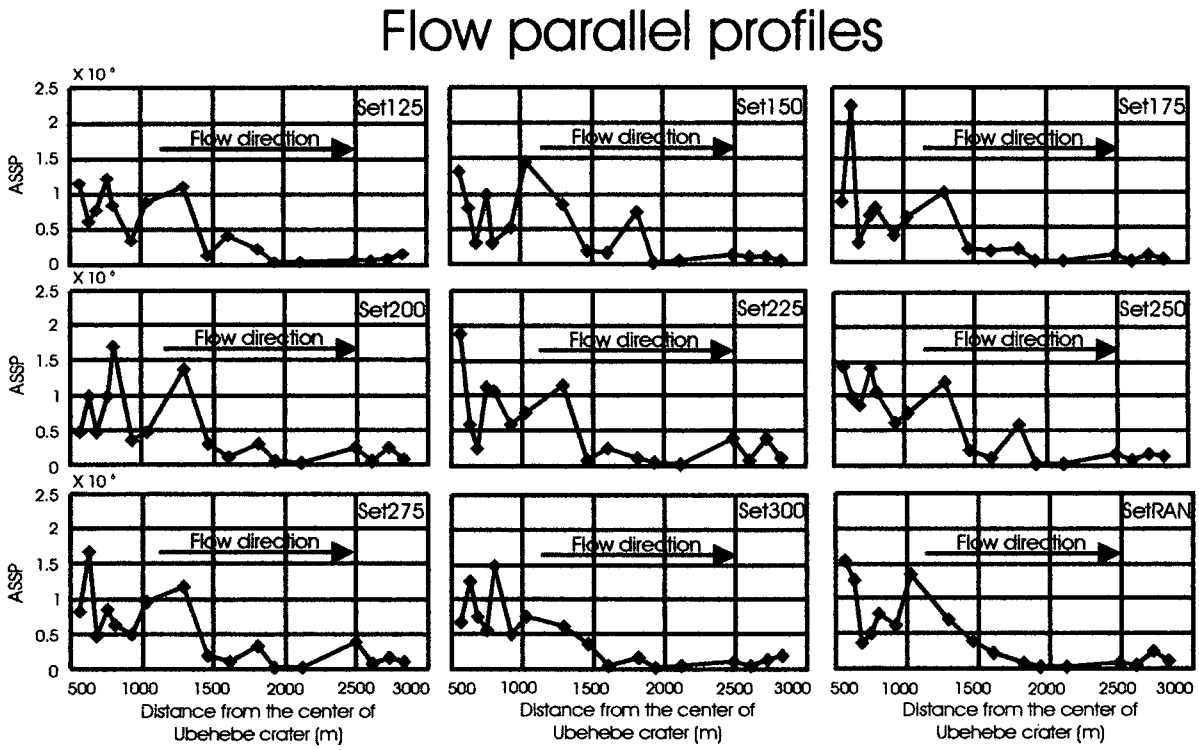

Fig. 6.7. Average square of sample points (ASSP) of nine sets of traces, one from each flow parallel profiles, plotted versus the distance from the center of the Ubehebe Crater.

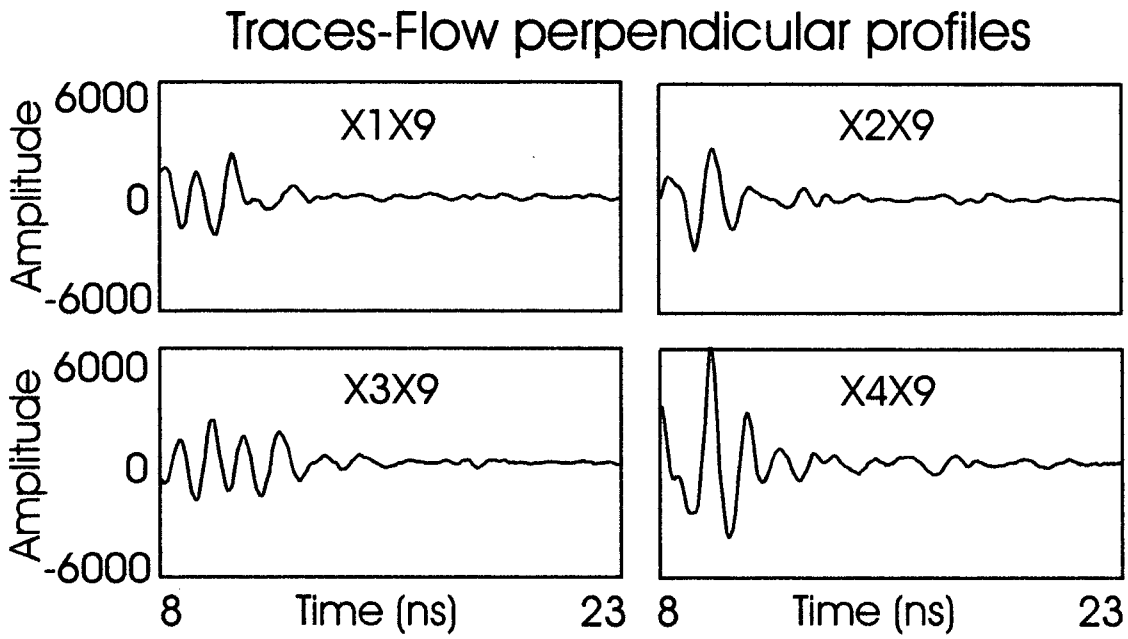

Fig. 6.8. Comparison of one trace from each flow perpendicular profile. The name of the profiles is indicated in the plots. The amplitudes are in microvolts.

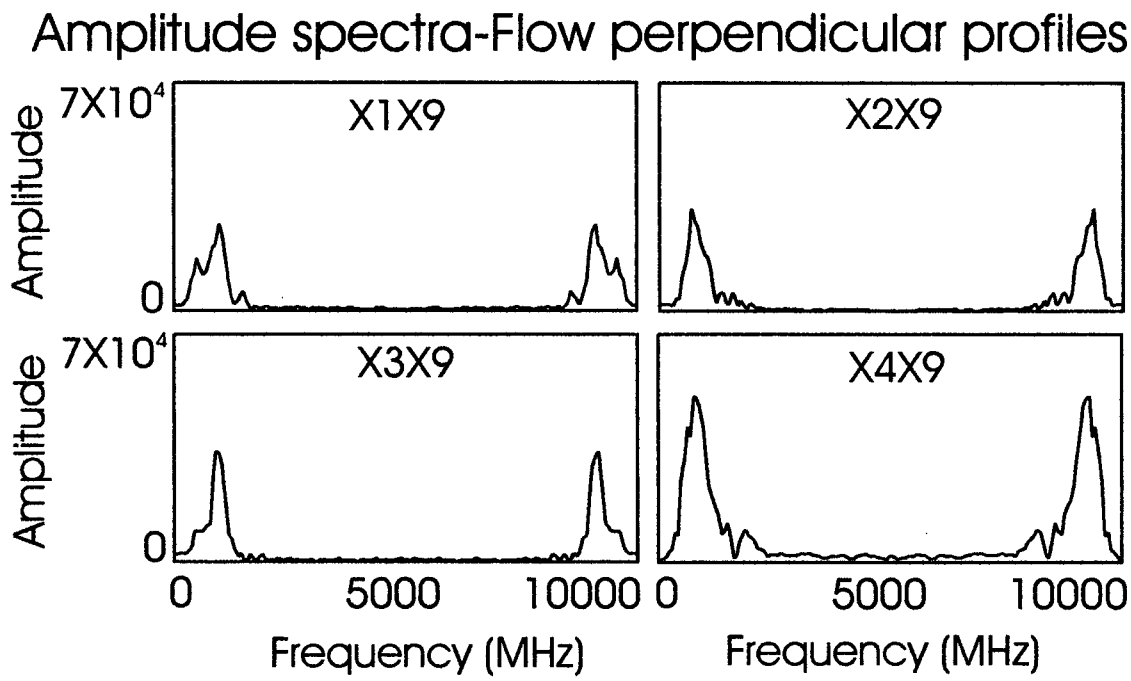

Fig. 6.9. Comparison of the amplitude spectra of the traces in Fig. 6.8. The name of the profiles is indicated in the plots. The Nyquist frequency is 5000 MHz.

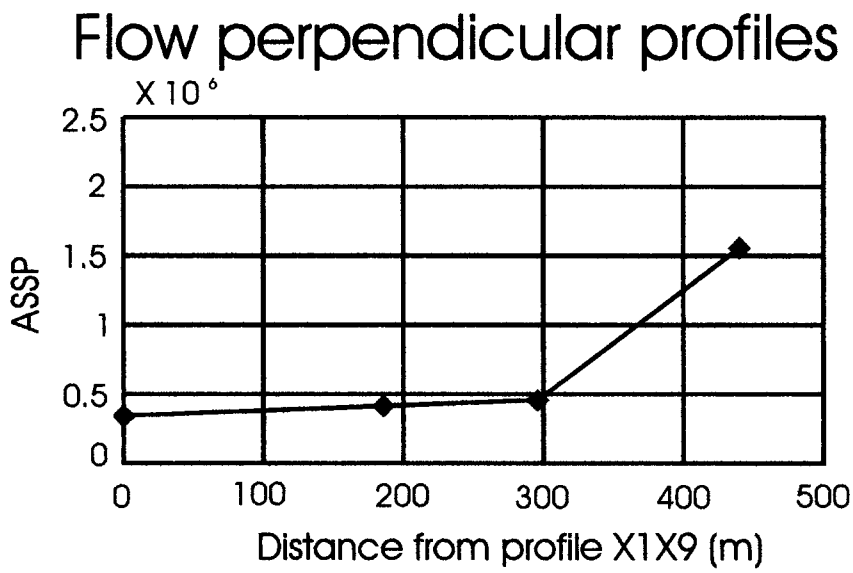

Fig. 6.10. Average square of sample points (ASSP) of the traces in Fig. 6.8 plotted versus the distance from profile X1X9. The vertical axes in Fig. 6.6 and Fig 6.10 are the same to enable comparison between the plots.

perpendicular profiles (Fig. 6.8) and their amplitude spectra (Fig. 6.9) show maximum amplitude values similar to those of the traces from the flow parallel ones located at the same distance from the vent (i.e. H4X9 and H5X9). This can be easily checked comparing the ASSP values in Fig 6.6 and Fig 6.10.

6.4 Models: method and results

Two sets of synthetic profiles have been computed to interpret the observed trend. These synthetic data have been generated using the PulseEKKO Synthetic Radargram Program (Sensors and Software) and making use of 200 MHz waves, which are vertically incident on flat layered earth models. The frequency of the electromagnetic waves that is smaller than that used in the field does not affect the generality of the conclusions. All reflections, including multiples, have been computed. All the earth models consist of 10 m thick successions of two alternate beds (i.e. A-B-A-B-A-B...) with different thickness, dielectric constants and attenuation coefficients.

The beds of the four earth models of the first set of synthetic profiles have the same thickness (1 m) and the same attenuation contrast (beds A with 9.5 dB/m and beds B with 10 dB/m), but different dielectric property contrast. The dielectric constant of beds A of the first earth model is 7. The dielectric constant of beds A of the second earth model is 7.5. The dielectric constant of beds A of the third earth model is 8. The dielectric constant of beds A of the fourth earth model is 8.5. The dielectric constant of beds B in all earth models is always 9. Summing up, the dielectric property contrast decreases from the first to the fourth earth model. Fig. 6.11, 6.12 and 6.13 present respectively traces, amplitude spectra and ASSP values of the traces of these four synthetic profiles. In order to discard the ground waves, we

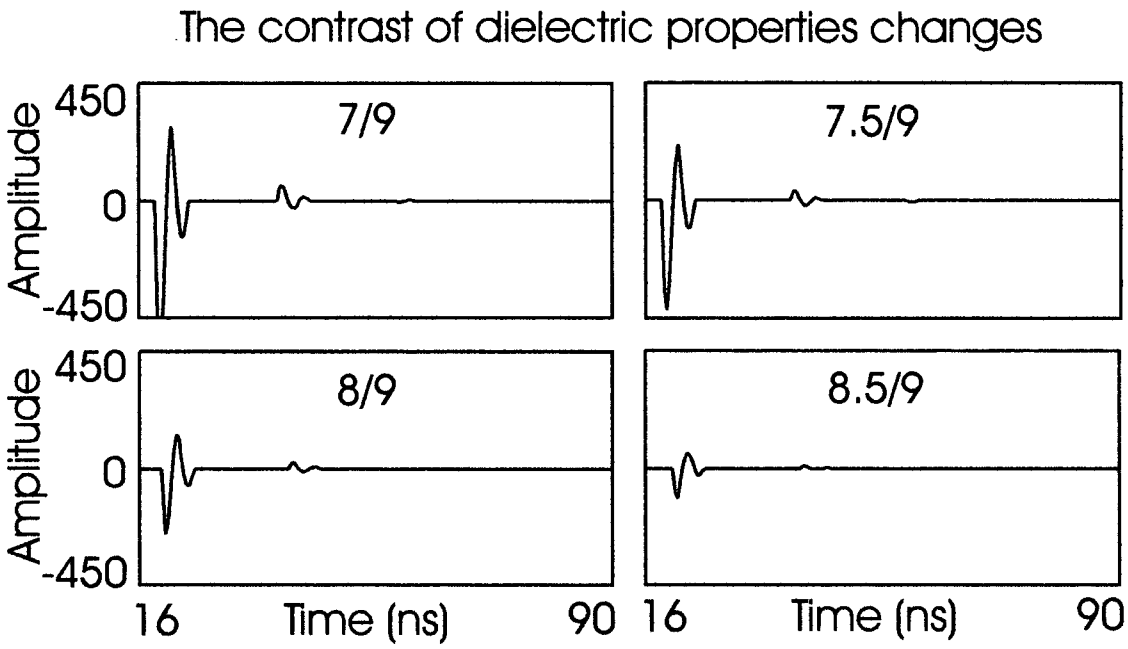

Fig. 6.11. Traces of four synthetic profiles obtained from a succession of two alternate beds (A-B-A-B...) with increasingly smaller dielectric property contrast. The numerator and denominator of the ratios (7/9, 7.5/9, 8/9, 8.5/9) show the dielectric constants of beds A and B respectively.

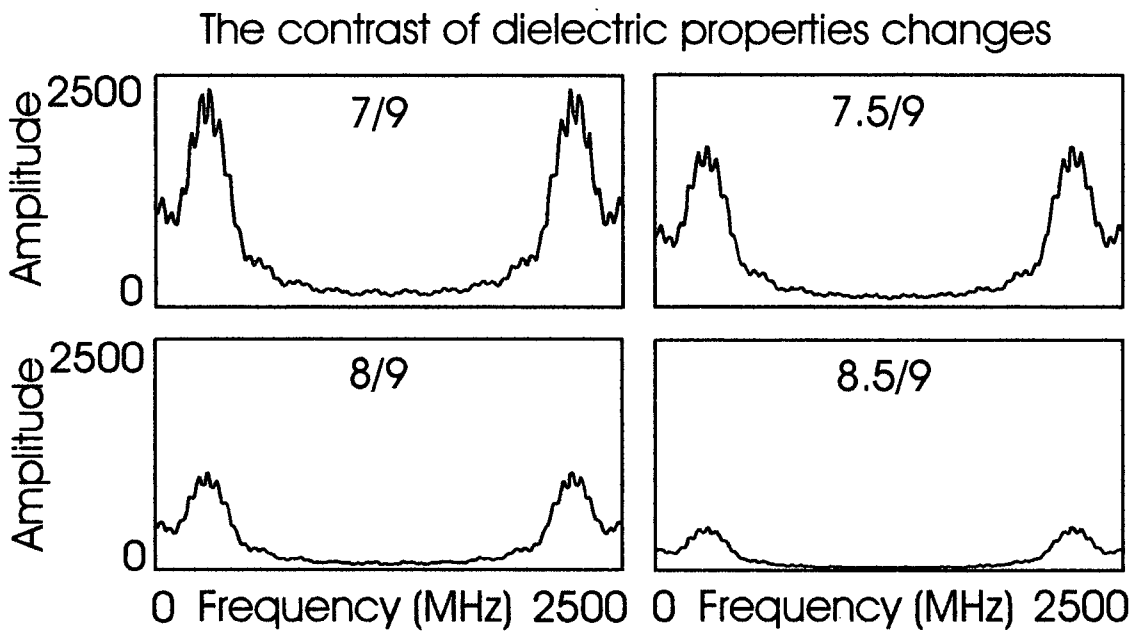

Fig. 6.12. Amplitude spectra of the four synthetic traces in Fig. 6.11. The synthetic profiles have been obtained from a succession of two alternate beds (A-B-A-B...) with increasingly smaller dielectric property contrast. The numerator and denominator of the ratios (7/9, 7.5/9, 8/9, 8.5/9) show the dielectric constants of beds A and B respectively.

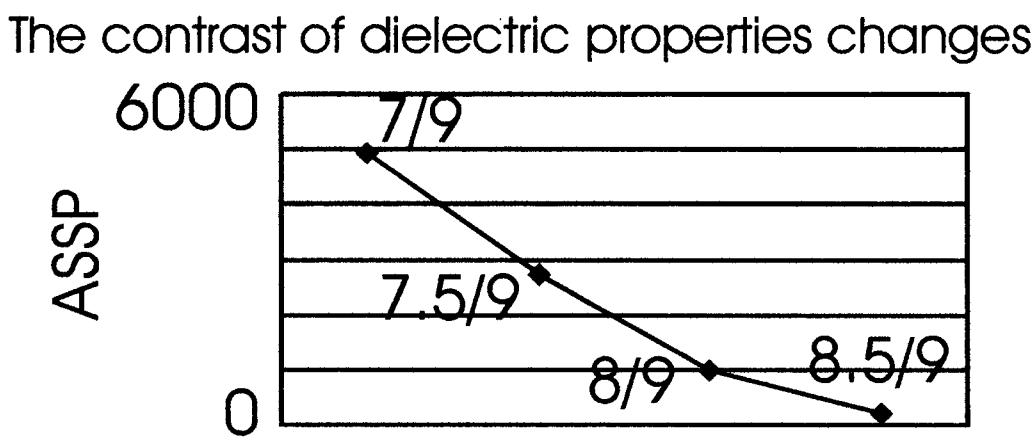

Fig. 6.13. Average square of sample points (ASSP) of the four traces in Fig. 6.11. The synthetic profiles have been obtained from a succession of two alternate beds (A-B-A-B...) with increasingly smaller dielectric property contrast. The numerator and denominator of the ratios (7/9, 7.5/9, 8/9, 8.5/9) show the dielectric constants of beds A and B respectively.

have taken into consideration the time window between 16 and 90 ns. These data show that the maximum amplitude of traces, main peaks of the amplitude spectra and the ASSP values decrease when the contrast in dielectric properties is reduced.

The second set of four earth models has the same contrast of dielectric constants (beds A and beds B have dielectric constants equal to 8.5 and 9 respectively) and the same attenuation contrast (beds A with 9.5 dB/m and beds B with 10 dB/m), but different bed thickness. The beds of the first earth model are 1 m thick. The beds of the second earth model are 50 cm thick. The beds of the third earth model are 10 cm thick. The beds of the fourth earth model are 5 cm thick. The bed thickness decreases from the first to the fourth earth model. Fig. 6.14, 6.15 and 6.16 shows respectively traces, amplitude spectra and ASSP values of the four synthetic profiles. Again, only the time windows between 16 and 90 ns have been taken into consideration to discard the ground waves. These data show that maximum amplitude of traces, main peaks of the amplitude spectra and ASSP values do not decrease when the bed thickness decreases.

6.5 Effects of console and computer position: experiment and results

A field experiment has been carried out to assess the presence and magnitude of artifacts related to console and computer position, because computer and cable connecting computer and console are considered strong sources of radio frequency noise (Sensors and Software, 1999). This experiment consists of a GPR data collection with the shielded antennae always in the same position and console and computer located at different distances from the antennae (25, 20, 15, 10, 5 and 0 m). The traces and their amplitude spectra are shown in Fig. 6.17 and 6.18 respectively. Fig. 6.17 shows that these traces are different. The largest

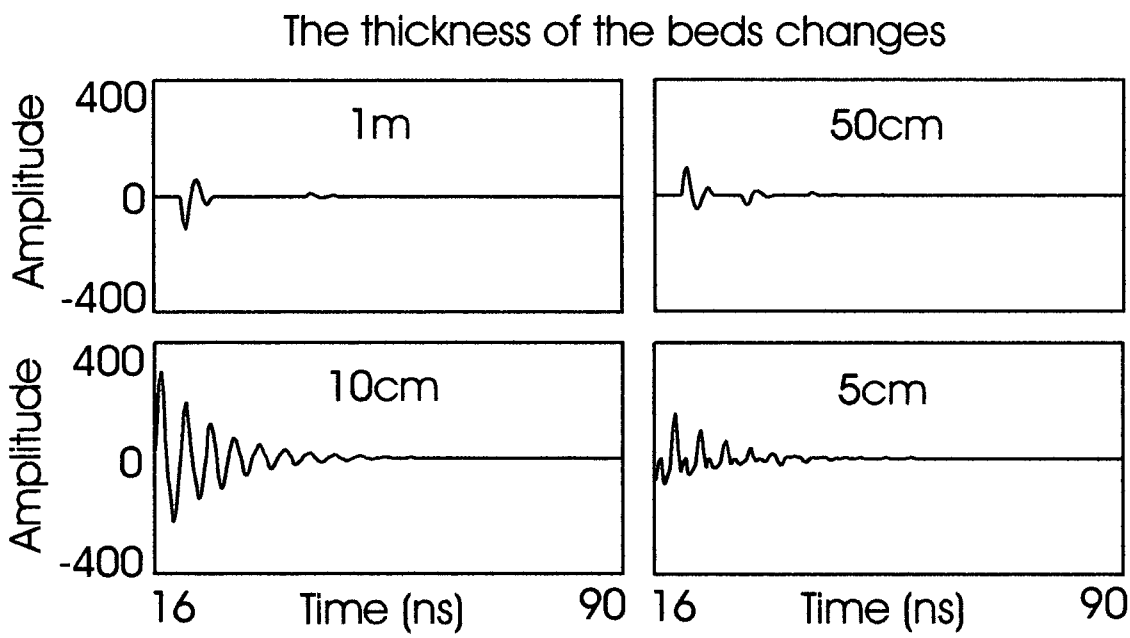

Fig. 6.14. Traces of four synthetic profiles obtained from earth models whose beds have different thickness as indicated in each plot.

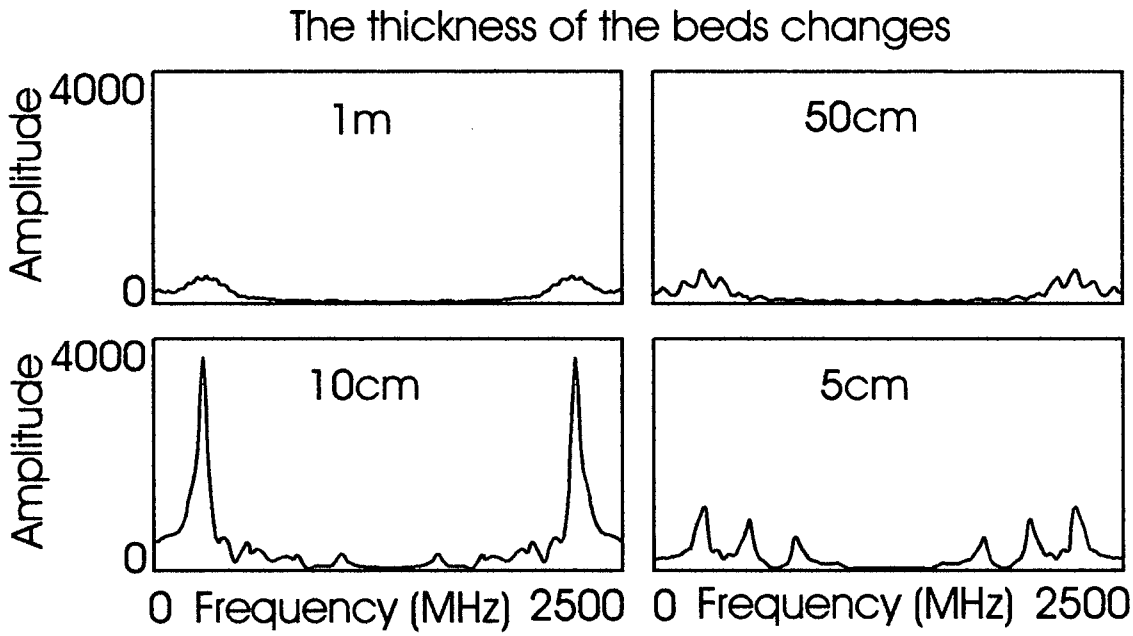

Fig. 6.15. Amplitude spectra of the traces in Fig. 6.14. The synthetic profiles have been obtained from earth models whose beds have different thickness as indicated in each plot.

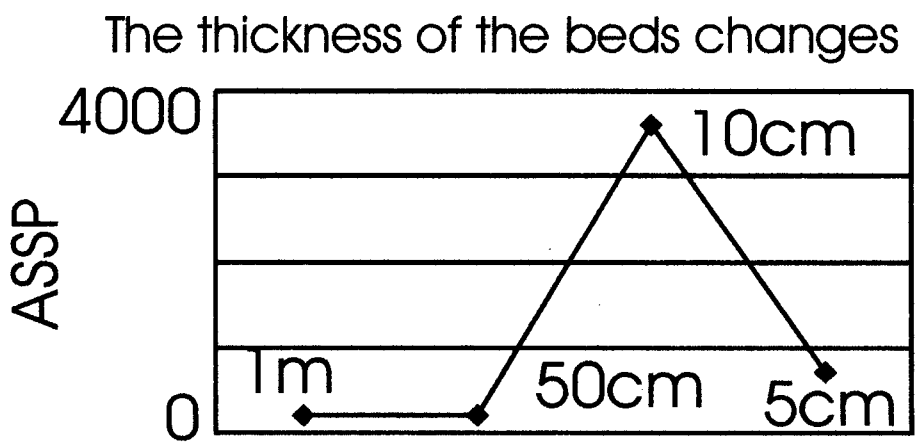

Fig. 6.16. Average square of sample points (ASSP) of the traces in Fig. 6.14. The synthetic profiles have been obtained from earth models whose beds have different thickness as indicated in the plot.

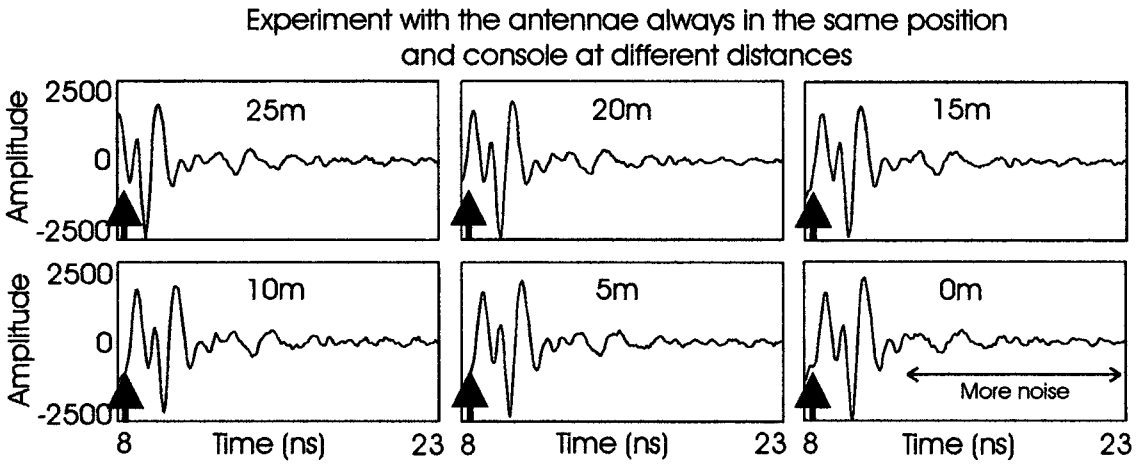

Fig. 6.17. Traces collected keeping the antennae always in the same position and console and computer at different distances from the antennae. These distances are shown in the plots. The arrows indicate the position of the larger differences between the traces. The amplitudes are in microvolts.

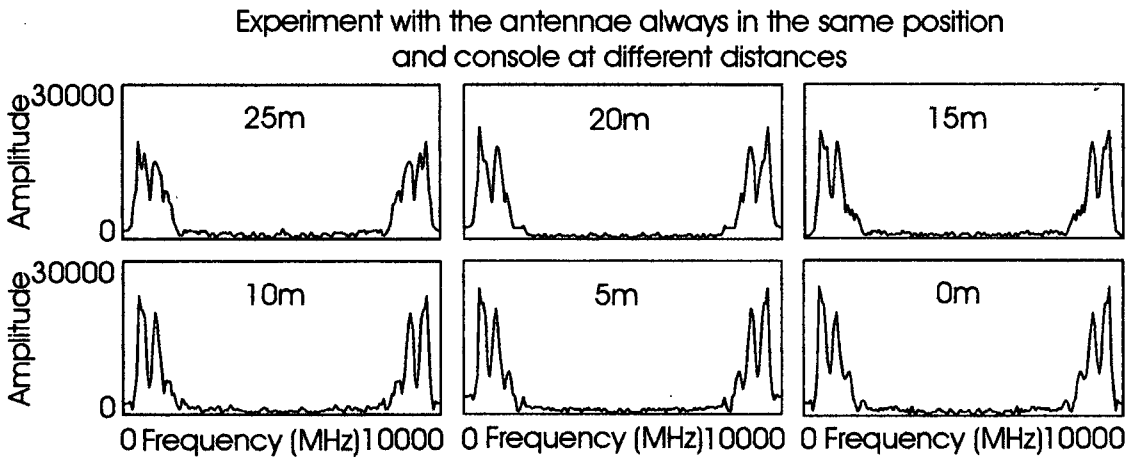

Fig. 6.18. Amplitude spectra of the traces in Fig. 6.17. These traces have been collected keeping the antennae always in the same position and console and computer at different distances from the antennae. These distances are shown in the plots.

differences are located in the earlier portions of the time windows (arrows), but the traces become also more affected by noise when the distance between antennae and console is reduced (this is visible in the lower part of the time windows). The plots of the amplitude spectra make the differences between the traces more evident (Fig. 6.18). In order to quantify these differences, the ASSP of the traces has been computed and displayed in Fig. 6.19. A time window between 8 and 23 ns has always been taken into consideration to enable a comparison with the data collected along flow parallel and flow perpendicular directions. A similar experiment was carried out with a PulseEKKO 100 instrument and unshielded 200 MHz antennae in Chapter 4.

6.6 Discussion

Amplitude spectra and traces of the flow parallel profiles (Fig. 6.4 and 6.5) show that the reflected energy decreases downflow. This is confirmed also by the CMP profiles, because the hyperbolas (which are due to subsurface reflections) are well identifiable only in proximal profiles and not in the distal ones where the reflections attenuate strongly when the antennae separation is larger than three or four step sizes (Fig. 6.3). The ASSP of the traces synthesizes well this downflow decrease of the reflected energy (Fig. 6.6 and Fig. 6.7). It is important to note that the differences between the traces are not obvious in traditional GPR profiles, because in these plots the traces are overlapping and the reflections are clipped (Fig. 6.2). The traces must be plotted separately and the calculations of Fourier transforms and ASSP values are very useful to detect the differences.

The experiment carried out reducing the distance between antennae and console (but keeping the antennae always in the same position) shows that differences between traces can

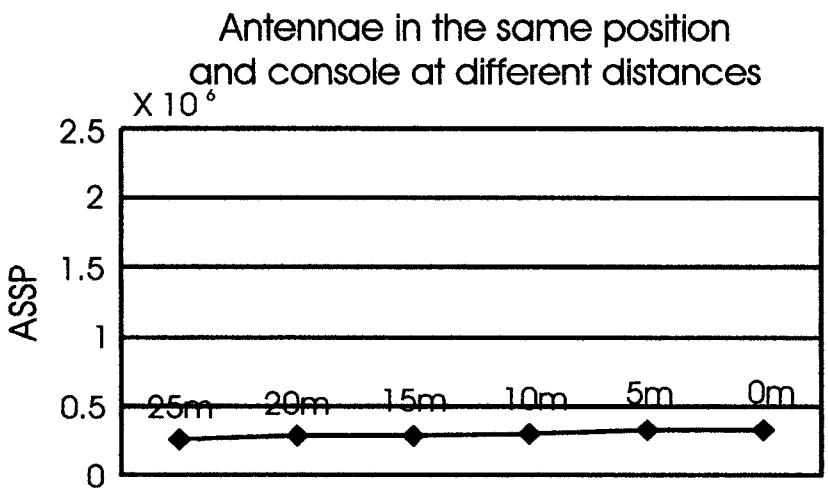

Fig. 6.19. Average square of sample points (ASSP) of the traces in Fig. 6.17. The traces have been collected keeping the antennae always in the same position and console and computer at different distances from the antennae. These distances are shown in the plot. The vertical axes in Fig 6.6, 6.7 and 6.19 are the same to enable comparison between the plots.

be related just to the console position (Fig. 6.17 and 6.18), because computer and cable connecting computer and console are sources of radio frequency noise that can affect also shielded antennae (Sensors and Software, 1999). This is the reason why, during the entire data collection, the distance between antennae and console has been no less than 20-25 m (the cable connecting antennae and console is 30 m long) and constant (to affect equally all traces). In any case, the difference between the ASSP of the traces collected when the separation between antennae and console was maximum (25 m) and when was minimum (0 m) is much smaller (Fig. 6.19) than most of the differences between the ASSP values of the traces of the flow parallel profiles (Fig. 6.6). For this reason, the decrease downflow of the amplitude of the reflections is probably due to the subsurface geology and not to artifacts related to the console position.

The downflow decrease of the amplitude of the reflections is probably caused by some aspects of the lateral facies variation in base surge deposits. In base surge deposits, grain size and bed thickness decreases whereas sorting increases downflow (Sohn and Chough, 1989; Chough and Sohn, 1990; Lajoie and Stix, 1992). These features are clearly visible also in the Ubehebe area, because for example coarse-grained, poorly sorted massive deposits crop out along the crater rim (Fig. 5.2), whereas fine-grained, thinly laminated better sorted deposits crop out in medial positions (Fig. 5.10) and along the wash (Fig. 2.5) in distal positions. One possible suggestion to explain the observed trend is that the increase of sorting and decrease of grain size produce beds that become increasingly more similar downflow with the consequence that the contrast between their dielectric properties is reduced. The first set of synthetic profiles (Fig 6.11, 6.12 and 6.13) shows that a decrease of the dielectric property contrast causes a decrease of the amplitude of the reflections. It is important to note that the

reduction alone of the bed thickness does not produce a decrease of the reflected energy, as suggested by the second set of synthetic profiles (Fig. 6.14, 6.15 and 6.16). But, the effect of the dielectric property contrast can compensate that arising from the bed thickness, because it decreases the differences between these beds. For an evaluation of the dielectric constants from CMP profiles see Appendix 1.

Unfortunately, the reflections in GPR profiles are not spike-like but wavelets comprising more than one peak (Daniels, 1996). This certainly decreases the resolution of the trend, but the general pattern does not appear to be masked. In any case, we assume that the wavelet is the same in all profiles because the conditions of data collection have been the same during the entire GPR survey (i.e. the differences between the traces are not due to different wavelets). The destructive interference of overlapping wavelets can explain why the amplitudes of the reflections in the earth model with 5 cm thick beds are smaller than those with 10 cm thick beds (although both are larger than in the others models with thicker beds).

The downflow attenuation of the signal could be used as a flow direction indicator when the position of the vent is unknown. But this trend is not regular and traces from profiles distributed along a large distance must be taken into consideration, because opposite trends can be observed in small portion of the data set (Fig. 6.6 and 6.7). For example, the traces of the few flow perpendicular profiles (Fig. 6.8, 6.9 and 6.10), although similar to those of the flow parallel ones which are at the same distance from the crater rim, form a west-east decreasing trend. This suggests that extreme care must be paid in assessing flow directions with this method and other geologic information and field constraints are probably necessary. The comparisons between traces are also affected by the position of the selected time window, because a too shallow time window can include the strong air and ground waves,

whereas a too deep time window is noisier. Other variables affecting the comparison between traces are for example the presence or lack of water in the deposits (i.e. the season) and local features such as large ballistic blocks or irregularities in the palaeotopography, which can cause strong reflections unrelated to the lateral facies variation.

6.7 Conclusions

Ground penetrating radar data are mainly used to image major underground discontinuities, but they probably contain a larger amount of subsurface information, because characteristics such as grain size, packing and composition of a rock control its dielectric properties. For example, the GPR data collected along a flow direction in the Ubehebe hydrovolcanic field present a decrease downflow of the amplitude of the reflections. This probably reflects some aspects of the lateral facies variation of base surge deposits. The downflow increase of sorting and decrease of grain size probably reduce the differences between the beds (i.e. the contrast between their dielectric properties) and consequently also the amplitude of the reflections. The downflow decrease of the amplitude of the reflections is due to the fact that the beds become more similar downflow. The concomitant downflow decrease of grain size and increase of sorting mean that in the more distal positions the deposits consist only of fine-grained laminae or thin beds with similar physical properties (it is important to say that the increase alone of sorting or decrease alone of grain size would not affect the amplitude of the reflections). But a simple visual inspection of GPR profiles does not enable the recognition of subtle degrees of similarities or dissimilarities between the traces. For this reason a numerical comparison of the traces is recommended and the

evaluation of amplitude spectra and the average of the squares of sample points is a very useful visual and computational aid.

CHAPTER VII

Quantification of the wavy reflections in GPR profiles using singular value decomposition

7.1 Introduction

The GPR profiles collected with 900 MHz antennae along a flow direction radial to the Ubehebe Crater have probably imaged the intermediate to distal portion of the lateral facies sequence by Chough and Sohn (1990). These profiles show a downflow decrease of the waviness of the reflections that is probably related to the characteristic downflow decrease of the size (wavelength and wave height) and quantity of the climbing dune-forms in the deposits (Sigurdsson et al., 1987; Sohn, 1996).

Unfortunately, in the GPR sections, it is not always possible to select confidently the position of the crests of the wavy reflections and measure the correspondent wavelength, in particular in the more distal positions where wavelength and wave height become smaller and not clearly resolved by the limited resolution. An attempt to measure the wavelength directly in the hard copy of the GPR profiles is shown in Fig. 7.1. These measurements are not representative of each entire profile, because questionable crests have been discarded from the calculations. But, these values are in the range of those measured in the field by Crowe and Fisher (1973) and will be used in Chapter 8 for further analyses. The purpose of Chapter 7 is to quantify the amount of wavy reflections in each profile using a fast,

quantitative and objective approach. This has been carried out by means of singular value decomposition and eigenimage processing of the GPR profiles.

7.2 Singular value decomposition

The singular value decomposition (Strang, 1986) is a factorization of a rectangular matrix **X** into orthogonal matrices, i.e. $\mathbf{X} = \mathbf{U}\,\Sigma\,\mathbf{V}^{T}$, where Σ is a diagonal matrix and T stands for transpose. The singular values of **X** are the positive entries of Σ which are distributed in decreasing order along its main diagonal and are equal to the positive square roots of the eigenvalues of the covariance matrices $\mathbf{XX}^{T}$ and $\mathbf{X}^{T}\mathbf{X}$. The application of the singular value decomposition to seismic profiles have been illustrated by Freire and Ulrych (1988) and Ulrych et al. (1999), but this technique can be applied to GPR profiles as well. For example, the singular value decomposition of a seismic or GPR profile **X** (with *m* traces and *n* sample points along each trace) can be written as

$$X = \sum_{i=1}^{r} \sigma_i u_i v_i^T , \qquad (1)$$

where: 1) *r* is the rank of **X**, 2) $\mathbf{u}_i$ is the *i*th eigenvector of $\mathbf{XX}^{T}$, 3) $\mathbf{v}_i$ is the *i*th eigenvector of $\mathbf{X}^{T}\mathbf{X}$, 4) σ_i is the *i*th singular value of **X** and 5) $u_i v_i^T$ is a *m* by *n* matrix of unitary rank called the *i*th eigenimage of **X**.

When all *m* traces are linearly independent (i.e., no trace can be represented in terms of a linear combination of the other traces), all σ_i are different from zero and the perfect reconstruction of **X** requires all eigenimages. On the other hand, when all *m* traces are linearly dependent (i.e. equal to within a scale factor), **X** can be perfectly represented by the first eigenimage (i.e. $\sigma_1 u_1 v_1^T$). In general, depending on the linear dependence among the

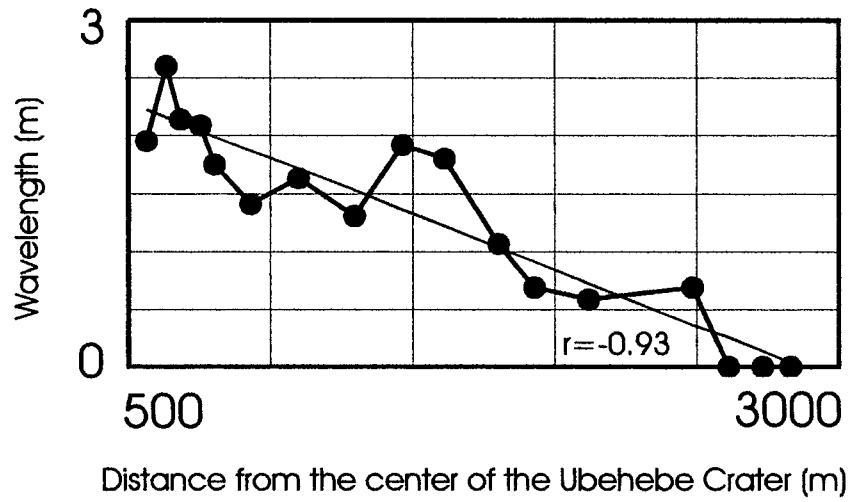

Fig. 7.1. Approximate wavelength in m of sandwaves estimated from the average distance of selected crests of the wavy reflections in GPR profiles. The straight line has been computed using the least squares method.

traces, a profile **X** can be reconstructed from only some eigenimages. Freire and Ulrych (1988) introduced band-pass, low-pass, and high-pass eigenimages according to the range of singular values, which has been used. Band-pass eigenimages are computed rejecting highly correlated as well as highly uncorrelated parts of the traces, i.e.

$$\mathbf{X}_{BP} = \sum_{i=p}^{q} \sigma_i \mathbf{u}_i \mathbf{v}_i^T , \tag{2}$$

where $1 < p \leq q < r$, whereas low-pass eigenimages are computed performing this summation from i=1 to p and high pass eigenimages from i=q to r.

7.3 Eigenimage processing: method and results

The GPR profiles collected in the Ubehebe hydrovolcanic field (with automatic gain control applied) were first energy normalized (the energy is the average of the squares of the sample points). This normalization consists in multiplying the sample points of the jth profile by $E_{av}/\sqrt{E_j}$, where E_{av} is the average energy of all profiles and E_j is the energy of the jth profile itself. Secondly, the high-pass eigenimages ($\mathbf{X}_{HP}$) of equal size windows (500 traces and 150 points along each trace) of all normalized GPR profiles were computed. The summation was performed from i=4 to r=150 (i.e. the first 3 eigenimages with the 3 highest singular values were discarded). The energy of the eigenimages of all profiles is plotted in Fig. 7.2. From this figure, it is clear that the energy of the eigenimages decreases moving away from the crater. All calculations have been performed using MATLAB® routines.

Figures 7.3, 7.4 and 7.5 show three original GPR profiles (with automatic gain control applied) and their correspondent high-pass eigenimages, which were computed as above. These three profiles were collected respectively at approximately 560, 1290 and 2600 m from

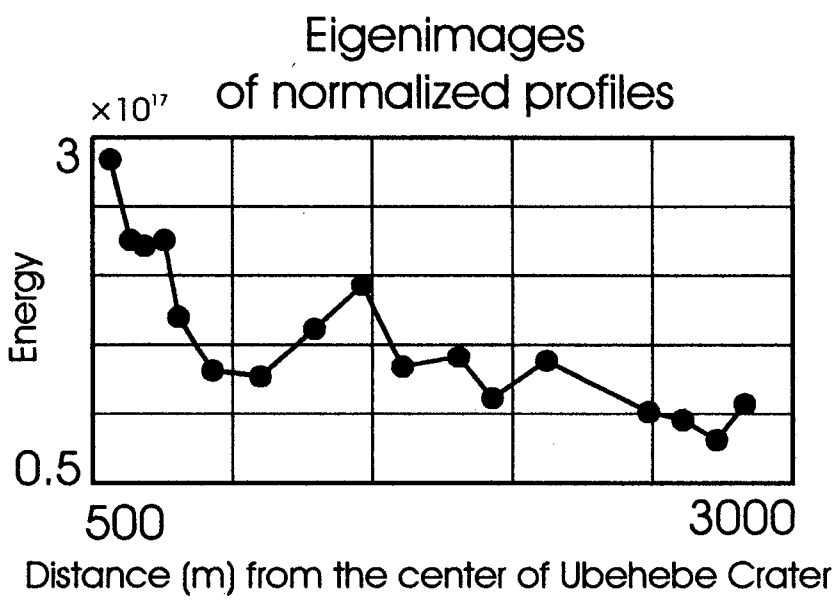

Fig. 7.2. Plot of the energy of the eigenimages of the normalized profiles versus the distance from the center of the Ubehebe Crater.

H1X9

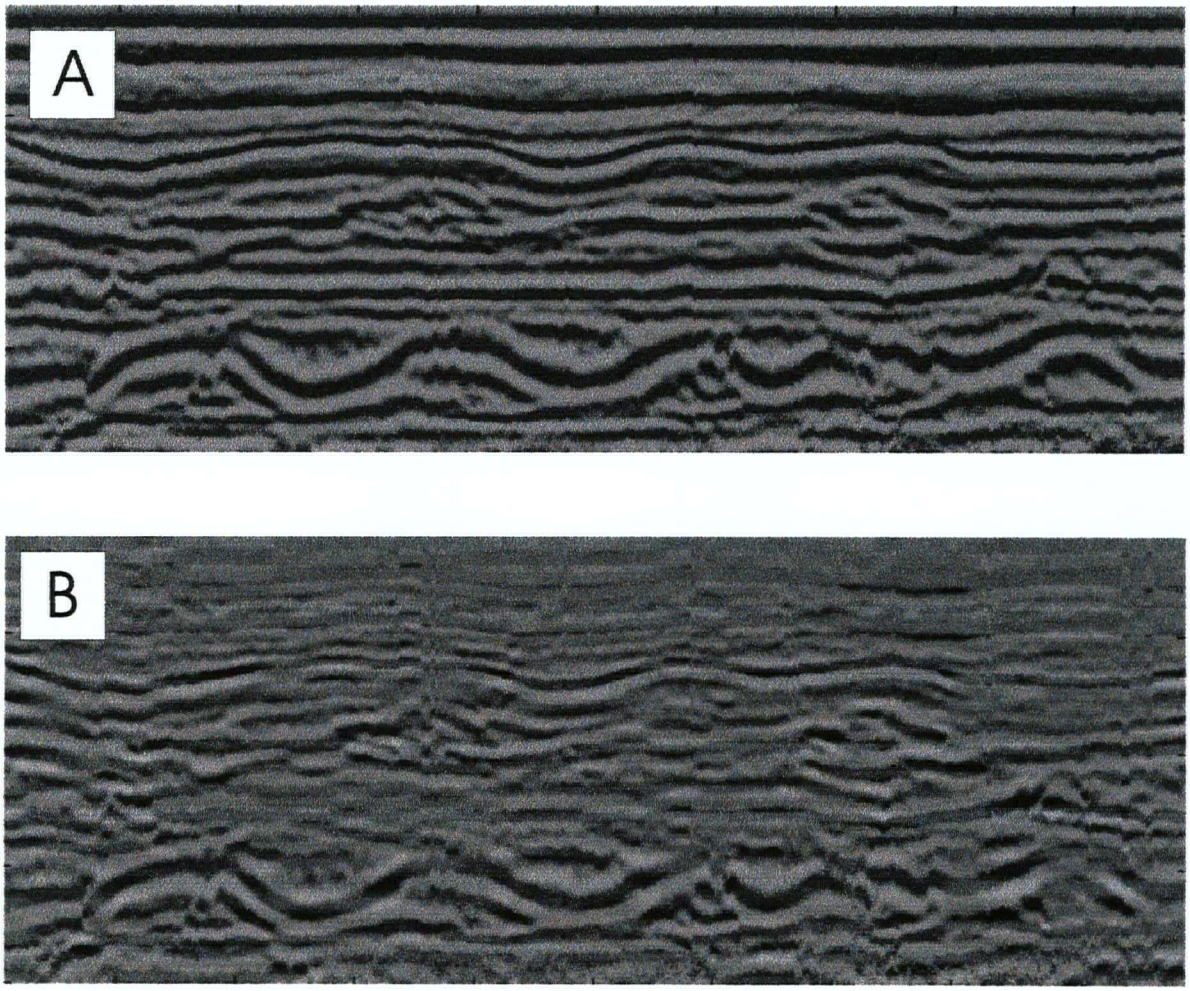

Fig. 7.3. These are GPR data displayed as images in MATLAB. Figure A shows the GPR profile with an automatic gain control applied and figure B is the high-pass eigenimage where the flat horizontal reflections have been selectively removed. The horizontal side of the profile corresponds to 10 m and the vertical to 1.2 m. The antennae separation and the step size were 17 cm and 2 cm respectively. This profile was collected at approximately 560 m from the center of the Ubehebe Crater.

H8X9

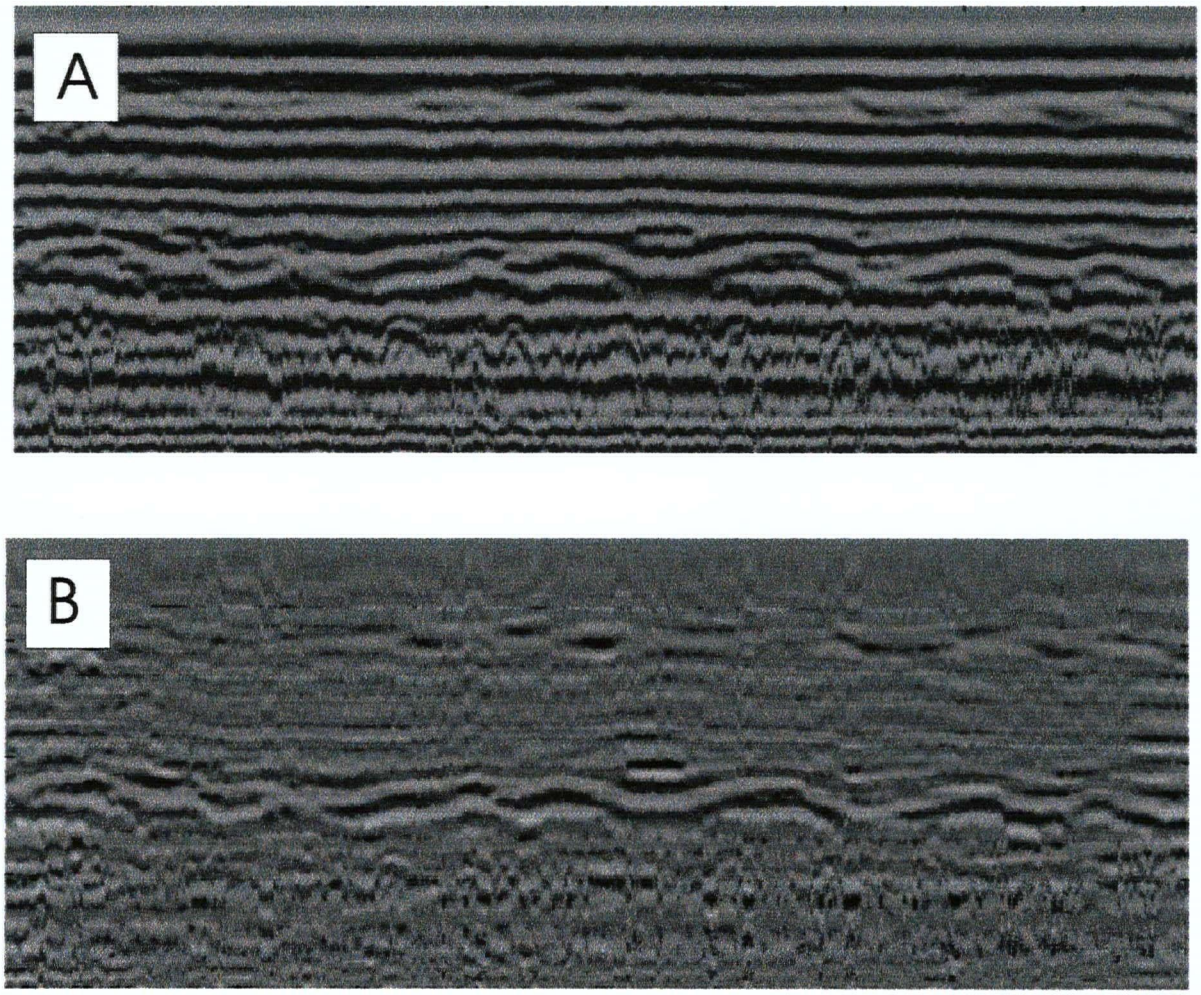

Fig. 7.4. These are GPR data displayed as images in MATLAB. Figure A shows the GPR profile with an automatic gain control applied and figure B is the high-pass eigenimage where the flat horizontal reflections have been selectively removed. The horizontal side of the profile corresponds to 10 m and the vertical to 1.2 m. The antennae separation and step size were 17 cm and 2 cm respectively. This profile was collected at approximately 1290 m from the center of the Ubehebe Crater.

K3X9

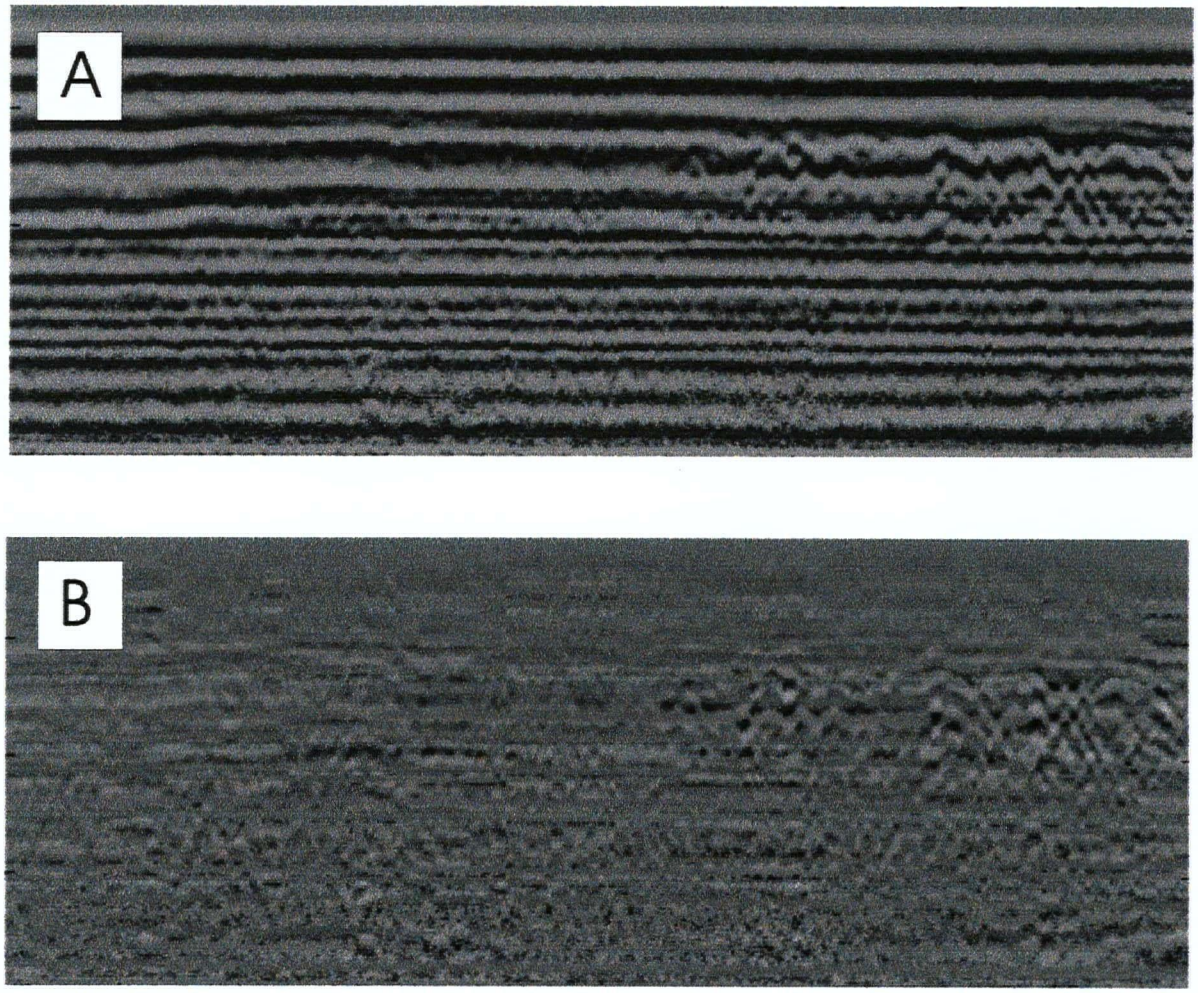

Fig. 7.5. These are GPR data displayed as images in MATLAB. Figure A shows the GPR profile with an automatic gain control applied and figure B is the high-pass eigenimage where the flat horizontal reflections have been selectively removed. The horizontal side of the profile corresponds to 10 m and the vertical to 1.2 m. The antennae separation and step size were 17 cm and 2 cm respectively. This profile was collected at approximately 2600 m from the center of the Ubehebe Crater.

the center of the Ubehebe Crater and show that the amount of wavy reflections decreases downflow. A comparison between the first eight singular values of all GPR profiles is presented in Fig. 7.6. It is possible to observe that the first singular values increase downflow, whereas the other singular values decrease downflow (with the exception of the second and third). Finally, Fig. 7.7 shows the first 36 singular values of the profile (shown in Fig. 7.3) collected at 560 m from the center of the Ubehebe Crater and those of the profile collected at 2600 m (shown in Fig. 7.5).

7.4 Discussion and conclusion

The high-pass eigenimage processing is a filter, which selectively removes the flat horizontal reflections from the GPR profiles, leaving the portions of the profiles with the wavy reflections. In this data set, tests have revealed that the removal of the first three eigenimages performs this filtering satisfactorily. For this reason, the values of the energy of the eigenimages depend on the amount of wavy reflections that has not been removed by the filter and the normalization of the GPR profiles assures that the energy was equal in all profiles before filtering. The energy of the eigenimages of the profiles decreases downflow (Fig. 7.2), because the reflections become increasingly less wavy in this direction and the filtering removes the increasingly larger parts of the traces, which are highly correlated (i.e. the flat reflections). This can be clearly observed comparing the GPR profiles and their correspondent high-pass eigenimages in Figs 7.3, 7.4 and 7.5. In general, if both wavy and flat reflections are not sub-horizontal, a rotation of the data matrix is obviously required before computing the eigenimages.

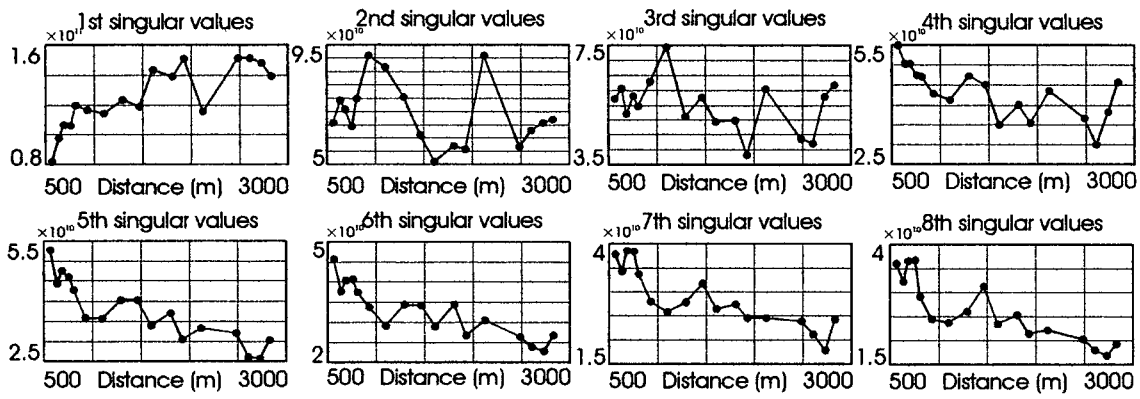

Fig. 7.6. Comparison between the first eight singular values of all GPR profiles plotted versus the distance from the center of Ubehebe Crater.

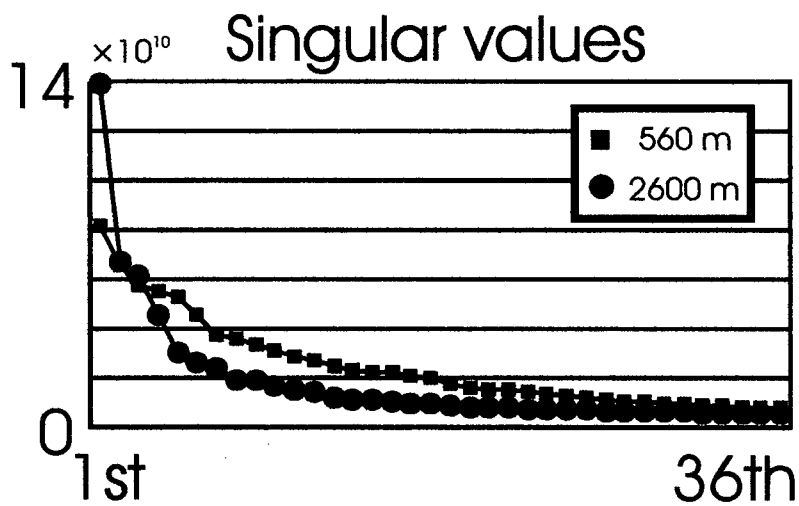

Fig. 7.7. The first 36 singular values of the GPR profile collected at approximately 560 m from the center of the Ubehebe Crater and those of the profile collected at 2600 m.

In short, the energy of the eigenimages can be considered an index of the amount of wavy reflections in the GPR profile, where the amount of wavy reflections encompasses both the number of trains of waves as well as the size of the waves. The computation of the energy does not distinguish between these two aspects of the waviness, but they present similar trends because they both decrease downflow. The wavy reflections in these profiles are caused by trains of sandwaves in the deposits and for this reason, the downflow decrease of the energy of the eigenimages gives an idea of the downflow decrease of both the number and size (i.e. wavelength and wave height) of the climbing dune-forms.

A few considerations are necessary before interpreting geologically the downflow distribution of the energies. First, not necessarily all non-horizontal reflections are always related to the presence of sandwaves. For example, the most distal profile has imaged no sandwaves at all, but the energy of its eigenimage is slightly larger than that of the previous three profiles. Second, two trains of waves have been identified in the GPR profiles, but they were deposited independently by different surges which did not necessarily leave sandwaves with the same size (i.e. wavelength and wave height). For this reason the energy gives only information about an average waviness of the reflections in each profile where more than one different surge unit has been imaged. It is also true that GPR may not be able to resolve very small dunes with small wavelength. Finally, it is interesting to note that the energy of the eigenimages does not decrease regularly, because after an initial decrease, it increases in correspondence of the eight and ninth profiles and decreases again after the ninth profile. This is exactly what happens to the distance between the crests of the waves in the profiles, although it is important to bear in mind that the GPR images of the sandwaves do not necessarily correspond always to their largest, central section. Furthermore, it is obvious that

the energy of the eigenimages does not give directly the value of the wavelength of the sandwaves.

Fig. 7.6 shows that the first singular values increase downflow, whereas the other singular values (with the exception of the second and the third) decrease downflow. This is related to two concomitant properties: 1) the singular values represent the weights associated with the eigenimages, i.e. the contribution of a particular eigenimage to the reconstruction of the original profile is proportional to the magnitude of the associated singular value (Ulrych et al., 1999), and 2) the first eigenimages are related to the highly correlated parts of the traces (i.e. those forming the flat reflections) whereas the others are related to the non correlated parts of the traces (i.e. those forming the wavy reflections). For these reasons, the weight of the first eigenimage (i.e. the first singular value) must be more important, i.e. higher, in the distal than in the proximal profiles, because the waviness of the reflections in the GPR profiles decreases downflow. On the contrary, the weights (i.e. the singular values) of the other eigeimages (which are related to the wavy reflections) must become less important, i.e. smaller, downflow. The distributions of the second and the third singular values are probably caused by the overlapping of these two opposite trends. Finally, Fig. 7.7 confirms that the first singular values are, in general, greater in the distal than in the proximal profiles. Furthermore, Fig. 7.7 confirms that the rate of decrease of the singular values is larger in the distal than in the proximal profiles.

CHAPTER VIII

Cluster Analysis of GPR profiles

8.1 Introduction

In order to classify the GPR profiles collected along the flow direction, three parameters have been simultaneously taken into consideration. These parameters are those computed in the previous chapters. They are: 1) the average square of the sample points of the traces of the GPR profiles (with no AGC applied), 2) the energy of the eigenimages and 3) the wavelength of the sandwaves measured on the hard copy of the profiles using simply a ruler. Unfortunately, each of these parameters does not present a regular decreasing trend along the flow direction. This means that, one single parameter is not able to locate precisely the position of each GPR profile along this direction. For this reason it seems natural to combine these parameters in a way suitable to balance their irregularities, i.e. a multivariate approach should be more efficient in classifying the profiles (or at least to better understand the structure of the data set). This has been attempted using a hierarchical cluster analysis (Davis, 1986), which is a multivariate procedure for detecting groups in a data set.

8.2 Cluster analysis: method and results

The clustering algorithm of a cluster analysis finds the closest profiles (as well as pairs of clusters or a profile and a cluster) according to a measure of distance and combines them.

The distance computed here is a simple *Euclidean distance*. The variables used are the three parameters mentioned in the previous paragraph. Each variable has been transformed into a range of values between 0 and 1 (i.e. the smallest value becomes 0 and the largest becomes 1), because otherwise the parameter with larger values would have biased the calculations of the distance. The clustering method used here is called *average linkage within groups*. This method combines initial clusters so that the average distance between all cases in the resulting cluster is as small as possible and the distance between two clusters is taken to be the average of the distances between all possible pairs of cases in the resulting clusters (Norusis, 1988). Finally, the clustering steps have been displayed in a dendrogram (Fig. 8.1), where the distances are rescaled to numbers between 0 and 25. These calculations have been performed using the software SPSS©.

8.3 Discussion and conclusions

The dendrogram in Fig. 8.1 clearly shows three main groups of GPR profiles, namely a proximal, a medial and a distal group. The proximal group comprises the four most proximal GPR profiles, the medial one comprises the seven intermediate profiles and the distal group the six most distal profiles. It is worth noting that the distal group is divided into two subgroups: each one with three consecutive profiles (H12X9, H13X9 and H14X9 on one side and K3X9, K2X9 and K1X9 on the other side). The cluster analysis seems a simple and efficient method to classify the GPR profiles collected at different distances from the vent and the fact that these profiles can be classified depends directly on GPR ability to detect the heterogeneities in the pyroclastic deposits, which are related to their lateral facies variation.

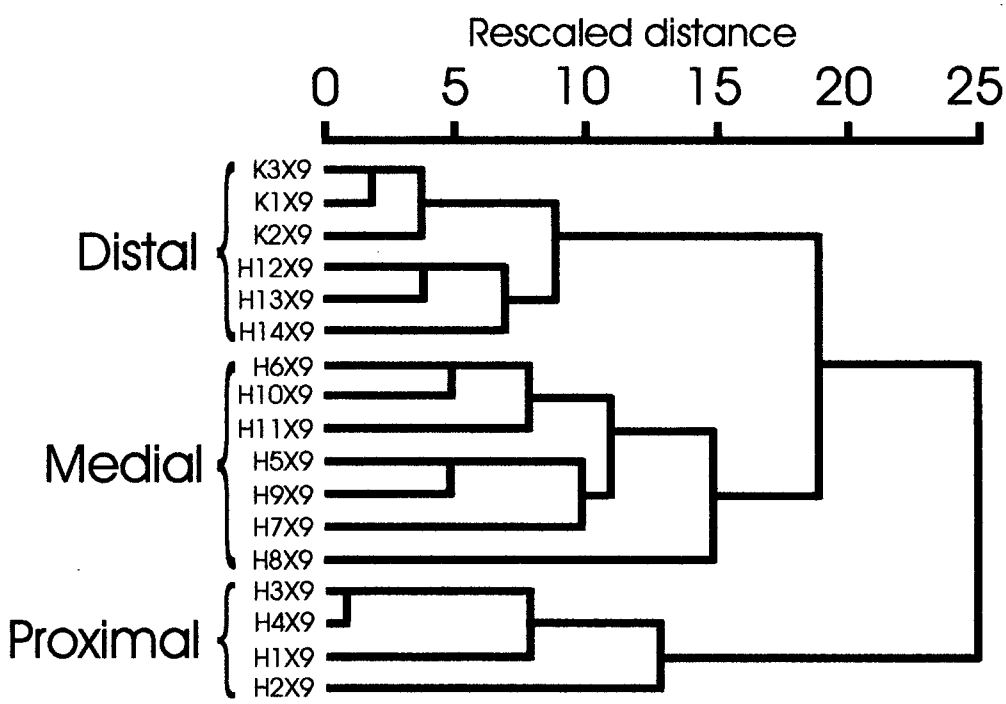

Fig. 8.1. Cluster analysis of the GPR profiles collected along the flow direction with 900 MHz antennae in the Ubehebe hydrovolcanic field.

A similar classification can be obtained inspecting qualitatively the plots of the variables, but, a cluster analysis has the advantages that can be carried out automatically by a computer and can express quantitatively the differences between the profiles. Furthermore, what makes this approach interesting is that we can include in the data set a profile collected in an unknown place within the same hydrovolcanic field. The analysis should be able to automatically classify it in the appropriate cluster. A more detailed classification probably requires a larger number of more suitable variables. The search for other variables in order to classify the GPR profiles is not a trivial task and constitutes a fascinating target for future research.

CHAPTER IX

SUMMARY

9.1 Summary

The GPR profiles collected along a flow direction in the Ubehebe hydrovolcanic field can be interpreted as images of the medial to distal portion of the lateral facies sequence distilled by Y.K. Sohn and S.K. Chough (Sohn and Chough, 1989; Chough and Sohn, 1990; Sohn, 1996), because the most proximal and intermediate radargrams show wavy reflections (i.e. sandwaves) together with plane-parallel reflections (plane-parallel beds and laminae), whereas the distal profiles present increasingly more plane-parallel reflections. The relative low resolution of the radar data does not, however, allows a reliable interpretation of the plane-parallel reflections. They could be due, for example, to plane-parallel laminated beds, fall deposits or thin massive beds. Unfortunately the GPR profiles alone cannot demonstrate the presence of one lateral facies sequence or the other because the resolution is not high enough to locate thin, fine grained massive beds, which could be present, for example, in medial positions such as in the model by Wohletz and Sheridan (1979). The presence of massive deposits along the southwest rim of the Ubehebe Crater probably confirms the Korean model because the massive facies is proximal in the sequence distilled by Y.K. Sohn and S.K. Chough and there is no evidence of massive deposits in the radar profiles.

Furthermore, the model suggested by Wohletz and Sheridan (1979) is probably based on wrong assumptions because they extend laterally within a single flow the results obtained with a statistical analysis of vertical bed-form transitions in different flow units, which are probably independent (Fisher and Schmincke, 1984). The main implication of the Korean model is that base surges are decelerating turbulent flows whose grain concentration decreases and degree of traction increases downcurrent, although these lateral facies variation models are probably an oversimplification of what actually occurs in nature. In any case, the work presented in this thesis demonstrates that GPR can locate trains of unexposed climbing dune-forms in the subsurface. This is the first time that climbing dune-forms have been imaged using ground penetrating radar. Furthermore, GPR allows also a 3-D study of these subsurface structures that would be otherwise impossible in the field.

Because the purpose of this research was to evaluate potential and limitations of GPR in studying the lateral facies variation of pyroclastic deposits, it is possible to say that, in areas with simple stratigraphy, ground penetrating radar can provide subsurface information and can integrate traditional geologic surveys. This is particularly useful when there are no exposures. For example, it has been possible to image the stratigraphic lower limit of the base surge deposits, suggesting that isopach maps can be obtained with this technique. The GPR data also show that it is possible to distinguish base surge deposits from the underlying sandstones (because they have different radar responses) and that different lithologies can be traced laterally in the subsurface. Furthermore, the presence of a small tuff ring, partly eroded and filled by alluvium, has been confirmed when an unconformity between the horizontal reflections from the alluvium and the underlying bowl-shaped reflections from the pyroclastic deposits has been imaged within the crater. It is important, however, to say that

the resolution of a GPR profile will always be worse than that obtained directly inspecting the surface of an outcrop. Furthermore, a GPR profile cannot be considered a true geologic section, because, among the other reasons, it shows the energy reflected from a 3-D cone of material underneath the antennae. These considerations show that it is extremely important to avoid over-interpretation of radar data.

The downflow decrease of the amplitude of the reflections is an extremely interesting result because it can be used as a flow direction indicator when the vent position is unknown. This trend probably reflects some aspects of the lateral facies variation of base surge deposits. The downflow decrease of the amplitude of the reflections is probably due to the fact that the beds become more similar downflow. The concomitant downflow decrease of grain size and increase of sorting mean that in the more distal positions the deposits consist only of fine-grained laminae or thin beds with similar physical properties. Unfortunately, a simple visual inspection of GPR profiles does not enable the recognition of subtle degrees of similarities or dissimilarities between the traces, but the amplitude spectra of the Fourier Transforms and the average square of the sample points of the traces are a very useful visual and computational aid. These results suggest that, although ground penetrating radar data are mainly used to image major underground discontinuities, they can probably be useful to obtain more subtle information about the heterogeneous distribution of subsurface physical properties. This constitutes a fascinating research field. In any case, it should be stressed that, experiments to assess presence and magnitude of artifacts, should always be carried out before quantitative measures are computed (Chapter 4).

The GPR profiles show also a downflow decrease of the waviness of the reflections, which is probably due to the downflow decrease of the size (i.e. wavelength and wave

height) of the climbing dune forms in the deposits. This trend can be used as a flow direction indicator when the vent position is unknown and has been evaluated numerically computing the energy of high-pass eigenimages of the radar profiles. The high-pass eigenimages act as a filter discarding the highly correlated parts of the traces (i.e. those forming the flat reflections) and leaving the portions of the profiles with the wavy reflections. For this reason, the energy of the eigenimages appears to be an index of the waviness of the reflections, which is useful because of the difficulties in selecting confidently the position of the crests (and measuring their correspondent wavelength) in the more distal GPR sections where the small wave heights are not well resolved by the limited resolution of radar data. But, it is important to realize that not necessarily all the wavy reflections in GPR profiles are related to climbing dune-forms in the deposits.

Finally, the parameters used to characterize the GPR profiles have been combined together in a cluster analysis. This analysis shows that it is possible to classify the profiles into proximal, medial and distal groups. This depends directly on the GPR ability to detect heterogeneities in pyroclastic deposits, which are related to their lateral facies variation. Further studies are probably necessary to select other parameters in order to obtain a better classification, but the search for parameters to classify GPR profiles is not a trivial task and constitutes a fascinating target for future research. GPR studies of pyroclastic deposits are still in their infancy but constitute a promising, new research field useful for the advancement of volcanology because they enable the collection of subsurface information without the presence of outcrops.

BIBLIOGRAPHY

Allen, J.R.L., 1982. Developments in sedimentology. Vol. 30A and B. Sedimentary structures, their character and physical basis. Elsevier, Amsterdam.

Allen, J.R.L., 1985. Physical sedimentology. Allen and Unwin, London.

Annan, A.P., Davis, J.L., Scott, W.J., 1975. Impulse radar wide angle reflection and refraction sounding in permafrost. Geological Survey of Canada, Paper 75-1C, 335-341.

Armstrong, M., 1998. Basic linear geostatistics. Springer Verlag, Berlin.

Beres, M., Green, A., Huggenberger, P., Horstmeyer, H., 1995. Mapping the architecture of glaciofluvial sediments with three-dimensional georadar. Geology, 23, 1087-1090.

Blatt, H., Middleton, G., Murrey, R., 1980. Origin of sedimentary rocks. Prentice-Hall, Englewood Cliffs.

Boudon, G., Lajoie, J., 1989. The 1902 Pelean deposits in the Fort Cemetery of St. Pierre: a model for the accumulation of turbulent nuées ardentes. J. Volcan. Geotherm. Res., 38, 113-130.

Bristow, C., Pugh, J., Goodall, T., 1996. Internal structure of aeolian dunes in Abu Dhabi determined using the ground penetrating radar. Sedimentology, 43, 995-1003.

Cai, J., McMechan, G.A., 1995. Ray-based synthesis of bistatic ground penetrating radar profiles. Geophysics, 60, 87-96.

Cas, R.A.F., Wright, J.V., 1987. Volcanic successions, modern and ancient. Chapman and Hall, London.

Chough, S.K., Sohn, Y.K., 1990. Depositional mechanics and sequences of base surges, Songaksan tuff ring, Cheju Island, Korea. Sedimentology, 37, 1115-1135.

Clark, I , 1979. Practical geostatistics. Applied Science Publishers LTD, London.

Crowe, B.M., Fisher, R.V., 1973. Sedimentary structures in base surge deposits with special reference to cross-bedding, Ubehebe Craters, Death Valley, California. Geol. Soc. Am. Bull., 84, 663-682.

Crowe, B.M., 1990. Ubehebe, California. In: Wood, C.A., Kienle, J., Eds., Volcanoes of North America, United States and Canada. Cambridge University Press, Cambridge.

Daniels, D.J., 1996. Surface penetrating radar. The Institution of Electrical Engineers, London.

Davis, J.C., 1986. Statistics and data analysis in geology. John Wiley and Sons, Singapore.

Davis, J.L., Annan, A.P., 1989. Ground penetrating radar for high-resolution mapping of soil and rock stratigraphy. Geophys. Prosp., 37, 531-551.

Druitt, T.H., Mellors, R.A., Pyle, D.M., Sparks, R.S.J., 1989. Explosive volcanism on Santorini, Greece. Geological Magazine, 126, 95-213.

Fisher, E., McMechan, G.A., Annan, A.P., 1992. Acquisition and processing of wide aperture ground penetrating radar data. Geophysics, 57, 495-504.

Fisher, R.V., 1983. Flow transformations in sediment gravity flows. Geology, 11, 273-274.

Fisher, R.V., Schmincke, H.-U., 1984. Pyroclastic rocks. Springer-Verlag, Berlin.

Fisher, R.V., Waters, A.C., 1970. Base surge bed forms in maar volcanoes. Am. J. Sci., 268, 157-180.

Freire, S.L.M., Ulrych, T.J., 1988. Application of singular value decomposition to vertical seismic profiling. Geophysics, 53, 778-785.

Gawthorpe, R.L., Collier, R.E.L., Alexander, J., Bridge, J.S., Leeder, M.R., 1993. Ground penetrating radar: application to sandbody geometry and heterogeneity studies. In: North, C.P., Prosser, D.J., Eds., Characterization of fluvial and aeolian reservoirs. Geol. Soc., Special Publication, London, 73, 421-432.

Gueguen, Y., Palciauskas, V., 1994. Introduction to the physics of rocks. Princeton University Press, Princeton, New Jersey.

Jol, H.M., Smith, D.G., 1991. Ground penetrating radar of northern lacustrine deltas. Can. J. Earth Sci., 28, 1939-1947.

Journel, A.G., Froidevaux, R., 1982. Anisotropic hole effect modeling. Mathematical Geology, 14, 217-239.

Hansen, W., Sill, W.R., Ward, S.H., 1973. The dielectric properties of selected basalts. Geophysics, 38, 135-139.

Heiken, G., Wohletz, K., 1992. Volcanic ash. University of California Press, Berkeley and Los Angeles.

Isaaks, E.H., Srivastava, R.M., 1989. Applied geostatistics. Oxford University Press, New York.

Kenyon, W.E., 1984. Texture effects on megahertz dielectric properties of calcite rock samples. J. Appl. Phys., 55, 3153-3159.

Knight, R., Tercier, P., Jol, H., 1997. The role of ground penetrating radar and geostatistics in reservoir description. The Leading Edge, 11, 1576-1582.

Lajoie, J., Lanzafame, G., Rossi, P.L., Tranne, C.A., 1992. Lateral facies variations in hydromagmatic pyroclastic deposis at Linosa, Italy. J. Volcan. Geotherm. Res., 54, 135-143.

Lajoie, J., Stix, J., 1992. Volcaniclastic rocks. In: Walker, R.G., James, N.P., Eds., Facies models, response to sea level change. Geological Association of Canada, pp. 101-118.

Mitchum, R.M., Vail, P.R., Thompson, S., 1977. Seismic stratigraphy and global changes of sea level, part 2: the depositional sequence as a basic unit for stratigraphic analysis. In: Payton, C.E., Ed., Seismic stratigraphy – applications to hydrocarbon exploration. The American Association of Petroleum Geologists, Tulsa, pp. 53-62.

McCoy, F.W., Papmarinopoulos, S., Doumas, C., Palyvou, C., 1992. Probing the Minoan eruption on Thera with ground penetrating radar: buried extent of Akrotiri, tephra stratigraphy and late-Bronze age volcanic hazard. Geol. Soc. Am., Abstracts with Programs, 24, 26.

McMechan, G.A., Gaynor, G.C., Szerbiak, R.B., 1997. Use of ground penetrating radar for 3-D sedimentological characterization of clastic reservoir analogs. Geophysics, 62, 786-796.

Mellett, J.S., 1990. Ground penetrating radar enhances knowledge of Earth's surface layer. Geotimes, 35, 12-14.

Norusis, M.J., 1988. SPSS-X advanced statistics guide. SPSS Inc., Chicago.

Olhoeft, G.R., 1984. Applications and limitations of ground penetrating radar. 54th Annual International Meeting., Society of Exploration Geophysicists, Expanded Abstracts, 147-148.

Pilon, J.A., Grieve, R.A.F., Sharpton, V.L., 1991. The subsurface character of Meteor Crater Arizona as determined by ground probing radar. J. Geophys. Res., 96, 15563-15576.

Rea, J., Knight, R., 1998. Geostatistical analysis of ground penetrating radar data: a means of describing spatial variation in the subsurface. Water Resources Research, 34, 329-339.

Reynolds, J.M., 1997. An introduction to applied and environmental geophysics. John Wiley and Sons, Chichester.

Robinson, E.A., Treitel, S., 1980. Geophysical signal analysis. Prentice Hall Inc., Englewood Cliffs.

Roddy, D.J., 1968. Minimum energy of formation of Ubehebe Crater, Death Valley, California. Geol. Soc. Am., Special Paper, 187-188.

Rubin, D.M., 1987. Cross-bedding, bedforms and paleocurrents. Society of Economic Paleontologits and Mineralogists, Tulsa.

Russell, J.K., Stasiuk, M.V., 1997. Characterization of volcanic deposits with ground penetrating radar. Bull. Volcan., 58, 515-527.

Russell, J.K., Stasiuk, M.V., *in press*. GPR studies of volcanic deposits on Thera. In: Volcanoes, Earthquakes and Archeology, Geol. Soc., Special Publication, London.

Sensors and Software, 1996. PulseEKKO 100 Run, User's guide, version 1.2.

Sensors and Software, 1999. PulseEKKO 1000 Run. User's guide, version 1.2.

Sigurdsson, H., Carey, S.N., Fisher, R.V., 1987. The 1982 eruption of El Chichon volcano, Mexico: physical properties of pyroclastic surges. Bull. Volcan., 49, 467-488.

Smith, D.H., Jol, H.M., 1992. Ground penetrating radar investigation of a Lake Bonneville delta, Provo level, Brigham City, Utah. Geology, 20, 1083-1086.

Smith, D.H., Jol, H.M., 1995. Ground penetrating radar: antenna frequencies and maximum probable depths of penetration in Quaternary sediments. J. Appl. Geophys., 33, 93-100.

Smith, D.H., Jol, H.M., 1997. Radar structure of a Gilbert-type delta, Peyto Lake, Banff National Park, Canada. Sedimentary Geology, 113, 195-209.

Sohn, Y.K., Chough, S.K., 1989. Depositional processes of the Suwolbong tuff ring, Cheju Island (Korea). Sedimentology, 36, 837-855.

Sohn, Y.K., 1996. Hydrovolcanic processes forming basaltic tuff rings and cones on Cheju Island, Korea. Geol. Soc. Am. Bull., 10, 1199-1211.

Stearns, S.D., David, R.A., 1996. Signal processing algorithms in Matlab. Prentice Hall, Upper Saddle River.

Strand, R.G., 1967. Mariposa Sheet. Geologic Map of California in scale 1:250.000. Division of Mines and Geology, Sacramento, CA.

Strang, G., 1986. Linear algebra and its applications. Saunders and Harcourt Brace Jovanovich Inc., Orlando.

Tercier, P., Knight, R., Jol, H., submitted. A comparison of the correlation structure in GPR images of deltaic and barrier spit depositional environment. Geophysics.

Troxel, B.W., Strand, R.G., 1964. Geologic map of the northern Death Valley and Eureka Valley area, scale 1:62.500. California Division of Mines and Geology.

Ulriksen, C.P.F., 1982. Application of impulse radar to civil engineering. Doctoral Thesis, Lund University.

Ulrych, T.J., Sacchi, M.D., Freire, S.L.M., 1999. Eigenimages processing of seismic sections. In: Kirlin, R.L., Done, W.J., Eds., Covariance Analysis for seismic signal processing, Society of Exploration Geophysicists, Tulsa, pp. 241-274.

Valentine, G.A., 1987. Stratified flow in pyroclastic surges. Bull. Volcanol., 49, 616-630.

Valentine, G.A., Fisher, R.V., 2000. Pyroclastic surges and blasts. In: Sigurdsson, H., Houghton, B.F., McNutt, S.R., Rymer, H., Stix, J., Eds., Encyclopedia of Volcanoes. Academic Press, San Diego, pp. 571-580.

Von Engeln, O.D., 1932. The Ubehebe craters and explosion breccias in Death Valley, California. Journal of Geology, 40, 726-734.

Waters, A.C., Fisher, R.V., 1971. Base surges and their deposits: Capelinhos and Taal volcanoes. J. Geophys. Res., 76, 5596-5614.

White R.E., 1991. Properties of instantaneous seismic attributes. The Leading Edge, 10, 26-32.

Wohletz, K.H., 1986. Explosive magma-water interactions: thermodynamics, explosion mechanisms and field studies. Bull. Volcan., 48, 245-264.

Wohletz, K., Heiken, G., 1992. Volcanology and geothermal energy. University of California Press, Berkely and Los Angeles.

Wohletz, K.H., Sheridan, M.F., 1979. A model of pyroclastic surge. Geol. Soc. Am., Special Paper, 180, 177-194.

Yilmaz O., 1987. Seismic data processing. Society of Exploration Geophysicists, Tulsa.

APPENDIX I

Dielectric constant

A1.1 Dielectric constant from CMP profiles: method and results

Dielectric constant of base surge deposits can be estimated from Common Mid Point (CMP) profiles. In these profiles the reflected electromagnetic waves plot as hyperbolas (Annan et al., 1975), whose equations enable the calculation of their velocities in the subsurface. The velocities V of the electromagnetic waves traveling through a particular medium can be written as:

$$V = \frac{c}{\left\{\left(\frac{K\mu_r}{2}\right)\left[\left(1+P^2\right)+1\right]\right\}^{1/2}}, \qquad (1)$$

where c is the speed of light in the free space, K is the relative dielectric constant and μ_r is the relative magnetic permeability (Reynolds, 1997). P is equals to $\sigma/\omega\varepsilon$ and is called the *loss factor*, where σ is the conductivity, ω is equal to $2\pi f$ (f is the frequency) and ε is the permittivity equals to $K\varepsilon_0$ (ε_0 is the permittivity of the free space). This formula, in non-magnetic (μ_r=1) and low loss material ($P\approx 0$), becomes:

$$V\,(\text{m/ns}) = 0.3\,(\text{m/ns}) / K^{1/2} \qquad (2)$$

The dielectric constant K can be easily computed from equation (2) using V estimated from CMP profiles (that I have determined using the software package Gradix©). Table A1 shows the values of the dielectric constants estimated using this method. These values are close to those (i.e. 7-15) determined experimentally for rock with basaltic composition (Hansen et al., 1973).

A1.2 Discussion

In dry rocks, the dielectric constant is usually dependent on bulk density (Gueguen and Palciauskas, 1994). The shape of the fragments (i.e. the amount of grain platiness) is also a very important factor affecting the amount of polarization of a rock material (Kenyon, 1984). The reflections in my GPR profiles are probably due to differences in density (i.e. porosity) across bed interfaces. In pyroclastic rocks, the packing density of clasts is determined for example by a combination of grain size distribution and sorting (Wohletz and Heiken, 1992), i.e. the texture of the rock (assuming, for example, that there are no changes in composition).

Table A1.1- Dielectric constants of base surge deposits from the Ubehebe hydrovolcanic field.

	Velocity (m/ns)	Dielectric constant
Cmpf3x2p	0.092	10.63
Cmpf2bis	0.091	10.87
Cmpg1x1	0.092	10.63
Cmpa1x5p	0.096	9.76
Cmph1x9	0.12	6.25

APPENDIX II

GPR IMAGES OF PYROCLASTIC DEPOSITS FROM SANTORINI (GREECE)

A2.1 Introduction

Ground penetrating radar surveys of basaltic pyroclastic deposits have been conducted in the island of Santorini (Fig. A2.1) in order to compare GPR profiles of pyroclastic deposits with different grain size. These profiles were collected parallel to the surfaces of outcrops using a PulseEKKO 100 instrument with unshielded 200 MHz antennae. In all GPR profiles, the step size is equal to 0.1 m, the antenna separation is 0.5 m and the number of stacks is 256. These data constitute an instructive database and can interestingly be compared to those collected in the Ubehebe hydrovolcanic field because the deposits have similar chemical composition (basic) but different grain size.

A2.2 Profiles SANT0 and CMPSANT0

Deposit

This deposit is exposed in a quarry along the road between the villages of Phira and Akrotiri and is located stratigraphically below the Minoan Member of the Thera Pyroclastic Formation (Druitt et al., 1989). It is a thinly laminated and very fine-grained deposit with

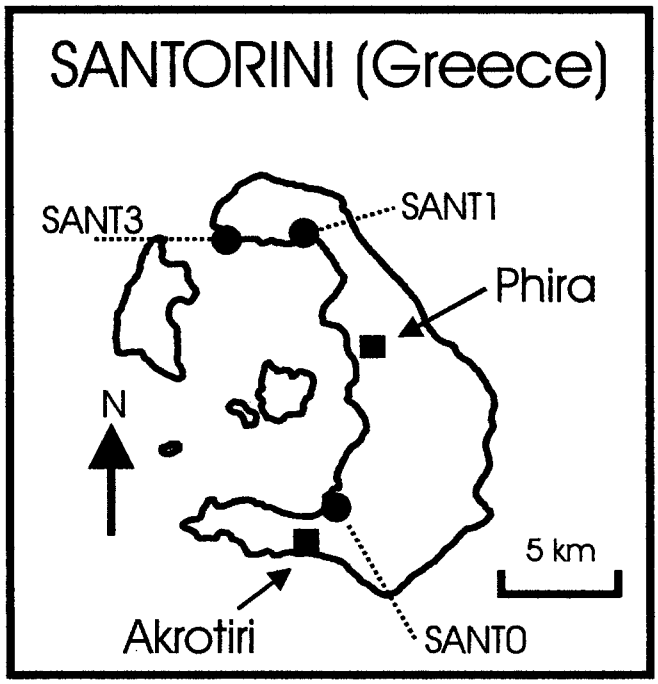

Fig. A2.1. Map of the island of Santorini (Greece) and locations of the GPR profiles.

blocky fragments less than 2 mm in diameter. The lamination is wavy (Fig. A2.2). The deposit is 3-4 m thick with a horizontal top (no soil cover) and horizontal base, it is well sorted and does not show grading. This deposit is interpreted as a distal base surge deposit.

GPR data

Survey SANT0 (Fig. A2.3) has been run on the horizontal top of the deposit and presents slightly inclined reflections. Some reflections are continuous, other discontinuous. The CMP data (Fig. A2.4) suggest subsurface velocities of the electromagnetic waves in this deposit equal to 0.08 m/ns. These velocities have been obtained using the software package Gradix© (Interpex).

A2.3 Profiles SANT1 and CMPSANT1

Deposit

This is an unconsolidated, well-sorted, scoria deposit with horizontal beds. This deposit is approximately 14 m thick, has a horizontal top and no soil cover. The clasts are black, angular and vesiculated with grain size ranging from 1 mm to 2.5-3 cm in diameter. This deposit is interpreted as a strombolian scoria fall deposit and belongs to the Megalo Vouno cinder cones (Druitt et al., 1989).

GPR data

The GPR profile SANT1 (Fig. A2.5) shows continuous, relatively horizontal and slightly wavy reflections. This survey was run on the horizontal top of the deposit. The CMP data

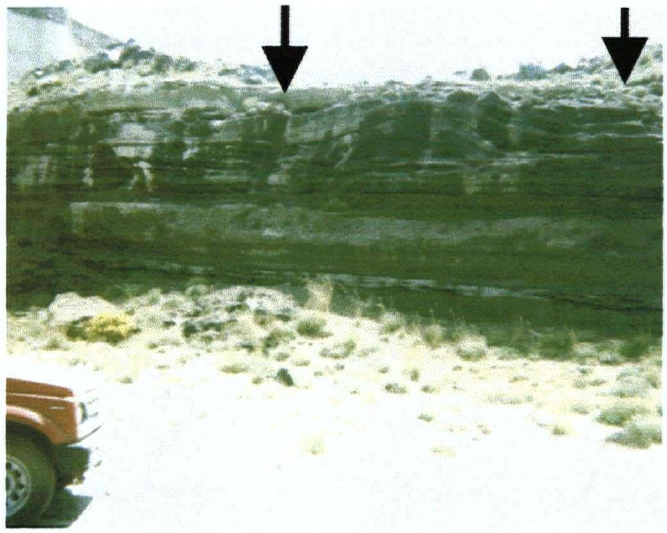

Fig. A2.2. Field photograph of the base surge deposits imaged by profile SANTO. Both GPR and CMP profiles have been run between the two vertical arrows.

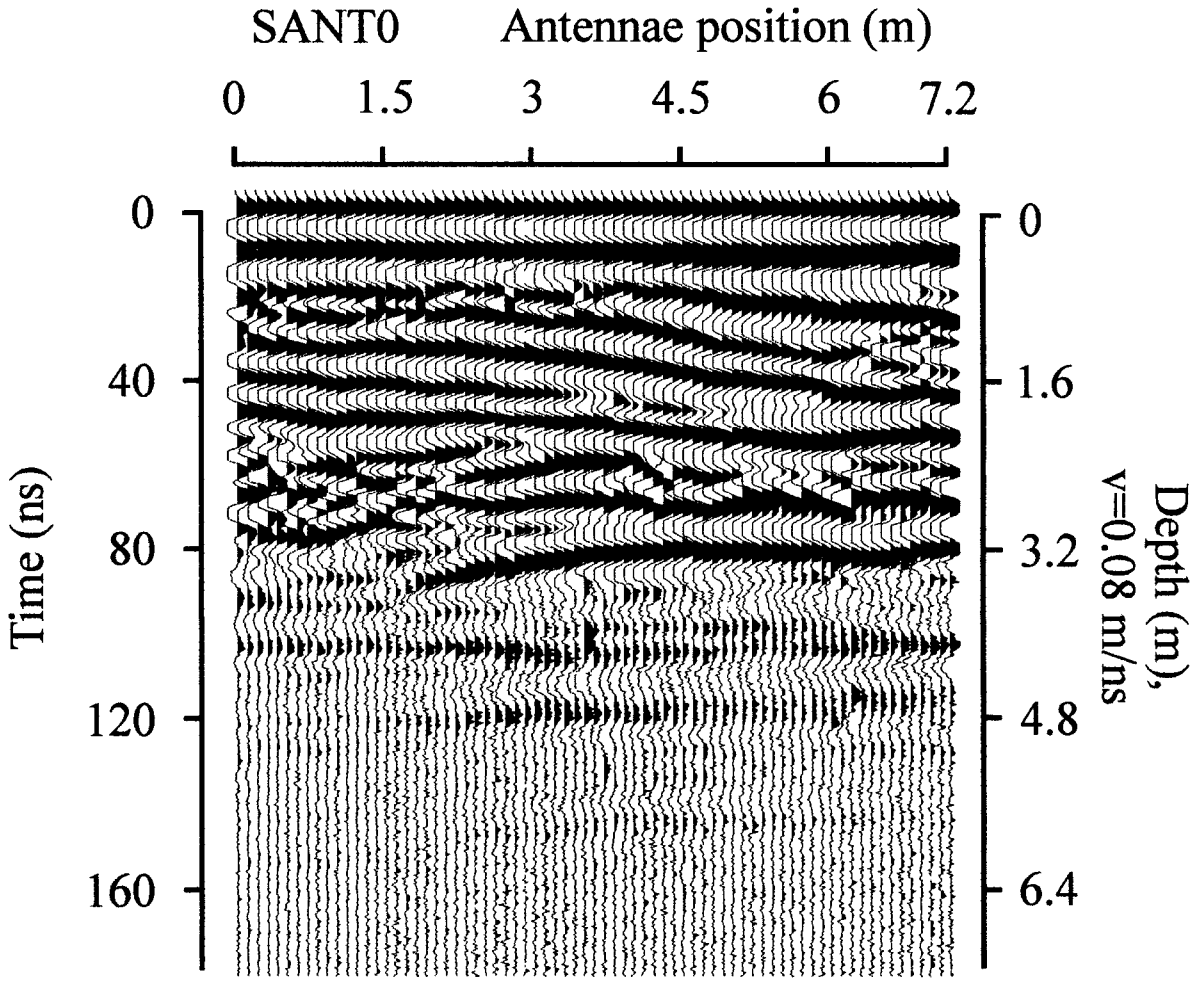

Fig. A2.3. GPR profile SANT0 obtained with 200 MHz antennae.

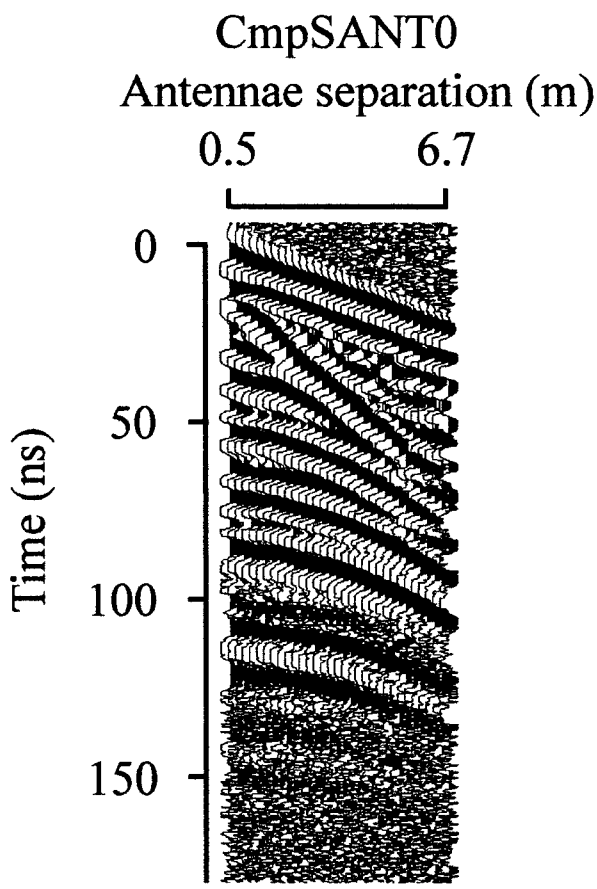

Fig. A2.4. Common Mid Point profile CMPSANT0. The hyperbolas suggest a subsurface velocity of the electromagnetic waves equal to 0.08 m/ns.

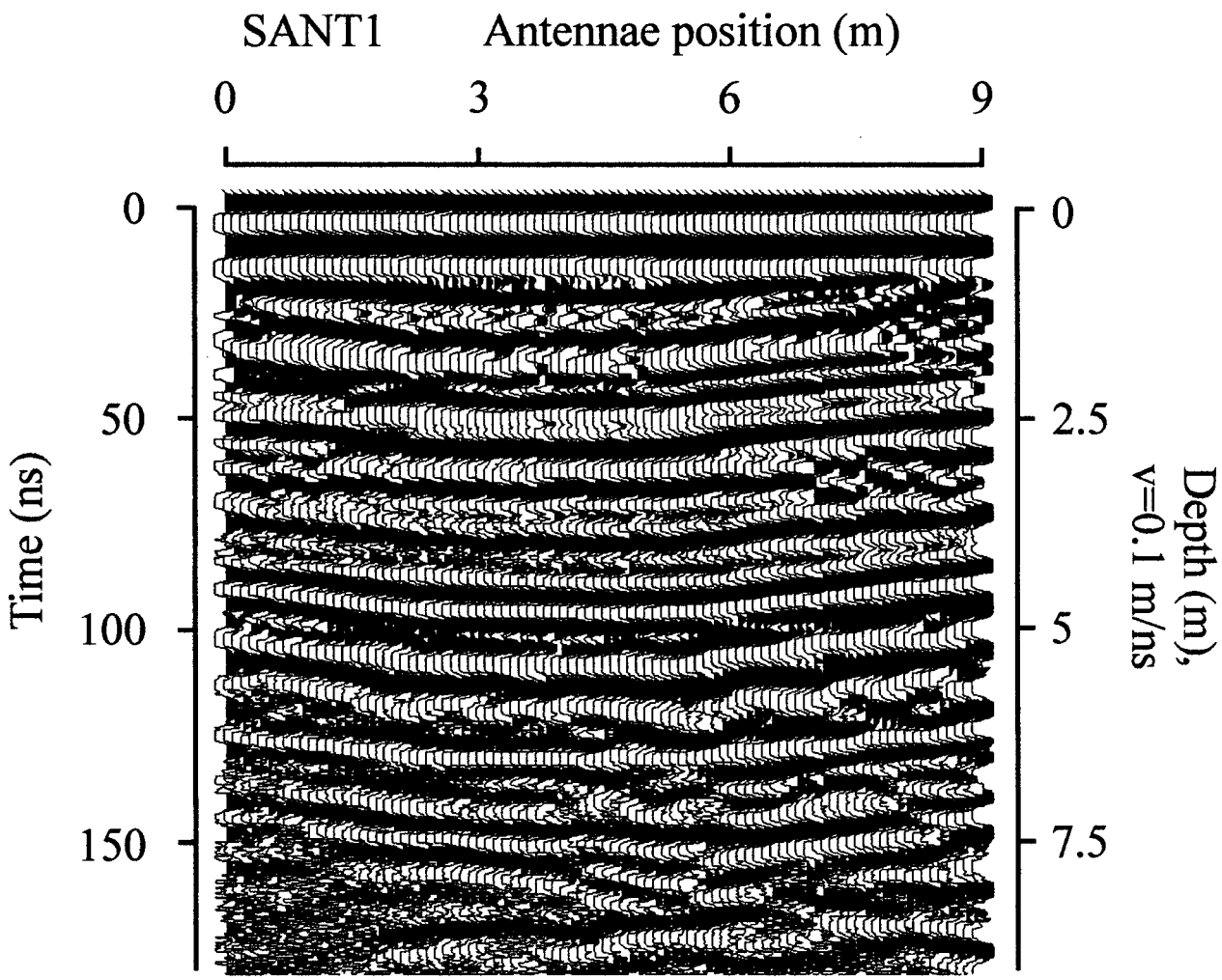

Fig. A2.5. GPR profile SANT1 obtained with 200 MHz antennae.

(Fig. A2.6) show that the subsurface velocities of the electromagnetic waves are between 0.09 and 0.12 m/ns. These velocities have been computed using the software package Gradix© (Interpex).

A2.4 Profiles SANT3 and CMPSANT3

Deposit

This is a partially welded, red scoria deposit with fragments ranging in size from few millimeters to 50-60 cm in diameter. Some porphyritic, non-vesiculated fragments are also present. This deposit crops out along the sea cliff near the village of Oia and belong to the 50 m thick spatter deposit described in Druitt et al. (1989).

GPR data

Profile SANT3 (Fig. A2.7) shows several hyperbolas. The tails of these hyperbolas are parallel to the lines of the air velocity grid superimposed to the profile and computed with the PulseEKKO software. The CMP data (Fig. A2.8) suggest that the subsurface velocities of the electromagnetic waves are between 0.08 and 0.09 m/ns. These velocities have been computed using the software package Gradix© (Interpex).

A2.5 Discussion

The GPR data collected in Santorini enable useful observations. For example, it is interesting to observe that the reflections in profile SANT0 (Fig. A2.3) and the laminae in the

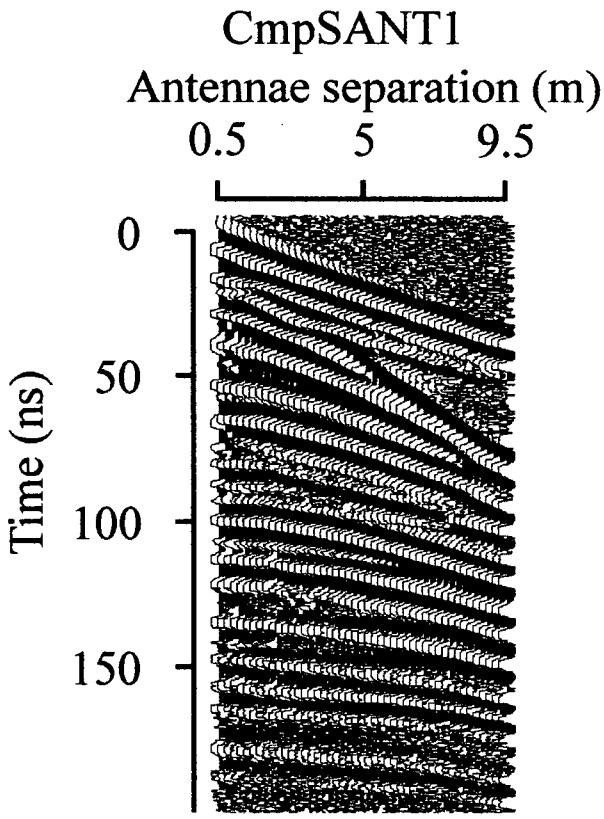

Fig. A2.6. Common Mid Point profile CMPSANT1. The hyperbolas suggest a range of subsurface velocities between 0.09 and 0.12 m/ns.

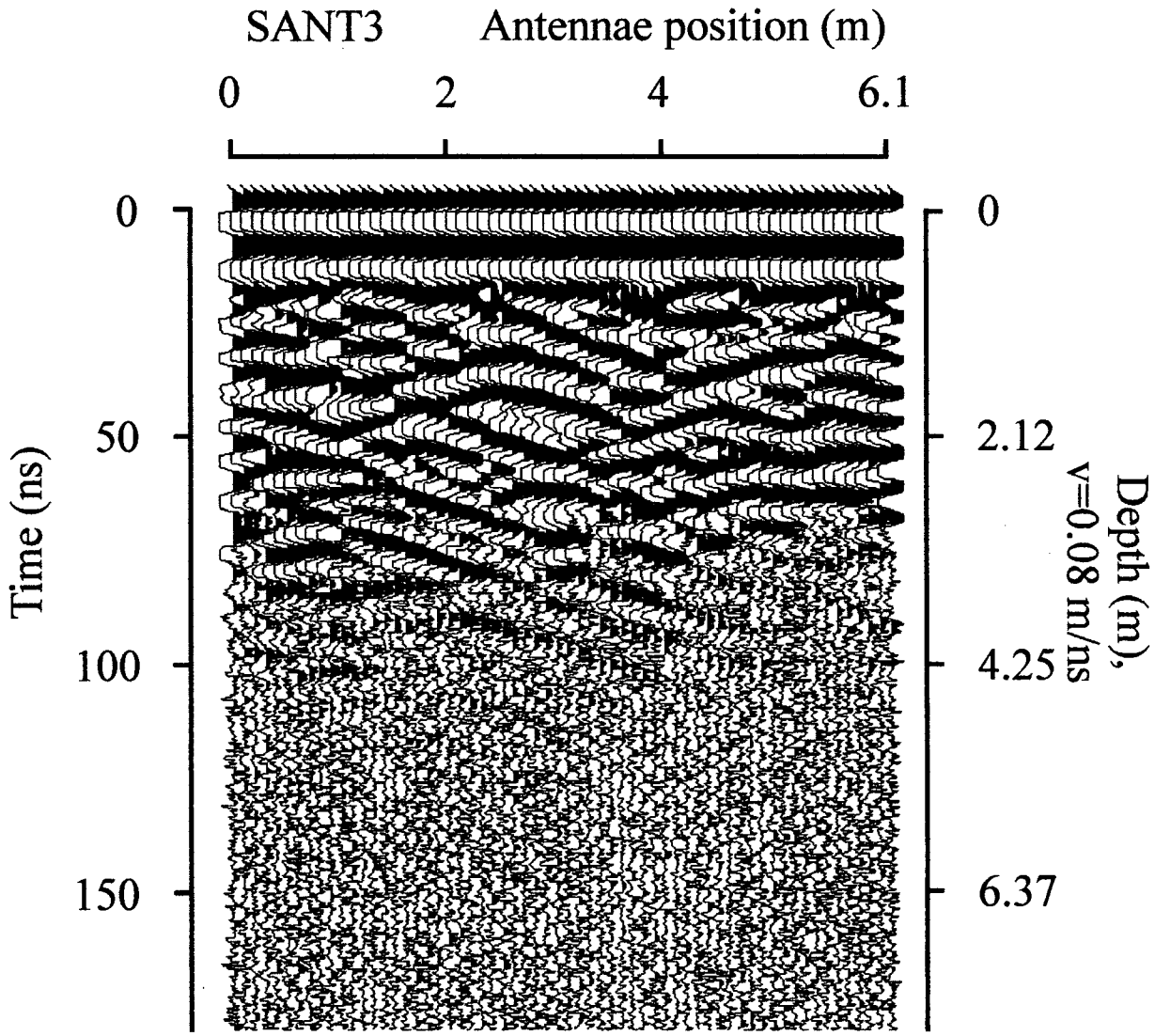

Fig. A2.7. GPR profile SANT3 obtained with 200 MHz antennae.

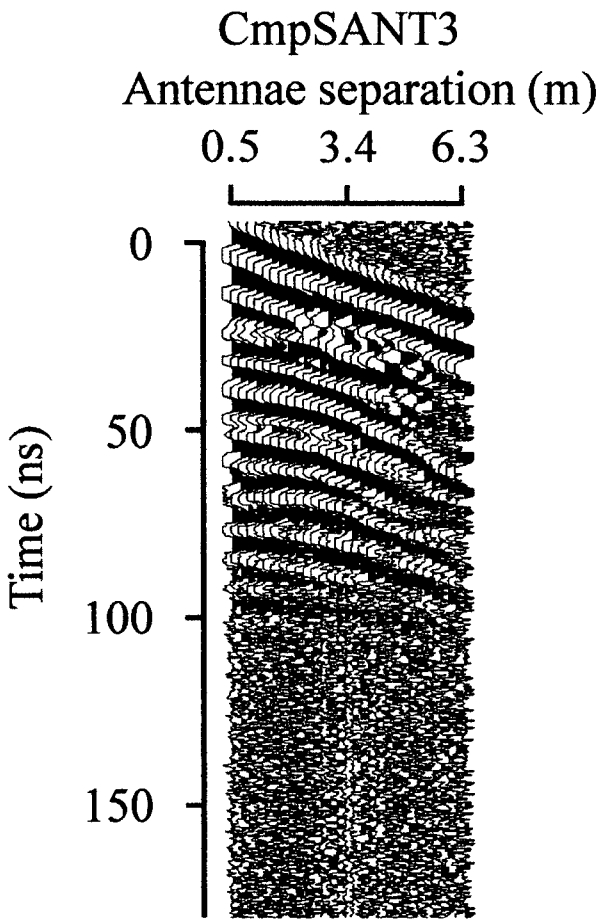

Fig. A2.8. Common Mid Point profile CMPSANT3. The hyperbolas suggest a range of subsurface velocities between 0.08 and 0.09 m/ns.

correspondent outcrop (Fig. A2.2) have different geometries. These differences could be due to the fact that the profile and the surface of the outcrop are parallel but few meters apart and pyroclastic deposits usually show high lateral variability. In this profile, the reflection located at 80-90 ns corresponds probably to the lowest stratigraphic limit of the base surge deposits, because located at approximately the same depth.

It is extremely interesting to note that in profile SANT1 (Fig. A2.5) there is a really good depth of penetration (~ 8 m) of the electromagnetic waves. In spite of the mineralogical composition of basaltic rocks (with a relatively high iron oxide contents) this deposit does not seem to have high conductivity that would have attenuated the propagation of the electromagnetic waves.

The tails of the hyperbolas in SANT3 (Fig. A2.7), which are parallel to the lines of the air velocity grid, show that the objects causing these reflections are located above the surface of the ground. For this reason, extreme care must be paid interpreting GPR data collected with unshielded antennae and the use of shielded antennae is recommended to study the lateral facies variation of base surge deposits.